FÁBIO RAFFAEL FELICE NETO

CONTACT MESH APPROACH IN EXPLICIT FINITE ELEMENT METHOD: AN APPLICATION TO A SEVERE CONTACT PROBLEM

UNIVERSIDADE FEDERAL DE UBERLÂNDIA

FACULDADE DE ENGENHARIA MECÂNICA - FEMEC

2016

SERVIÇO PÚBLICO FEDERAL
MINISTÉRIO DA EDUCAÇÃO
UNIVERSIDADE FEDERAL DE UBERLÂNDIA
FACULDADE DE ENGENHARIA MECÂNICA
PROGRAMA DE PÓS-GRADUAÇÃO EM ENGENHARIA MECÂNICA

ALUNO: Fábio Raffael Felice Neto

NÚMERO DE MATRÍCULA: 11223EMC010

ÁREA DE CONCENTRAÇÃO: Mecânica dos Sólidos e Vibrações

LINHA DE PESQUISA: Projetos de Sistemas Mecânicos

PÓS-GRADUAÇÃO EM ENGENHARIA MECÂNICA: NÍVEL DOUTORADO

TÍTULO DA TESE:

"Contact Mesh Approach in Explicit Finite Element Method: an Application to a Severe Contact Problem"

ORIENTADORA: Profa. Dra. Sonia A. Goulart Oliveira

CO-ORIENTADOR: Prof. Dr. Rafael Weyler Perez – UPC/Espanha

A Tese foi **APROVADA** em reunião pública, realizada no Anfiteatro B - Bloco 5O, Campus Santa Mônica, em 10 de outubro de 2016, às 13:00 horas, com a seguinte Banca Examinadora:

NOME		ASSINATURA
Profa. Dra. Sonia A. Goulart Oliveira	UFU	
Prof. Dr. Francisco José de Souza	UFU	
Prof. Dr. Washington Martins da Silva Júnior	UFU	
Prof. Dr. Gilmar Ferreira Batalha	Poli/USP	
Prof. Dr. Jánes Landre Júnior	PUCMinas	

Uberlândia, 10 de outubro de 2016

FÁBIO RAFFAEL FELICE NETO

CONTACT MESH APPROACH IN EXPLICIT FINITE ELEMENT METHOD: AN APPLICATION TO A SEVERE CONTACT PROBLEM

Dissertation submitted to the Mechanical Engineering Graduation Program of the Federal University of Uberlândia, in partial fulfillment of the requirements for the degree of **Doctor in Mechanical Engineering**

Focus Area: Solid Mechanicsand Vibration

Advisor: Prof. Dr. Sonia A. Goulart de Oliveira

Co-advisor: Prof. Dr. Rafael Weyler Perez

Uberlândia -MG

2016

Dados Internacionais de Catalogação na Publicação (CIP)
Sistema de Bibliotecas da UFU, MG, Brasil.

F314c
2016

Felice Neto, Fábio Raffael, 1989-
Contact mesh approach in explicit finite element method : an application to a severe contact problem. / Fábio Raffael Felice Neto. - 2016.
135 f.

Orientadora: Sonia A. Goulart de Oliveira.
Coorientador: Rafael Weyler Perez.
Tese (doutorado) -- Universidade Federal de Uberlândia, Programa de Pós-Graduação em Engenharia Mecânica.
Disponível em: http://dx.doi.org/10.14393/ufu.te.2017.3
Inclui bibliografia.

1. Engenharia mecânica - Teses. 2. Método dos elementos finitos - Teses. I. Oliveira, Sonia A. Goulart de, 1959-. II. Perez, Rafael Weyler. III. Universidade Federal de Uberlândia. Programa de Pós-Graduação em Engenharia Mecânica. IV. Título.

CDU: 621

DEDICATION

I dedicate this toeveryone that, anyhow, helped me making all this possible.

AKNOWLEDGEMENTS

First of all I would like to thank my family, for unconditional support in every step of my life. They are the base of everything I am, did or will going to do.

My sincere gratitude to my friends, which were there with meat all times, to celebrate together or to cheer me up when I needed. It's a privilege to be surrounded by such good fellows.

I am especially thankful to my advisor Sonia, for all the academic support, partnership and for arousing in me the interest in science.And I am also thankful to my co-advisor Rafael Weyler, for the knowledge given, patience, dedication to our partnership and specially friendship.

I would like to acknowledge my CIMNE colleagues, from whom I learned a lot and who helped me in every stage of this work.

My gratitude to CNPq and the development agencies, which enabled this research by granting my scholarship and the proper tools to keep the research.

I would like to thank the Polytechnic University of Catalonia, for receiving me with open arms.

Finally, my profound gratitude to every professor, technician, the Federal University of Uberlândia and the Graduation Program of the Mechanical Engineering School, which granted me with a great course and opportunity.

FELICE-NETO, F. R. F**. CONTACT MESH APPROACH IN EXPLICIT FINITE ELEMENT METHOD: AN APPLICATION TO A SEVERE CONTACT PROBLEM.** 2016. 117f.PhD Thesis, Universidade Federal de Uberlândia, Uberlândia.

Abstract

The contact problem in Finite Element Method formulations is characterized as an optimization problem, in which the boundary conditions generate a contact penetration gap that must be minimized to maintain the physics of the problem. Normally the contact initiation depends on a search frequency and bodies' velocities, resulting inconsiderable errors when in severe contact cases. So this work aims to propose a contact mesh approach in an Explicit Finite Element Method. This contact mesh links the probable contact regions and minimizes the potential error. To validate the material formulation and properties a tensile strength experiment was simulated. And in order to test the method efficiency, a microindentation experiment that represents a severe contact problem was simulated using explicit and implicit time integration methods. As results both methods showed similar good results when compared to experimental tests, but the implicit approach had better results in total time execution. It was possible to understand the deformation phenomenon in the microindentation test and also other related phenomena, such as the stress field and the pile up.

Keywords: Finite Element Method, Contact Mesh, Microindentation Simulation, Explicit Finite Element Method.

LIST OF SYMBOLS

$\boldsymbol{a}$	Characteristic length of the contact area	[m]
$\boldsymbol{b^{-1}}$	Finger Deformation Tensor	
$\boldsymbol{b^{e-1}}$	Elastic part of the Finger Deformation Tensor	
$\boldsymbol{C}$	Cauchy-Green Tensor	
$\boldsymbol{d}$	Element Position	[m]
$\dot{\boldsymbol{d}}, \boldsymbol{v}$	Element position derivative or velocity	[m/s]
$\ddot{\boldsymbol{d}}, \boldsymbol{a}$	Element velocity derivative or acceleration	[m/s^2]
$\boldsymbol{e}$	Almansi deformation tensor	
$\boldsymbol{e^e}$	Elastic Part of the Almansi deformation tensor	
$\boldsymbol{e^p}$	Plastic Part of the Almansi deformation tensor	
$\tilde{\boldsymbol{e}}$	Almansi deformation tensor in the intermediate stage configuration	
$\boldsymbol{e^{e^{TR}}}$	Trial Elastic Part of the Almansi deformation tensor	
$\tilde{\boldsymbol{e}}^{\boldsymbol{TR}}$	Trial Almansi deformation tensor in the intermediate stage configuration	
$\tilde{\boldsymbol{e}}^{\boldsymbol{p^{TR}}}$	Trial Plastic part of the Almansi deformation tensor in the intermediate stage configuration	

$\boldsymbol{E}$	Young Modulus	[GPa]
$\overline{\boldsymbol{E}}$	Green-Lagrange Deformation	
$\boldsymbol{E}^{*}$	Equivalent Young Modulus	[GPa]
$\overline{\boldsymbol{E}}^{\boldsymbol{P}}$	Plastic part of the Green-Lagrange Deformation	
$\boldsymbol{f}(\boldsymbol{\sigma})$	Yield function	
$\boldsymbol{f}, \boldsymbol{f}^{-1}$	Configuration Transformations	
$\boldsymbol{f}^{\boldsymbol{int}}$	Internal forces vector	
$\boldsymbol{f}^{\boldsymbol{ext}}$	External forces vector	
$\boldsymbol{F}^{\boldsymbol{e}}$	Elastic part of the deformation gradient tensor	
$\boldsymbol{F}^{\boldsymbol{p}}$	Plastic part of the deformation gradient tensor	
$\boldsymbol{F}_{\boldsymbol{z}}$	Z force applied in the microindentation test	
$\boldsymbol{g}$	Metric tensor related to the spatial configuration	
$\overline{\boldsymbol{G}}$	Metric tensor related to the intermediate configuration	
$\boldsymbol{G}$	Metric tensor related to the material configuration	
$\boldsymbol{H}$	Characteristic element size	[m]
$\boldsymbol{H}_{\boldsymbol{d}}$	Hardness	
$\boldsymbol{i}, \boldsymbol{j}, \boldsymbol{k}, \boldsymbol{l}\ \boldsymbol{and}\ \boldsymbol{m}$	Vector Coordinates (Dimension).	
$\boldsymbol{I}$	Identity Matrix	

J_2, J_3	Second and third deviatoric stresses invariant	
k	Hardening modulus	[MPa]
l_0	Initial specimen length	[m]
l_f	Final specimen length	[m]
M	Mass Matrix	
n	Hardening Exponent	
n_T	Total number of simulation steps	
P	Normal Force applied to the bodies in the Hertz contact	[N]
r	Contact radius	[m]
R_1	First Hertz Contact body radius	[m]
R_2	Second Hertz Contact body radius	[m]
R	Equivalent contact radii	[m]
S_{ij}	Deviatoric Stresses tensor	
T	Final time	[s]
t	Time	[s]
t_E	Simulation end time	[s]
U	Deformation gradient tensor	
w	Work of adhesion	

$\boldsymbol{x}$	Displacement field
$\boldsymbol{x_i}$, $\boldsymbol{x_j}$	Element position in the X axis
$\boldsymbol{x_{i-1}}$, $\boldsymbol{x_{j-1}}$	Previous position of an element in the X axis
$\boldsymbol{y_i}$, $\boldsymbol{y_j}$	Element position in the Y axis
$\boldsymbol{y_{i-1}}$, $\boldsymbol{y_{j-1}}$	Previous position of an element in the Y axis
$\boldsymbol{z}$	Distance between two atomic planes
$\boldsymbol{z_0}$	Equilibrium distance between two atomic planes
$\boldsymbol{\alpha}$	Critical time step factor
$\bar{\boldsymbol{\alpha}}$	Scalar hardening
$\boldsymbol{\delta_1}$	Interference given by the deformation undergone by the first body of the Hertz contact
$\boldsymbol{\delta_2}$	Interference given by the deformation undergone by the second body of the Hertz contact.
$\boldsymbol{\delta}$	Total interference by both bodies in Hertz contact
$\Delta\boldsymbol{\varepsilon_p}$	Incremental Plastic part of the total deformation
$\Delta\boldsymbol{x}$	Element increment position in the X axis
$\Delta\boldsymbol{y}$	Element increment position in the Y axis
$\Delta\boldsymbol{t}$	Simulation Time Step

Δt_{crit}	Critical time step	
ε_p	Plastic part of the total deformation	
φ	Deformed body configuration	
ϕ^*	Pullback operator	
ϕ_*	Push-forward operator	
Φ^{TR}	Limit surface of the Yield function	
ν	Poisson's ratio	
Ω_0	Set of points that defines a body	
Ω_t	Set of point that defines the deformed configuration	
ψ	Plasticity Index	
ρ	Material density	[kg/m³]
$\sigma(z)$	Adhesive stress	
σ^*	Aperities height distribution	
σ_n	Stress field in the initial configuration	
σ_y	Yielding Stress	[MPa]
$\sigma_1, \sigma_2, \sigma_3$	First, second and third principal stresses	[MPa]

LIST OF FIGURES

Fig. 2.1. Hertz Non-Conformable Contact between two elastic bodies. (ADAMS *et.al.* 2000)

Fig. 3.1.$f(x,y)$ function

Fig. 3.2. Mesh in Oxy

Fig. 3.3. Imposition of contact constraints in: (a) Classical Methods; (b) Contact Domain Method. (Adapted from Oliver *et al.*, 2009)

Fig. 3.4. Possible patch definitions for a 2D problem. (OLIVER *et al.*, 2009)

Fig 3.5. 3D Contact Domain approximated with Tetrahedral Elements. (Adapted from Hartmann *et al.*, 2010)

Fig. 3.6. Generating of the contact mesh: (a) Original Mesh; (b) Removal of internal nodes and shrinkage; (c) Creation of the contact mesh; (d) Original boundary and mesh retrieved.

Fig. 4.1. Representative design of the incremental formulation.

Fig. 5.1. Westergaard space (JORGE NATAL, 2005)

Fig. 5.2. Orthogonally Condition in $\sigma_1 - \sigma_2$ space (JORGE NATAL, 2005)

Fig. 5.3. Hardening Rules (GONZALES, 2009)

Fig.6.1. Schematic diagram of a Microindentation test. (Adapted from HOLMBERG, 2009)

Fig.6.2. 5N Brinell Microindentation Force vs. Depth curve (DA SILVA, 2009)

Fig. 6.3. 10N Brinell Microindentation Force vs. Depth curve (DA SILVA, 2009)

Fig. 6.4. Pile up and sink in phenomena. (Adapted from TALJAT & PHARR, 2004)

Fig. 6.5. Schematic Design of the Laser Interferometry operation mechanism

Fig. 6.6. Laser Interferometry of the 5N Brinell microindentation (DA SILVA, 2009)

Fig. 6.7. 5N Brinell microindentation roughness profile. (DA SILVA, 2009)

Fig. 6.8. Laser Interferometry of the 10N Brinell microindentation (DA SILVA, 2009)

Fig. 6.9. 10N Brinell microindentation roughness profile. (DA SILVA, 2009)

Fig. 7.1. Tensile Strength FEM models with Tetrahedral and Hexahedral Elements.

Fig. 7.2. Distribution of nodes in the top surface of the tensile strength experiment test model.

Fig. 7.3. Time vs. Force Graph applied to the tensile strength test top nodes.

Fig. 7.4. Representation of the microindentation test.

Fig. 7.5. Mesh of the Top and Bottom face of the indenter.

Fig.7.6. Mesh of the Top and Bottom face of the specimen.

Fig. 7.7. Mesh of the FEM Microindentation model.

Fig. 7.8. Restricted points in the model symmetry surfaces with and without the global mesh.

Fig.7.9. Time vs Displacement curve imposed on the top surface indenter nodes

Fig. 7.10. Second 'Time vs Displacement' curve imposed on the top surface indenter nodes

Fig. 8.1. Error minimization algorithm curve

Fig. 8.2. Validation Force vs. Displacement Curves

Fig. 8.3. Tensile strength stress FEM simulation

Fig. 8.4. Equivalent Von Mises Stresses for the tensile strength simulation.

Fig. 8.5. Centre Specimen node Z Displacement for 10-4 Scale

Fig. 8.6. Centre Specimen node Z Displacement for 10-3 and 10 -4 Scale

Fig. 8.7. Z Displacement of the Explicit Model

Fig.8.8. Top and Bottom surface of the Explicit Contact Mesh

Fig. 8.9. Z Displacement Explicit Results for the Copper Specimen

Fig.8.10. Z Displacement Explicit Results for the Indenter

Fig.8.11. Effective Plastic Deformation Explicit Results for the Indenter

Fig. 8.12. Z Displacement of the Implicit Model

Fig. 8.13. Top and Bottom surface of the Implicit Contact Mesh

Fig. 8.14. Z Displacement Implicit Results for the Copper Specimen

Fig. 8.15. Z Displacement Implicit Results for the Indenter

Fig. 8.16. Effective Plastic Deformation Implicit Results for the Indenter

Fig. 8.17. Nodes taken in the surface, X axis, to analyse the microindentation Z displacement profile.

Fig. 8.18. Implicit and Explicit Indentation depth half-area mark

Fig. 8.19. Implicit Indentation depth half-area mark for the first Time vs. Displacement curve

Fig. 8.20. Force vs. Depth Implicit curve for the second T x D curve.

Fig.8.21. Z Displacement in a node within the pile up area

LIST OF TABLES

Table 7.1. Copper specimen properties.

Table 7.2. Microindentation Simulation Indenter Properties.

Table 8.1. Simulation time for different number of CPUs

Table 8.2. Material Properties approximation Algorithm Results

Table 8.3. Minimization Algorithm Seeds Test

Table 8.4. Total Execution Time for different Time vs. Displacement curve scales

SUMMARY

CHAPTER I 1

INTRODUCTION 1

CHAPTER II 6

CONTACT MECHANICS 6

2.1. Hertz Contact Theory 7

2.2. Inelastic Bodies Contact 9

2.3. Friction and Tangential Loading 10

2.4. Nanometric Scale Contact 11

2.5. Multi-asperity Contact 12

CHAPTER III 14

THE FINITE ELEMENT METHOD (FEM) 14

3.1.Time Integration 15

3.1.1. Finite difference method 16

3.1.2. Central difference method 18

3.2. Contact in FEM 21

3.2.1 Contact Mesh 22

CHAPTER IV 26

CONSTITUTIVE MODEL FORMULATION 26

4.1. Kinematic analysis 26

4.2. Incremental Formulation 29

4.2.1 Predictor-corrector algorithm 31

CHAPTER V 33

YIELD SURFACE AND HARDENING LAW 33

5.1. Von Mises Yield Surface 37

5.2. Ludwik Nadai hardening law 38

CHAPTER VI 39
INSTRUMENTED MICROINDENTATION 39
6.1. Microindentation Test 40
6.2. Pile up and Sink in 42
6.3. Laser Interferometry 43
CHAPTER VII 47
METHODOLOGY 47
7.1. Implementing the Constitutive Model in COMFORM 47
7.2. Validation of the Implemented Model 48
7.3. Material properties from tensile strength test curve 52
7.4. Simulation of a Micro-indentation test 53
7.4.1. Explicit FEM 60
7.4.2. Scale Problem 61
7.4.3. Implicit FEM 61
7.4.4. SecondT x D (Time vs. Displacement) Simulation 62
CHAPTER VIII 63
RESULTS AND DISCUSSION 63
8.1. Number of Cores convergence 63
8.2. Convergence and Interaction of the implemented modulus inside COMFORM 64
8.3. Hardening properties for the Copper Specimen 65
8.4. Validation of the model with tensile strength test 67
8.5. Microindentation FEM Simulation 70
8.5.1. Explicit Time Integration Microindentation FEM Model 72
8.5.2. Implicit Time Integration FEM Model 75
8.5.3. Pile up 81
CHAPTER IX 83

CONCLUSION 83
CHAPTER X 86
FUTURE WORK 86
CHAPTER XI 87
REFERENCES 87
APPENDIX A 95
ANNEX A 98

CHAPTER I

INTRODUCTION

Numerical Methods are often used to solve mathematical problems which describe physical phenomena, when they have several variables or even does not have analytical solution. A heavily widespread numerical method is the Finite Element Method (FEM), which provides an approximate solution to differential equations that usually represent physical phenomena, such as continuum mechanics and fluid mechanics.(FELICE-NETO, 2012,BARKANOV, 2001, DESAI,1972, ZIENKIEWICZ, 1991)

When the described phenomenon needs to perform contact between different bodies or even self-contact, it is usually performed an optimization problem, with the objective function being the minimization of the penetration gap formed by the boundary condition which imposed one surface against the other. This problem is normally solved by searching the surrounding of the possible contact surfaces and considering contact from a distance (cut-off). The main problem of this approach is that the penetration can be already happening when the algorithm detects the contact, leading to a non-realistic compensation force that could give wrong results for micro sized analysis.(OYSU, 2006,SILVA, 2016,BANDEIRA, 2015)

A relatively new approach on the contact problem is the contact domain approach, or contact mesh, which creates a mesh linking the nodes that will possibly begin contact from one surface to another, with a single layer of elements. This mesh is responsible for predicting the contact and reduce the error, by virtually shrinking the elements and transmitting the conditions from one surface to another. The contact domain is currently implemented with an Implicit FEM time integration inside the COMFORM software, which is a project developed by the Polytechnic University of Catalonia (UPC) in collaboration with other institutes. Even considering the Implicit FEM as a powerful simulation method, its resolution is based on a single step matrix inversion and that could lead to simplified results when analysing deformation development.(OLIVER *et al.*, 2009, HARTMANN *et al.*,2009, HARTMANN *et al.*, 2010, WEYLER *et al.*, 2012).

Thus, the general objective of this work is to implement inside the COMFORM software the contact mesh with Explicit Time Integration Method that should work with all the modules already existent in the software. As specific objectives, is important to validate the postulated methodology and for that it must be used a problem in which the contact is severe and the gap error of the usual methods could lead to a divergence between experimental and simulated results.

The problem chosen to validate the explicit contact methodology was the microindentation test problem, where a known shaped indenter is pressed against a specimen surface, with controlled force and displacement. In this test the maximum value of depth is in micrometre scale (~2µm) and the indentation marks are evaluated by a Laser Interferometry process (GU *et al.*, 2003, FELICE NETO, 2012, RUTHERFORD, 1997, CHEN, 2007, HOLMBERG, 2009).The Explicit Method results were compared with experimental data and the previous validated Implicit Method for the same model (HARTMANN *at.al.,*2009, HARTMANN *at.al.,* 2010).

The microindentation experimental tests data were taken from experiments carried by Da Silva (2008), using a Copper Specimen and a Tool Steel Indenter. Considering the Copper behaviour and the micrometric scale of the problem, it was necessary to implement inside COMFORM a Small Elastic

and Large Plastic Deformations Material Formulation, which configures another specific objective of this work. This formulation allows the stress and strain field analysis and the indentation mark final shape. To validate the material formulation were created a FEM simulation based on an experimental tensile strength data.

An error minimization approach were used in order to obtain the Copper hardening properties, in which the experimental stress vs. strain curve from the tensile strength experiment were used as base. A Ludwik-Nadai hardening law curve were calculated, by the iteration of the hardening exponent and modulus, until they converge to the minimum error configuration when compared to the experimental data.

The results show that, the Explicit Time Integration Method and the Small Elastic and Large Plastic Deformations COMFORM modules implemented converged with the whole algorithm. The tensile test simulation was used to validate the material formulation and the methodology used to obtain the Ludwik-Nadai hardening properties. The Explicit model, with contact mesh, was validated with the comparison between the experimental and FEM simulation data from the microindentation test. The implicit and the explicit time integration methods, both using contact mesh, gave similar results for the microindentation simulation, which were different from the experimental data. Using different boundary conditions were possible to infer that the machine which performed the microindentation tests had a stiffness/assembly gap problem that mask the real displacement underwent by the Copper Specimen. Finally, it was observed that the Copper, like other metallic materials, shows a pile up in the indentation mark surroundings, mainly influenced by the hardening properties (hardening exponent) and friction. The pile up were analysed, and it was more evident during the elastic recuperation, probably because of a difference in the deformation direction, when performing an indentation mark.

In order to study the contact related phenomena in the microindentation test and the referred simulations, this work were organized as it follows:

- The second chapter studies the Contact Mechanics Theory, starting in the Hertz contact theory, after that the contact between inelastic

bodies, friction phenomenon and finishing with nanometric scale contact, considering different approaches to comprehend the asperity contact.

- The third chapter explains the Finite Element Theory, including the time integration Methods (Explicit/Implicit) and the contact approach, especially the Contact Mesh.
- The fourth chapter is about the Constitutive Model Formulation, in which is postulated the kinematic analysis used, also the predictor-corrector algorithm that leads the incremental formulation development.
- The fifth chapter studies the Yield Surface Theory, in this work the Von Mises Yield Surface Theory. The yield surface describes the plastic behaviour of materials. This chapter also presents the material constitutive law, Ludwik-Nadai.
- The sixth chapter were dedicated to explain the phenomena related to the abrasive wear simulation, i.e., the microindentation test and the Scanning Electron Microscopy. In this chapter were also presented the experimental data from Da Silva (2008).
- The seventh chapter explains the Methodology used, with the implementation, validation, material properties obtainment methodology, simulation models construction and conditions used for all simulations.
- The results are shown in the chapter eight, where all the result comparisons, validations and analysis were made.
- The ninth chapter presents the conclusions obtained from the results analysis and also the whole work conclusions, considering the objectives proposed.
- The tenth chapter proposes some Future Work ideas, i.e., the next possible work that could start from the conclusions and results achieved in this work.
- The References used in the whole work are organized in the eleventh chapter.

- APPENDIX A contains the algorithm implemented to calculate the material hardening properties, following the methodology proposed.
- Finally the Annex A presents the structural organization of the Contact parameters input in the COMFORM software, such as the explanation of each variable.

CHAPTER II

CONTACT MECHANICS

Contact Mechanics is the science field which studies strain and stresses that occurs in a two body contact. The contact can be subdivided in non-conformable and conformable contact. The first one occurs when the contact area is too small when compared to the geometry and bodies radii. On the other hand, the second occurs with bigger contact areas, compared to the bodies' radii, usually already presenting plastic deformation in the contact region.

The contact starts in one point or line, depending on the geometry of the contacting bodies. In a non-conformable contact, when the deformation of the contact region starts, this point or line becomes a contact area, with characteristics such as: i. Usually the contact area is very small, compared to the size of the contacting bodies; ii. The stresses are concentrated near the contact region and are not really affected by the bodies shape, far from the contact region. (BRAGA, 2008)

The main model which describes the elastic contact is the one developed by Hertz, in 1882, who published an article about the increase on the area size related to the normal force applied in contact, based in a linear elastic model. (JOHNSON, 1985)

2.1. Hertz Contact Theory

The Hertz contact theory starts from the proposition that, to calculate local deformations, each body must be considered as an elastic half-space loaded on a small elliptic area. For this to be true, the contact area must be small when compared to the contacting bodies dimension and the surfaces relative radii. (PENNEC *et.al.*, 2007)

Herewith those considerations, Hertz also postulated the following assumptions. (FRANCO, 2002)

- The surfaces are non-conformable and continuous;
- Small deformations;
- Each body can be considered as an elastic half space;
- There is no friction.

These assumptions ensure that the stress field, calculated on a solid body, is not affected by boundaries of high stressed regions and also that the deformations in contact area are small enough in order to the linear elastic theory be valid. Fig. 2.1 shows the Hertz contact between two non-conformable bodies, where **P** is the normal force applied, **a**is the characteristic length of the contact area(half-space contact area), $\boldsymbol{\delta_1}$e $\boldsymbol{\delta_2}$ represents the interference given by the elastic deformation undergone by the first and the second body, respectively. The dimension$\boldsymbol{\delta}$ is the total interference undergone by both bodies in contact.

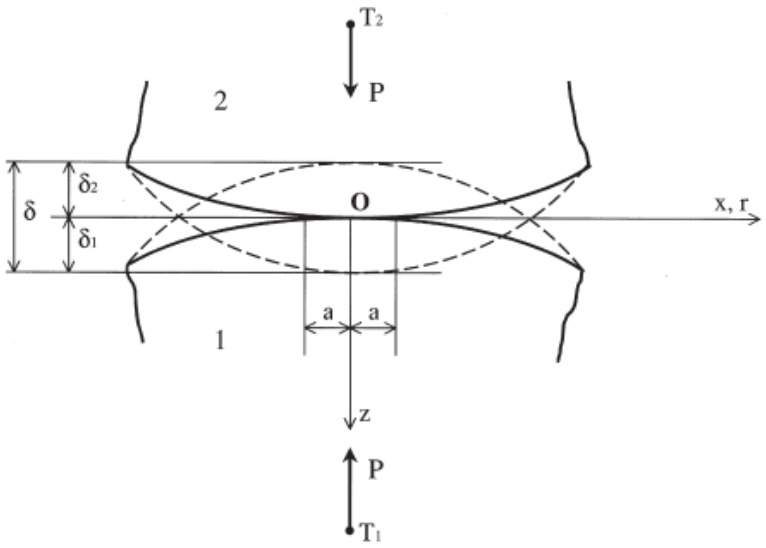

Figure 2.1. Hertz Non-Conformable Contact between two elastic bodies. (ADAMS *et.al.*, 2000)

For solids of revolution, the interference, contact area and maximum contact pressure (in $R = 0$) shown in Fig.2.1, can be calculated using the equations 2.1 to 2.3.

$$\delta = \left(\frac{9P^2}{16RE^{*2}}\right)^{\frac{1}{3}} \tag{2.1}$$

$$a = \left(\frac{3PR}{4E^*}\right)^{\frac{1}{3}} \tag{2.2}$$

$$p_0 = \left(\frac{6PE^{*2}}{\pi^3 R^2}\right)^{\frac{1}{3}} \tag{2.3}$$

Where E^* is the equivalent Young Modulus, which depends on Poisson and Young Modulus for both materials and is given by the equation (2.4). This assumption is possible because the pressure acting on the first body is equal to the pressure on the second one (JOHNSON, 1985).

$$\frac{1}{E^*} = \frac{1-\upsilon_1^2}{E_1} + \frac{1-\upsilon_2^2}{E_2} \quad (2.4)$$

The equivalent radius, represented by R, depends on both bodies radii (R_1 e R_2) and is given by the equation 2.5.

$$\frac{1}{R} = \frac{1}{R_1} + \frac{1}{R_2} \quad (2.5)$$

2.2. Inelastic Bodies Contact

The necessary load to start a plastic contact is usually related to the contact stress field in the most ductile material, governed by a yield criterion, for example, Von Mises or Tresca. (JOHNSON, 1985)

Even considering the plastic effect on the contact region, which means that there is material flux in this area, the plastic zone is fully contained by the surrounded material and this material is still showing elastic deformation behaviour. For smooth geometry body shapes, such as spheres and cylinders, the plastic region is underneath the surface. For pointed shape bodies, such as cones, the plastic zone is adjacent to the tip, always surrounded by the rest of the body, with elastic behaviour. This implies in a decrease on the plastic zone size, when the tip angle increases or when the penetration depth decreases. The plastic zone can decrease until there is just elastic zone, so the Hertz contact can be considered as an initial contact condition or a mildest contact. (ADAMS, 2000; JOHNSON, 1985)

In an extreme scenario, where the plastic deformation is too big when compared to the elastic one, the body should be considered as a purely plastic

material. In this case, the elastic deformation is not considered, so there will be just a region with plastic deformation, proportional to the material properties and the stress field. The rest of the material, out of the plastic deformation zone, will be considered as a non-deformable or rigid region. The rigid region can undergo stress fields big enough to start elastic deformation, but these will not be considered until they start plastic behaviour.

2.3. Friction and Tangential Loading

A tangential loading in a Hertz Contact must be analysed with one of three cases: (ADAMS, 2000)

- A pair of identical materials;
- One rigid material and the other one considered incompressible, which means $\nu = \frac{1}{2}$.
- Both materials considered incompressible.

In any of those cases, normal stresses do not cause tangential displacements and also, no tangential stresses cause normal displacements. This is important to simplify the first analysis and it is considered as an uncoupling.

For a plane strain contact, there will be an adhesion zone (stick zone) surrounded by two slip zones. When the tangential stress increases, the stick zone decreases until there is just the slip zone, which is governed by the Coulomb friction law, with no distinction between static and kinematic friction coefficient. (JOHNSON, 1985)

After that, a sliding between asperities starts, and the friction works on superimpose the tangential contact stress. These stresses change the stress field inside the half-space and also change the necessary stress to start plastic

deformation. For elevated friction coefficients, the maximum shear stress happens in the surface and not underneath it, making a faster transition to the plastic deformation behaviour, when compared to a frictionless situation. (JOHNSON, 1963)

2.4. Nanometric Scale Contact

In a nanometric scale, solid bodies are still considered as continuum, but the adhesion effect on the surroundings is more evident, creating an adhesive stress ($\sigma(z)$), governed by the Lennard-Jones potential relation, given by the equation 2.6. (ADAMS, 2000; JOHNSON, 1998)

$$\sigma(z) = -\frac{8w}{3z_0}\left[\left(\frac{z}{z_0}\right)^{-3} - \left(\frac{z}{z_0}\right)^{-9}\right] \tag{2.6}$$

Where z is the distance between two atomic planes, z_0 is the equilibrium distance between atomic planes and w is the work of adhesion, that can be calculated by the sum of the surface energies in the system. The equation 2.7 is an adhesion model to rigid spheres, where R is the sphere radius.

$$p = -\frac{8\pi wR}{3}\left[\frac{1}{4}\left(\frac{z}{z_0}\right)^{-8} - \left(\frac{z}{z_0}\right)^{-2}\right] \tag{2.7}$$

In an inelastic contact, it is necessary to consider the effect of the adhesion hysteresis, i.e., an additional work to separate the deformed surfaces, because of the dissipated energy.

2.5. Multi-asperity Contact

The formulation proposed so far, works for single contacts, even in the nanometric scale, so it becomes necessary to come up with a methodology to study a group of asperities together. This is very important to correctly study the surface roughness in a contact pair.

The first possible approach is to uncouple the problem, working with each asperity properties (height, radius of curvature etc.) and the asperities are statistically distributed. The effect of a single asperity is considered local, independent of the other asperities. The Global effect will be a sum of each asperity effect. (ADAMS, 2000)

Another approach is the coupled one, on which a mathematical model considers all the system as one and calculate the global effects at once, including the cross effect between asperities.

The multi-asperity contact approach is very important when studying contact, because there is a great difference between the apparent contact and the actual contact area. This causes variations on the tribological contact and, by consequence, variation on the global friction.

Greenwood & Williamson (1966) proposed a model to describe the elastic contact between two nominally flat surfaces, with a great number of spheric asperities, different heights and randomly distributed in the area (Gaussian or exponential distribution). According to them, the contact area increases proportionally to the load applied (increase on the asperity area and contact of

new asperities). To predict if the contact is elastic or plastic was also proposed a plasticity index, which combines the material and topographical properties of the solids in contact (“elastic hardness” and actual hardness), given by the equation 2.8.

$$\psi = \frac{E'}{H_d}\left(\frac{\sigma^*}{R}\right)^{\frac{1}{2}} \tag{2.8}$$

Where ψ is the plascicity index, H_d is the material hardness and σ^* is the aperities height distribution.

Considering that this work aims to simulate a microindentation experiment, in which a spherical indenter presses a plane surface (infinite radius) and also both bodies are deformable, the most suitable approach is the uncoupled asperity problem.

CHAPTER III

THE FINITE ELEMENT METHOD (FEM)

In order to understand, describe and predict physical phenomena, mathematical formulations, in the form of differential equations, can be a powerful method. These problems exact solution (analytic solution) could be too difficult or even impossible to achieve. In order to try to solve this problem, are often used approximate solutions by numerical methods, such as the FEM, which configures a powerful and versatile method. (FELICE-NETO, 2012)

According to Barkanov (2001), the FEM can be considered as a numerical analysis method that aims to achieve approximate solutions to problems governed by differential equations. The FEM consists in discretize the continuum in an arbitrary number of nodes, which are interconnected becoming elements. The group of elements which compose the discretization is called mesh. (DESAI, 1972)

The main idea is that the model is obtained by the reverse process, from the component equation to substructure equations, all governed by the classical principals of mechanics (FELLIPA, 2015). This means that the equations which govern the phenomena and the interpolation functions are inserted in those elements, together with the conditions that ensure the node continuity, when this node is shared by more than one element. The unknown variables are the

problem degrees of freedom, and become the field variable values for the nodes. The solution can be analysed in the nodes or through the hole problem (global), when the nodal solutions are interpolated, ensuring the problem continuity. The solution quality will be linked to the number of elements in the mesh, the equations inserted and also the boundary conditions imposed to the problem. (ZIENKIEWICZ, 1991).

One of the greatest advantages in using FEM consists in the possibility of fixing as many parameters as the user wants to, and change just one or a few of those parameters, making more evident the effect of one parameter or the cross effect of some. As a disadvantage, can be pointed out the difficulty of creating non homogenous materials (with gradual material properties or even imperfections such as vacancies or impurities), especially when working with nanometric scale and contact. In those cases, the micro deformations, pointed high temperatures, adsorption etc. can transform the material in a way which will be hard to predict by numerical methods.

3.1.Time Integration

To solve Finite Element Method (FEM) problems, such as structural dynamic and transient problems, is used direct time integration schemes. These schemes are divided in two main groups; i) Implicit methods, in which the solution requires the factorization of a matrix that considers the stiffness of the materials and nonlinear symmetrical formulation. Thisimplies that the simulation occurs as if the bodies move slowly enough to make a quasistatic process.Therefore,the phenomenon analysed becomes a two stages problem (before and after solution), ignoring what happens during the process andmaking the division in a number of steps a user decision. One way to study dynamic problems with implicit methods is to add inertial components and to analyse the problem development it is possible to divide the simulation in several stages, increasing the

computational cost.Also the implicit method have unconditional stability, so the time step size can be chosen by problem characteristics and it requires a larger computational effort to each step, compared to explicit methods. ii) Explicit methods normally use a lower computational cost by each step, because it may use only vector calculations, but it is conditionally stable. So the time step size must be calculated in order to maintain the problem stability. This calculus normally use the material properties, such as density and elastic modulus, and the minimum element size in the mesh.(ZIENKIEWICZ, 1991; NOH, 2013)

3.1.1. Finite difference method

Considering that the continuous function $f(x_1, y_2) = f(x, y)$ has known values at discrete points (i, j etc.), the derivative of f at i, j can be determined using finite difference methods. Fig.3.1 represents the continuous function $f(x, y)$.

point	coord.x	coord.y	f(x,y)
...	...	...	...
i-1	x_{i-1}	y_{i-1}	f_{i-1}
j-1	x_{j-1}	y_{j-1}	f_{j-1}
...	...	...	...
i	x_i	y_i	f_i
j	x_j	y_j	f_j
...	...	...	...

Figure 3.1. $f(x, y)$Function

Considering Fig. 3.1, the coordinates were used in the form of the Equation (3.1).

$$x_i - x_{i-1} = x_j - x_{j-1} = \cdots = \Delta x \; ; y_i - y_{i-1} = y_j - y_{j-1} = \cdots = \Delta y \tag{3.1}$$

In this first case the increments (Δx and Δy) are constants according to x and y axes just to simplify the explanation, but it is not a rule or necessary condition to the finite difference method. The mesh assumes the form shown by the Fig.3.2.

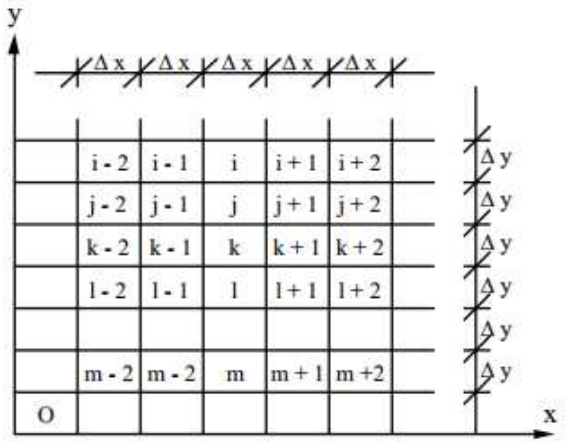

Figure 3.2. Mesh in Oxy.

The derivative form of the function $f(x, y)$ with respect to x is given by the equation (3.2).

$$\frac{\delta f}{\delta x} = \lim_{\Delta x \to 0} \frac{\Delta f}{\Delta x} \tag{3.2}$$

If Δx is sufficiently small, the equation (3.2) becomes the equation (3.3)

$$\frac{\delta f}{\delta x} \cong \frac{\Delta f}{\Delta x} \tag{3.3}$$

Thus, the derivative form of $f(x, y)$ can be obtained by forward, equation (3.4), backward, equation (3.5), or central difference method. The Central Difference Method calculates the velocity in the $t + \frac{1}{2}\Delta t$ time and the position and

acceleration in $t + \Delta t$, using the equation (3.6) for velocity and position and the acceleration can be obtained from the conservation of momentum.

$$\left(\frac{\delta f}{\delta x}\right)_k \cong \frac{f_{k+1} - f_k}{\Delta x} \quad (3.4)$$

$$\left(\frac{\delta f}{\delta x}\right)_k \cong \frac{f_k - f_{k-1}}{\Delta x} \quad (3.5)$$

$$\left(\frac{\delta f}{\delta x}\right)_k \cong \frac{f_{k+1} - f_{k-1}}{2\Delta x} \quad (3.6)$$

For this work, were used the central difference method, considered a better approximation than the other two difference methods. (DINIS, 2004)

3.1.2. Central difference method

To apply the central difference method to this study, first is assumed that the simulation time is $0 \leq t \leq t_E$, where t_E is the end of the simulation, subdivided in time steps Δt^n, with $n = 1, \dots, n_T$, where n_T is the total number of steps. The time step will be considered variable due to mesh deformations that occur during the simulation process and change on the wave speed caused by the stress. This variation occurs to maintain the problem stability, considering the conditional stability. The time increment is in the form presented in equation (3.7). (BELYTSCHKO, 2001)

$$\Delta t^{n+\frac{1}{2}} = t^{n+1} - t^n, \; t^{n+\frac{1}{2}} = \frac{1}{2}(t^{n+1} + t^n), \; \Delta t^n = t^{n+\frac{1}{2}} - t^{n-\frac{1}{2}} \quad (3.7)$$

The central difference method applied to the velocity(v) is given by the equation (3.8), where d represents the displacement.

$$\dot{d}^{n+\frac{1}{2}} = v^{n+\frac{1}{2}} = \frac{d^{n+1}-d^{n}}{t^{n+1}-t^{n}} = \frac{1}{\Delta t^{n+\frac{1}{2}}}(d^{n+1} - d^{n}) \tag{3.8}$$

To transform the equation (3.8) into an integration formula, it can be rearranged, becoming the equation (3.9).

$$d^{n+1} = d^{n} + \Delta t^{n+\frac{1}{2}} v^{n+\frac{1}{2}} \tag{3.9}$$

The acceleration $(a)$is given by the equation (3.10)

$$\ddot{d}^{n} = a^{n} = \frac{v^{n+\frac{1}{2}}-v^{n-\frac{1}{2}}}{t^{n+\frac{1}{2}}-t^{n-\frac{1}{2}}} \quad , \quad v^{n+\frac{1}{2}} = v^{n-\frac{1}{2}} + \Delta t^{n} a^{n} \tag{3.10}$$

The equation (3.10) shows that the velocities are defined at time half-steps $\left(n+\frac{1}{2}\right)$. The equation (3.11) shows the acceleration in terms of displacement, by substitute the equation (3.8) into the equation (3.10).

$$\ddot{d}^{n} = a^{n} = \frac{\Delta t^{n-\frac{1}{2}}(d^{n+1}-d^{n})-\Delta t^{n+\frac{1}{2}}(d^{n}-d^{n-1})}{\Delta t^{n+\frac{1}{2}}\Delta t^{n}\Delta t^{n-\frac{1}{2}}} \tag{3.11}$$

For an equal time step, the equation (3.11) reduces to the equation (3.12), which is the second derivative of a function, same equation as the derivative form of the equation (3.6).

$$\ddot{d}^n = a^n = \frac{d^{n+1} - 2d^n + d^{n-1}}{(\Delta t^n)^2} \tag{3.12}$$

The equation of motion in a time step n is given by the equation (3.13), where M is the mass matrix, f^{int} the internal forces vector and f^{ext} is the external forces vector. Substituting the equation (3.13) into the equation (3.10), the equation to update the nodal velocities and displacements is obtained from equation (3.14).

$$Ma^n = f^n = f^{ext}(d^n, t^n) - f^{int}(d^n, t^n) \tag{3.13}$$

$$v^{n+\frac{1}{2}} = v^{n-\frac{1}{2}} + \Delta t^n M^{-1} f^n \tag{3.14}$$

It is possible to update the nodal velocities and/or displacements without solving any equations provided, by the diagonalization of the mass matrix. This approximation allows the explicit method to develop. This is the main characteristic of the explicit methods. (BELYTSCHKO, 2001)

The explicit methods are conditionally stable, which means that the stability occurs only if the time step does not exceed a critical time step, also called stable time step. This critical time step can be calculated by the equation (3.15), where Δt_{crit} is the critical time step, H is the characteristic element size, ρ is the material density, E is the material Young modulus and α is a critical time step factor, to ensure that the time step will be smaller than the critical time step, which means that the α values must be smaller than 1. (SVENSSON, 2008)

$$\Delta t = \alpha \Delta t_{crit} \ , \ \Delta t_{crit} = H\sqrt{\frac{\rho}{E}} \tag{3.15}$$

3.2. Contact in FEM

FEM simulations are often used to study problems which consider more than one body, with interaction between them. This could be done adding a prediction of the forces and restrictions directly to the body that will be analysed, as boundary conditions. Sometimes these conditions are hard or even impossible to find analytically, becoming the contact a necessary feature. Another point to consider is that the contact problems became a major concern in several engineering applications, such as gears, rollers and abrasive wear. (OYSU, 2006)

The contact method most used in FEM commercial programs is the Penalty Method, in which is used a force to avoid the penetration of volumes. Itscalculationconsiders geometrical and space conditions (such as body shape and penetration gap), other variables (material properties and process parameters) and a penalty constant to multiply the penetration, which is chosen by the user. A small value for the penalty could violate the contact condition (allow penetration) and a big value could destabilize the simulation. This method achieves good results for macro sized problems, like stamping process, but for micro and nano sized process, like microindentation tests, the error can be greater than the tolerances for a correct analysis. Another problem is the penalty constant given by the user, which is highly non-linear and dependent on the user experience. (SILVA, 2016)

Another method to understand the contact is the Lagrange Method, which establishes a minimization with boundary conditions, creating a Lagrangian function. This function relates the objective function to the problem restrictions and is ensured by the Kuhn-Tucker conditions (BANDEIRA, 2015). Based on the

Lagrange and Penalty Method the Augmented Lagrange Method can be also postulated, using both the penalty factor and the Lagrange multipliers, but in this case the Lagrange multipliers are updated each step and a finite penalty factor guarantee the convergence. This method is stable but it must iterate each step, which is a problem for explicit methods (BERTSEKAS, 1995)

3.2.1 Contact Mesh

According to Oliver *et al.* (2009), the contact domain is a fictive intermediate region, with the same dimension as the contacting bodies, connecting the potential contact surfaces of those bodies. This leads to a purely displacement problem, because the contact function is now based on the dimensionless measure of the normal and tangential gaps.

So, the difference between this method and the node-to-node or segment-to-segment strategy lays on the interpretation of the contact domain. In the classical methods, the contact conditions are formulated due to a projection of the contact surface or point (slave contact surface) onto the other contact surface (master contact surface), as shown in Fig. 3.3 (a). Considering that, the contact problem is a subdomain, with lower dimension. On the other hand, the contact mesh establishespatches, connecting the potential contact surfaces, in other words, an intermediate domain with the same dimension as the bodies in contact, Fig. 3.3 (b). (OLIVER *et al.*, 2009, HARTMANN *et al.*,2009, HARTMANN *et al.*, 2010, WEYLER *et al.*, 2012)

In order to connect the potential contact surfaces, the patches created must not overlap, it must be a unique layer and it converge to the contact domain as the number of vertices increases. As shown on Fig. 3.4, the contact patches can be designed in multiples ways. In our study, we will use only tetrahedrical linear-linear shaped patches due to the best results in the contact formulation, according to Oliver *et al.* (2009).

For the 3D problem the same assumption is considered, using linear Tetrahedral patches to approximate the contact domain. For this case, two

element types are considered: Type A patches, with 3 vertex nodes placed on one contact boundary and one on the other and Type B, with 2 vertex nodes placed on each contact body. Type B elements are used to ensure that in 3D models all the contact domain is meshed. The 3D contact mesh, with both types of elements is shown in Fig. 3.5.

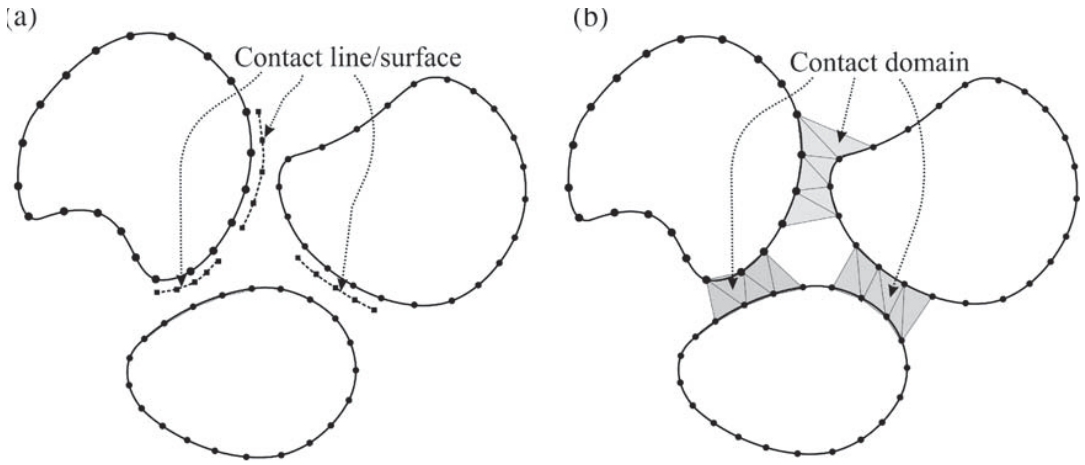

Figure 3.3. Imposition of contact constraints in: (a) Classical Methods; (b) Contact Domain Method. (Adapted from Oliver *et al.*, 2009)

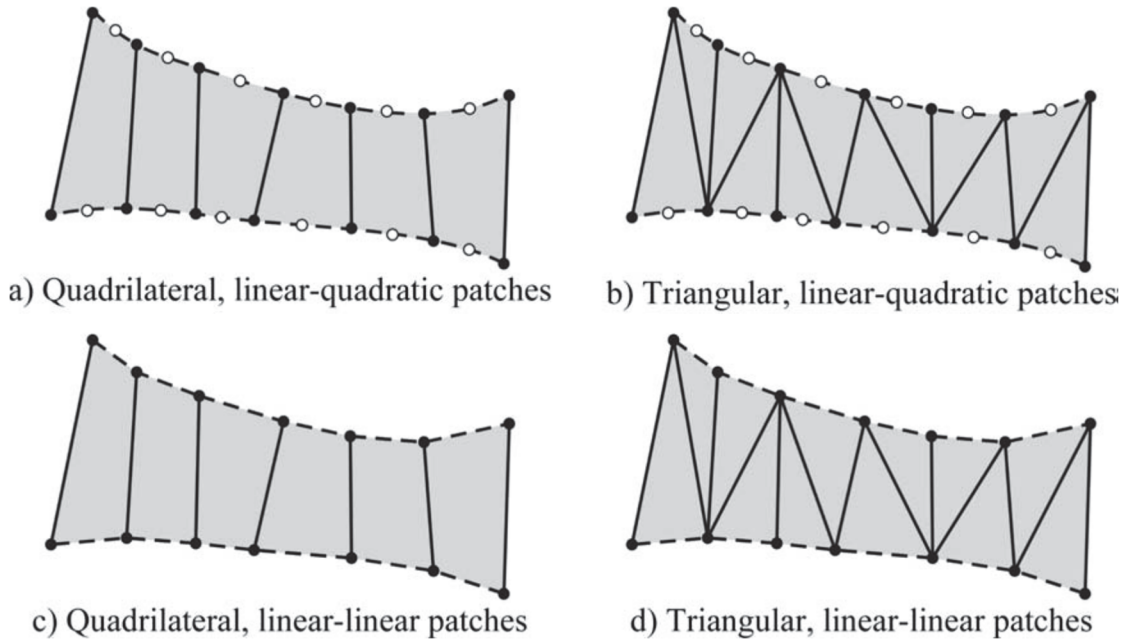

Fig 3.4. Possible patch definitions for a 2D problem. (OLIVER *et al.*, 2009)

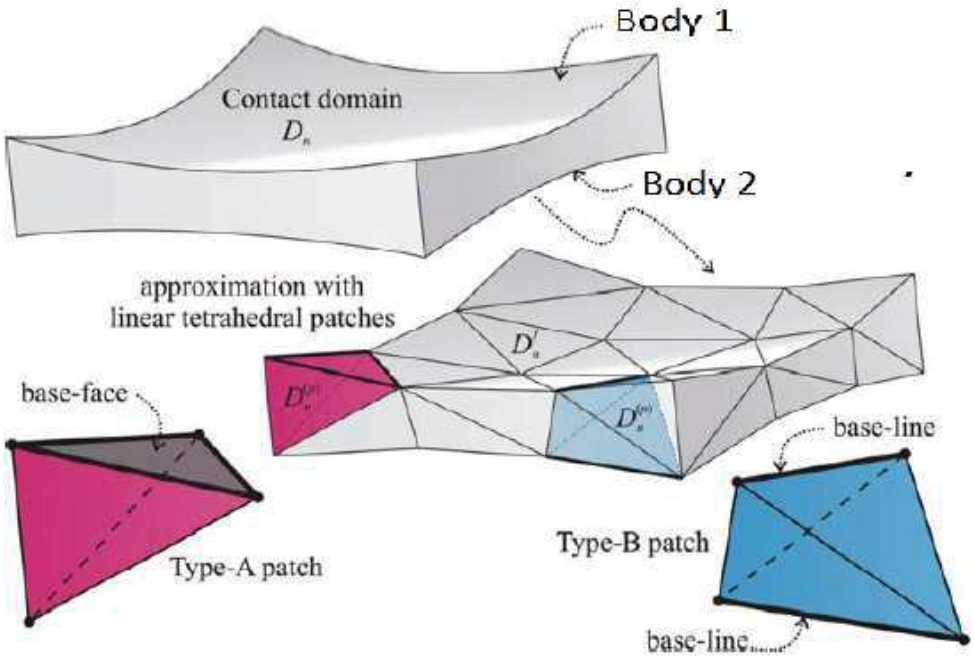

Fig 3.5. 3D Contact Domain approximated with Tetrahedral Elements. (Adapted from Hartmann *et al.*, 2010)

It is important to note that the creation of a contact mesh is independent of the master/slave relation, it means that it doesn't matter which body will be considered as master or slave in the contact pair. The determination of the contact mesh, i.e., which points of each contact pair will be connected and when the mesh will be created is defined by an active strategy. So the creation process of the contact mesh follows 4 steps: i. the process starts with a FEM meshed pair of bodies, where the element chosen doesn't affect the contact approach (Fig. 3.6 (a)); ii. the interior nodes are removed and the boundaries are shrunk (Fig. 3.6 (b)); iii. the contact mesh is created, linking both bodies in the probable contact areas (Fig. 3.6 (c)); iv. The original boundary and mesh are retrieved (Fig. 3.6 (d)). (HARTMANN *et.al.,*2010)

The definition of variables and program structure of the contact domain in the form of the COMFORM software are presented in ANNEX A, which describes each variable and exemplify the contact part of the COMFORM data input.

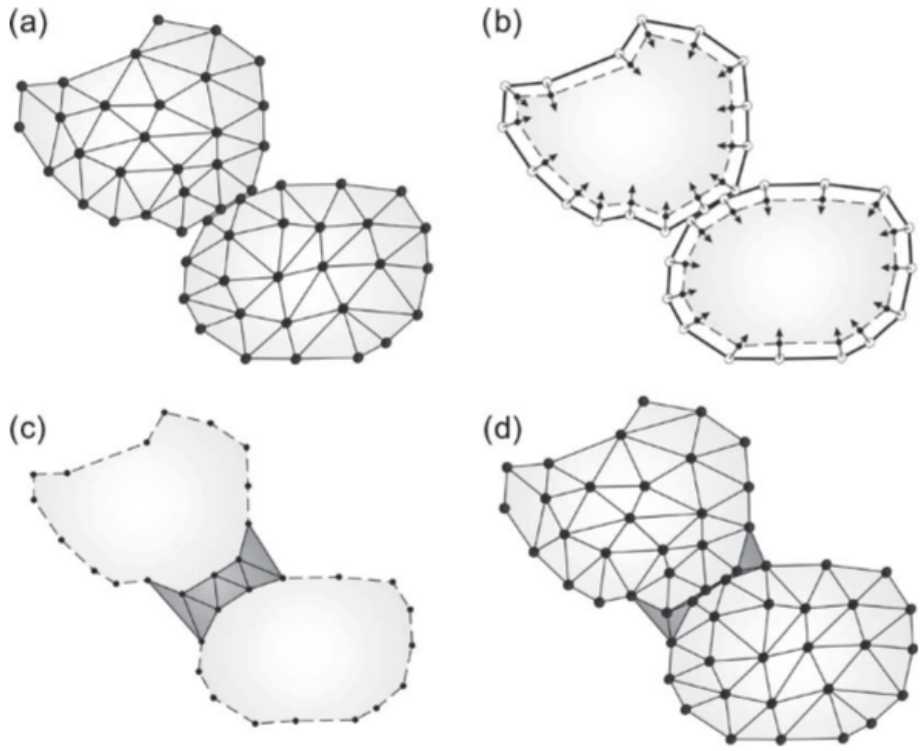

Fig. 3.6. Generating of the contact mesh: (a) Original Mesh; (b) Removal of internal nodes and shrinkage; (c) Creation of the contact mesh; (d) Original boundary and mesh retrieved.

CHAPTER IV

CONSTITUTIVE MODEL FORMULATION

A microindentation experiment can be simulated as if the plastic deformations are greater when compared to elastic ones, enough to neglect the elastic part of the total deformations in the material formulation. Considering that, the formulation respected the big plastic deformation continuum mechanics theory, in whichthe process were considered purely mechanic, because in a quasistatic process, velocities are sufficiently low to neglect any heat or heat transfer.

4.1. Kinematic analysis

In order todefine the formulation, it is necessary first to describe the kinematics of the problem, i.e.the large strain theory. In this case, the body is defined as a set of points(Ω_0), with defined boundaries and belonging to a reference configuration ($\Omega_0 \subset R^{n_{\dim}}$). This body can be in two or three dimensions

$(n_{dim} = 2{,}3)$. The process, microindentation or micro-scratch test, occurs in a time interval$[0, T]$ C R_+, where T is the final time of the process. (WEYLER, 2000)

The deformation can be defined as $\varphi : \Omega_0 \, x \, [0, T] \rightarrow R^{n_{\dim}}$, so any particle of the body $(X \in \Omega_0)$ in a given time $(t \in [0, T])$ is ruled by the equation of motion (4.1), leading to a deformed body configuration given by the set of points $\Omega_t = \varphi(\Omega_0, t)$, in time t. The equation (4.2) defines the displacement field $(\boldsymbol{U})$ from the equation of motion and equation (4.3) the deformation gradient tensor $(\boldsymbol{F})$ (WEYLER, 2000).

$$x = \boldsymbol{\varphi}(X, t) \tag{4.1}$$

$$\boldsymbol{U}(X, t) = \boldsymbol{\varphi}(X, t) - X \tag{4.2}$$

$$\boldsymbol{F}(X, t) = \frac{\partial \boldsymbol{\varphi}(X,t)}{\partial X} = \boldsymbol{I} + \frac{\partial \boldsymbol{U}(X,t)}{\partial X} \tag{4.3}$$

Where $\frac{\partial \boldsymbol{U}(X,t)}{\partial X} = GRAD \, \boldsymbol{U}(X, t)$, given by the equation (4.3), represents the material displacement gradient tensor.

To work with plastic deformation in elastoplastic materials, it must be considered that it goes through an elastic deformation stage before the permanent deformationstarts. This leads to the problem of coupling those two different deformation mechanisms of the material.

For moderate plastic behaviours, which means up to 30%, the structural phenomena caused by the plastic flow are small enough to be neglected concerning to the structural crystal properties which rules the elastic behaviour(FISH, 2000). This means that the two deformation mechanisms can be treated as separated phenomena, coupled in a multiplicative form, as shown in equation (4.4) with the deformation gradient tensor. In this equation,F^e is the elastic part of the deformation gradient tensor and F^p is the plastic part.

$$F(X,t) = F^e(X,t).F^p(X,t) \tag{4.4}$$

An important consideration to be made is that the elastic part of the deformation is so small compared to the plastic part and it is possible to assume $F \approx F^p$and $F^e \approx I$. This leads to the assumption that the effects of rotation in the rigid body movement are not great enough to cause major errors. In the reference configuration (Ω_0), the Cauchy Green tensor ($\boldsymbol{C}$) is given by the equation (4.5) and then the Green Lagrange deformation ($\boldsymbol{E}$) in shown in the equation (4.6).

$$\boldsymbol{C} = \boldsymbol{F}^T\boldsymbol{F} \tag{4.5}$$

$$\boldsymbol{E} = \frac{1}{2}(\boldsymbol{C} - \boldsymbol{I}) \tag{4.6}$$

In the deformed configuration Ω_t, the Finger deformation tensor (b^{-1})is given by the equation (4.7) and its elastic part $\left(b^{e^{-1}}\right)$ is given by the equation (4.8), where $\bar{G}$ is the metric tensor related to the intermediate configuration and G is the metric tensor related to the material configuration.

$$b^{-1}(x,t) = \boldsymbol{F}^{-T}(\varphi^{-1}(x,t),t).\boldsymbol{G}.\boldsymbol{F}^{-1}(\varphi^{-1}(x,t),t) \tag{4.7}$$

$$b^{e^{-1}}(X,t) = \boldsymbol{F}^{e^{-T}}(\varphi^{-1}(x,t),t).\overline{\boldsymbol{G}}.\boldsymbol{F}^{e^{-1}}(\varphi^{-1}(x,t),t) \tag{4.8}$$

From the equations (4.7) and (4.8) it is possible to calculate the Almansi deformation tensor (known also as Euler strain tensor) in its total by equation (4.9). Theelastic part of this tensor is given by equation (4.10) and plastic part by the equation (4.11). On these equations, g is the metric tensor related to the spatial configuration.

$$e(x,t) = \frac{1}{2}\left(g - b^{-1}(x,t)\right) = e^{e}(x,t) + e^{p}(x,t) \tag{4.9}$$

$$e^{e}(x,t) = \frac{1}{2}\left(g - b^{e^{-1}}(x,t)\right) \tag{4.10}$$

$$e^{p}(x,t) = \frac{1}{2}\left(b^{e^{-1}}(x,t) - b^{-1}(x,t)\right) \tag{4.11}$$

4.2. Incremental Formulation

The incremental formulation aims to determine the internal and dependent variables from the free and boundary variables (Total deformation, Plastic deformation and internal variables). For that, the time is subdivided in incremental steps $[0,T] = \cup_{n=0}^{N}[t_n, t_{n+1}]$. Also for all the particles belonging to the domain $X \in \Omega_0$, it is known the displacement field $\Delta U_{n+1}: \Omega_0 \rightarrow R^{n_{dim}}$ in the time increment $[t_n, t_{n+1}]$ and the variables $\{\varphi_n, E_n^p, \sigma_n\}$ at t_n, where $\sigma_n$is the stress field in the initial configuration. The Integration will consist in determine the variables $\{\varphi_{n+1}, E_{n+1}^p, \sigma_{n+1}\}$ at t_{n+1}. Once these variables were determined, all the other ones are automatically determined aswell. (WEYLER, 2000)

Figure 4.1 represent the incremental formulation design, where $\boldsymbol{E}$ is the deformationin the initial configuration of the body, $\boldsymbol{e}$ is thedeformation in the final configuration and $\tilde{\boldsymbol{e}}$ is the deformation in an intermediate stage defined by t_n.

To relate material tensors with spatial tensor it is used the transfer operators $pullback\ \phi^*$and $pushforward\ \phi_*$, which can use the transformation $f$represented by the equation (4.12) or the transformation f^{-1} represented by the equation (4.13), depending on which variable will be transformed. In the Fig. 4.1 these two operators are used to go from the last converged configuration to the

final configuration (f) and from the final configuration to the last converged one (f^{-1}).

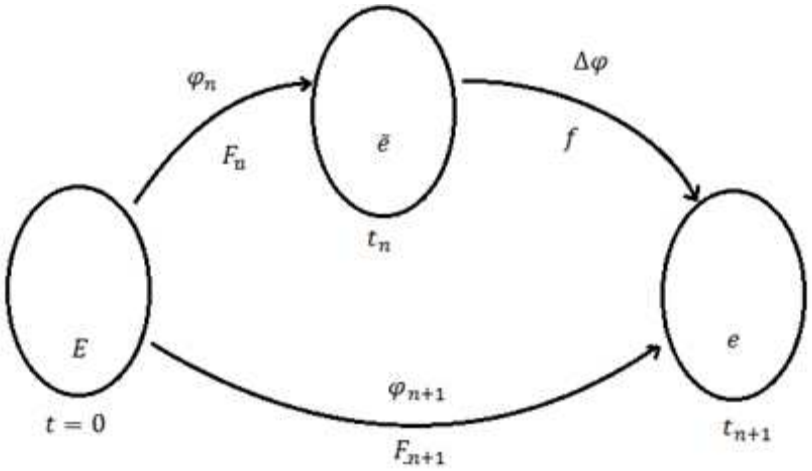

Figure 4.1. Representative design of the incremental formulation.

$$\boldsymbol{f = \frac{\partial \varphi_{n+1}}{\partial \varphi_n} = 1 + \frac{\partial \Delta\varphi}{\partial \varphi_n}} \tag{4.12}$$

$$\boldsymbol{f^{-1} = \frac{\partial \varphi_n}{\partial \varphi_{n+1}} = 1 - \frac{\partial \Delta\varphi}{\partial \varphi_{n+1}}} \tag{4.13}$$

The Finger tensor, in the intermediate configuration, is now in the form of the equation (4.14), its elastic part the equation (4.15) and the additional split of the Almansi tensor, also in the intermediate configuration and isolated for the elastic part, is shown by the equation (4.16).

$$\boldsymbol{(b_n)^{-1} = 1 - 2e_n} \tag{4.14}$$

$$\boldsymbol{(b_n^e)^{-1} = 1 - 2e_n^e} \tag{4.15}$$

$$\boldsymbol{e_n^e = e_n - e_n^p} \tag{4.16}$$

4.2.1 Predictor-corrector algorithm

The time integration uses a predictor-corrector algorithm, and for that the integration is composed by two stages. In the first stage, is calculated an elastic prediction, as known as *trial*, in which the irreversible variables are frozen, such as the internal variables. The second stage works as a plastic correction, where the solution of the first stage is corrected back to the yield surface if it's out, in other words, until the Kuhn-Tucker conditions are satisfied. (WEYLER, 2000)

The process starts with the calculation of the Almansi tensor in the intermediate stage at t_{n+1}, equation (4.17), by applying a *pullback*(transforming to the equation material form) in $\boldsymbol{e_{n+1}}$and then in equation (4.18), calculate the trial of elastic part of the Almansi tensor at t_{n+1}, applying a *pullback* at $\boldsymbol{e_{n+1}^{e^{TR}}}$. The equation (4.19) shows the trial of the elastic part in the deformation tensor. With the equations (4.17), (4.18) and the additional split, shown at equation (4.16), it is possible to calculate the plastic part of the Almansi tensor in the intermediate stage, equation (4.20). From the equation (4.20) it is possible to notice that the plastic part of the Almansi tensor at the initial configuration (which is an input data) stays the same for the other two configurations and also for the trial at t_{n+1}.

$$\tilde{\boldsymbol{e}}_{\boldsymbol{n+1}} = \phi^*(\boldsymbol{e}_{\boldsymbol{n+1}}) = \frac{1}{2}(\boldsymbol{f}^{\boldsymbol{T}}.\boldsymbol{f} - \boldsymbol{b}_{\boldsymbol{n}}^{-\boldsymbol{1}}) \tag{4.17}$$

$$\tilde{\boldsymbol{e}}_{\boldsymbol{n+1}}^{\boldsymbol{e^{TR}}} = \phi^*\left(\boldsymbol{e}_{\boldsymbol{n+1}}^{\boldsymbol{e^{TR}}}\right) = \frac{1}{2}(\boldsymbol{f}^{\boldsymbol{T}}.\boldsymbol{f} - (\boldsymbol{b}_{\boldsymbol{n}}^{\boldsymbol{e}})^{-\boldsymbol{1}}) \tag{4.18}$$

Where

$$\boldsymbol{e}_{\boldsymbol{n+1}}^{\boldsymbol{e^{TR}}} = \frac{1}{2}.(\boldsymbol{g} - (\boldsymbol{b}_{\boldsymbol{n+1}}^{\boldsymbol{e}})^{-\boldsymbol{1}}) \tag{4.19}$$

$$\tilde{\boldsymbol{e}}_{\boldsymbol{n+1}}^{\boldsymbol{p^{TR}}} = \tilde{\boldsymbol{e}} - \tilde{\boldsymbol{e}}_{\boldsymbol{n+1}}^{\boldsymbol{e^{TR}}} = \frac{1}{2}((\boldsymbol{b}_{\boldsymbol{n}}^{\boldsymbol{e}})^{-\boldsymbol{1}} - \boldsymbol{b}_{\boldsymbol{n}}^{-\boldsymbol{1}}) = \tilde{\boldsymbol{e}}_{\boldsymbol{n}}^{\boldsymbol{p}} = \boldsymbol{e}_{\boldsymbol{n}}^{\boldsymbol{p}} \tag{4.20}$$

With the result from the equation (4.20), the stress tensor, the internal variables and the yield surface is possible to calculate a function $\Phi^{\mathrm{TR}}(\boldsymbol{\sigma}, p)$, that determines if the current equivalent stress is still inside the yield surface ($\Phi^{\mathrm{TR}} \leq 0$), which means that the trial responses are the actual values for the time step t_{n+1}. In the case that the current equivalent stress is outside the yield surface ($\Phi^{\mathrm{TR}} > 0$), there must be calculated the return of this point to the yield surface border, and then use the values obtained. In both cases, to obtain the values of the Almansi tensor and the plastic part of the Almansi tensor, the *push-forward* operator must be applied, as presented by the equations (4.21) and (4.22).

$$\boldsymbol{e_{n+1}} = \phi_*(\tilde{\mathbf{e}}_{\mathbf{n+1}}) = \mathbf{f}^{-\mathbf{T}}.\,\tilde{\mathbf{e}}_{\mathbf{n+1}}.\,\mathbf{f}^{-\mathbf{1}} \tag{4.21}$$

$$\boldsymbol{e^{p}_{n+1}} = \phi_*\left(\tilde{\mathbf{e}}^{\mathbf{p}}_{\mathbf{n+1}}\right) = \mathbf{f}^{-\mathbf{T}}.\,\tilde{\mathbf{e}}^{\mathbf{p}}_{\mathbf{n+1}}.\,\mathbf{f}^{-\mathbf{1}} \tag{4.22}$$

The formulations presented in this chapter were then implemented in the FORTRAN90 based COMFORM algorithm, considering that the variables used must come from the main program and the algorithm implemented must return variables respecting the COMFORM software logic, in order to allow the whole software to work properly.

CHAPTER V

YIELD SURFACE AND HARDENING LAW

Yield surface is defined as a map in stress space, in which is drawn a boundary that separate non-yielded regions from the ones that already undergo flowing due to the problem conditions.(COURTNEY, 2005)

The yield will be the criteria to define a material plasticity, according to the equation (5.1), in which the first term represents a function of stress tensor and hardening variables. Considering an isotropic material, the yield depends only on the principal stresses, so the *F*function becomes dependent only on the scalar hardening – α. (NATAL JORGE, 2004)

$$F(\boldsymbol{\sigma}, \alpha) = f(\boldsymbol{\sigma}) - \sigma_y(\alpha) = 0 \tag{5.1}$$

Where the $f(\boldsymbol{\sigma})$ represents the equivalent stress. This function can be represented in space by a Westergaard bearing pressure, where three orthogonal axes coincide with the principal stresses, Fig.5.1. (NATAL JORGE, 2004, WESTERGAARD, 1939)

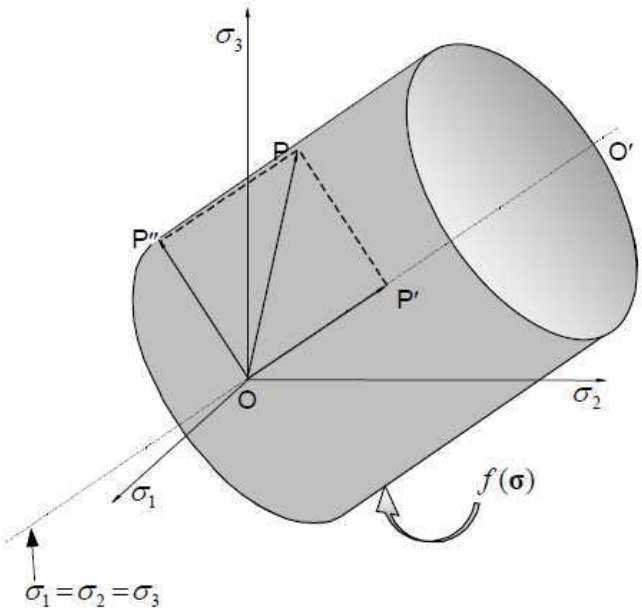

Figure 5.1- Westergaard space (JORGE NATAL, 2005)

The increment of the point P is represented by the vector $\overline{OP}$, which can be decomposed and its components coincide with the hydrostatic stress(axis where the three principal stresses has the same value) and the deviatoric stress , where $\overline{OP''}$ is normal to OO'. So the yield will depend only on the vector $\overline{OP''}$ (*shape changing* stresses or deviatoric stresses). This is only true if the hydrostatic pressure (*volume changing* stresses) does not affect the material yield, which can be demonstrated by experimental tests. Given that, the yield will depend only on the second and the third invariants of the deviatoric stresses (S_{ij}), shown in the equations (5.2) and (5.3).(JORGE NATAL, 2005, KACHANOV, 1974)

$$J_2 = \frac{1}{2} tr(\boldsymbol{s}^2) = \frac{1}{2} S_{ij} S_{ji} \tag{5.2}$$

$$J_3 = \frac{1}{3} tr(\boldsymbol{s}^3) = \frac{1}{3} S_{ij} S_{jk} S_{ki} \tag{5.3}$$

The geometric representation can be obtained by these two invariants, in the form of the equation (5.4).

$$\theta = \frac{1}{3} sen^{-1}\left(-\frac{3^{\frac{1}{3}} x\, J_3}{2 J_2^{\frac{1}{3}}}\right) ; \ \theta \in \left[-\frac{\pi}{6}, +\frac{\pi}{6}\right] \tag{5.4}$$

Considering a deformable material, if $f(\boldsymbol{\sigma}) < \sigma_y(\alpha)$, the analysed point is showing elastic behaviour. On the other hand, if $f(\boldsymbol{\sigma}) = \sigma_y(\alpha)$, the material behaviour is considered plastic. The material behaviour after that point will depend on the f variation due to $\boldsymbol{\sigma}$, as shown by the equation (5.5), which is a vector normal to the yield surface called associated plastic flow, Fig. 5.2.

$$df = \left(\frac{\partial f}{\partial \boldsymbol{\sigma}}\right)^T d\boldsymbol{\sigma} + \cdots \tag{5.5}$$

In summary,

- If $df < 0$, the material shows elastic behaviour and the incremental stress is located inside the yield surface.
- If $df = 0$, the material shows perfectly plastic behaviour, constant α, and the stresses are located on the yield surface boundaries.
- If $df > 0$, the material is undergoing hardening, which means that the yield surface will change. It can evenly expand, in the case of isotropic hardening (KACHANOV, 1974). It can dislocate in stresses space, in the case of kinematic hardening (OWEN, 1980). If the yield surface dislocates, change its size, its shape or even rotate, the hardening is considered distortional (EKMARK, 1983). The kinematic and the isotropic hardening geometric representation is shown by the Fig. 5.3 (a) and (b) respectively.

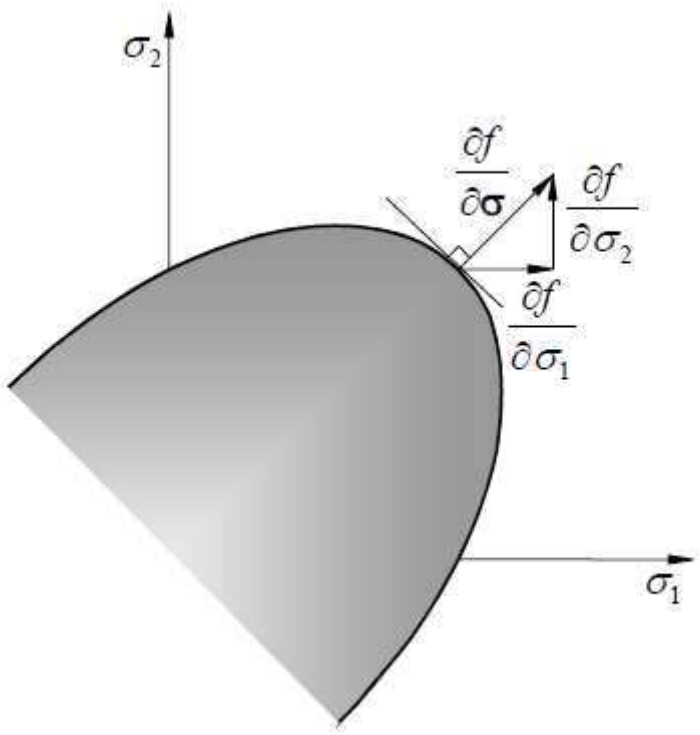

Figure 5.2 – Orthogonally Condition in $\sigma_1 - \sigma_2$ space (JORGE NATAL, 2005)

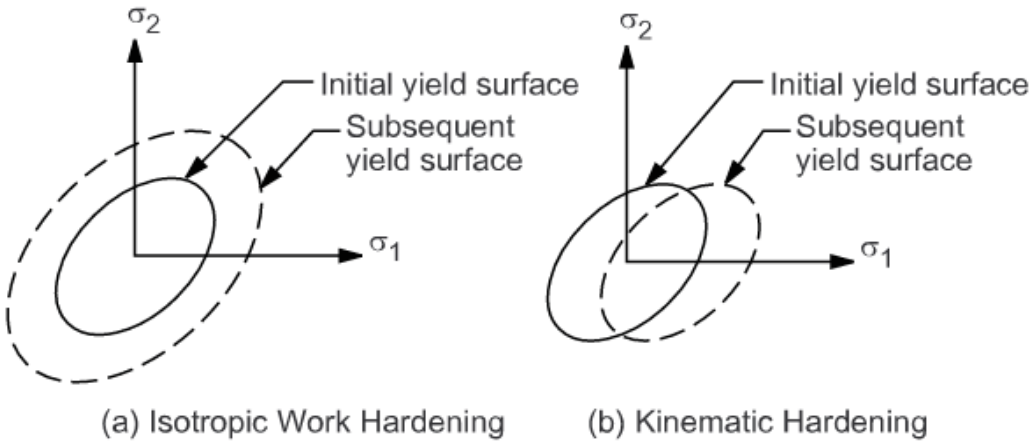

Figure 5.3 – Hardening Rules (GONZALES, 2009)

5.1. Von Mises Yield Surface

According to Von Mises (1913), the yield occurs when the second invariant of the deviatoric stresses J_2 reaches a critical value, depending on the hardening (α). This hypothesis considers the distortion energy density and should be true for an uniaxial stress state aswell, where $\phi(\alpha) = \sqrt{\frac{2}{3}}\sigma_y$ and the effective stress is given by the equation (5.6).

$$\bar{\sigma} = \sqrt{3J_2} = \sqrt{\frac{3}{2}\boldsymbol{s}:\boldsymbol{s}} = \sqrt{\frac{3}{2}S_{ij}S_{ji}} \;\rightarrow\; \bar{\sigma} - \sigma_y(\alpha) = 0 \tag{5.6}$$

According to Hill (1950), the deformation energy in terms of the second deviatoric and the volumetric expansion (equation (5.7)) will only ensure incompressibility if the Poisson Ratio$(\nu)$is iqual to 0.5 and therefore the second part of the equation (5.7) will became null, resulting in the equation (5.8).

$$U_0 = \frac{1}{2\mu}J_2 + \frac{3(1-2\nu)}{2E}\sigma_m^2 \tag{5.7}$$

$$F(\boldsymbol{\sigma}, \alpha) = \frac{1}{2\mu}J_2 - \frac{1}{6\mu}\sigma_y^2(\alpha) = 0 \tag{5.8}$$

The equation (5.6) and (5.8) can be combined, resulting in the effective stress in terms of the second deviatoric stress J_2 (equation (5.9)), which shows that Von Mises yield surface is applicable to materials with no volumetric deformation.

$$\bar{\sigma} = \sqrt{3J_2} = \sqrt{\left(\frac{1}{2}\right)((\sigma_1 - \sigma_2)^2 + (\sigma_2 - \sigma_3)^2 + (\sigma_3 - \sigma_1)^2)} \tag{5.9}$$

5.2. Ludwik Nadai hardening law

After the analysis of the deformation being inside or outside the yield surface, it becomes necessary to understand and prescribe the hardening experienced by the material when it goes under plastic deformation. Many are the mathematical models with the purpose of describe the behaviour of the hardening curve and for this work were used the Ludwik-Nadai hardening law. (MELCONIAN, 2014)

This law is exponential and considers the variation of the plastic deformation, as it can be seen on equation (5.10).

$$\sigma_y = k\left(\varepsilon_{ps0} - \varepsilon_{ps}\right)^n \tag{5.10}$$

Where,

- σ_y is the yield stress
- k is the hardening modulus
- ε_{ps0} is a initial equivalent plastic strain that defines the initial yield stress
- $\varepsilon_{ps}$is the current equivalent plastic strain.
- $n$is the hardening exponent.

The current stress value is equal to the yield stress when the current plastic deformation is equal to zero, as given by the equations (5.11) and (5.12)

$$\varepsilon_{ps0} = \left(\frac{\sigma_y}{k}\right)^{\frac{1}{n}} \tag{5.11}$$

$$\sigma = k\left(\left(\frac{\sigma_y}{k}\right)^{\frac{1}{n}} - \varepsilon_{ps}\right)^n = k\left(\left(\frac{\sigma_y}{k}\right)^{\frac{1}{n}} - 0\right)^n = \sigma_y \tag{5.12}$$

CHAPTER VI

INSTRUMENTED MICROINDENTATION

According to Jost (1966), Tribology is the science field which studies contacting surfaces, in relative motion, and related subjects. This concept unifies the friction, lubrication and wear subjects in only one field of study. This is important, considering that the wear phenomenon is a complex interfacial process, which is irreversible, progressive and with difficult theoretical characterization. (NOGUEIRA, 1988, MARTINS, DA SILVA, 2008)

Aiming to comprehend and predict the wear, more specifically the abrasive wear phenomenon, experimental simulations are often used. These simulations are divided in two groups:

i- Global Approach, which tries to represent the abrasive wear in an area, using abrasometric techniques. (Costa *et al.*, 2001, FRANCO *et al.,* 1989);

ii- Local approach, which studies the interaction between a single asperity or particle and the counter-body material. The experiment which best representsthe rolling particle abrasive wear is the microindentation test. (DEVARAJU, 2015)

6.1. Microindentation Test

The microindentation test consists in an experimental method in which the specimen is pressed by a known shaped indenter, with controlled load and displacement. Analysing the load, displacement and also the indentation mark, it is possible to calculate the bulk or multi-layered materials properties. It is also possible tocharacterize the multi-layered material adhesion between layers and analyse other phenomena, such as the pile-up and sink-in. (GU *et al.*, 2003, FELICE NETO, 2012, RUTHERFORD,1997, CHEN, 2007, HOLMBERG, 2009)

The microindentation test schematic diagram is represented inFig. 6.1.

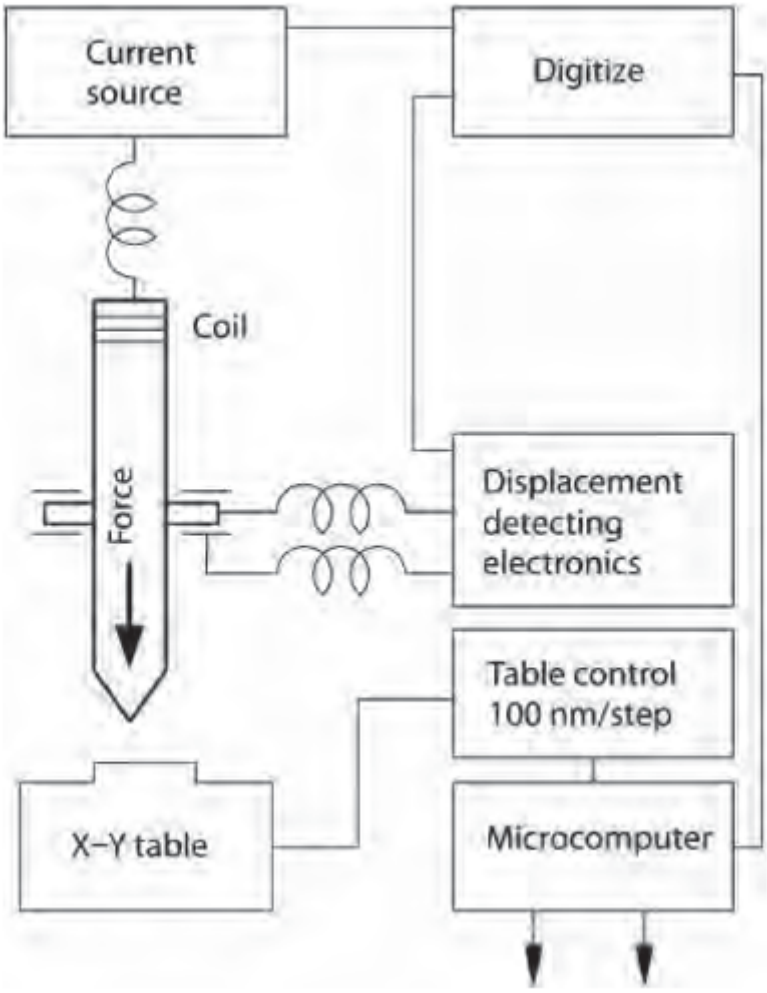

Fig.6.1. Schematic diagram of a Microindentation test. (Adapted from HOLMBERG, 2009)

The microindentation experiments carried by Da Silva (2008) gave as results for microindentation depth vs. Applied Force, for 5N and 10N Brinell indenter experiment, the Fig. 6.2 and 6.3 respectively. For the Brinell indenter, the standard used was ASTM E10-15a.

It is important to note that the curve separates from zero in the X axis only with 8 µm depth, which means the indenter approximation, i.e., the indenter does not start touching the specimen and the total depth actually is the subtraction between the greatest value for depth and the value where the force became different from zero, approximately 7 and 15µm, for 5N and 10N experiment respectively.

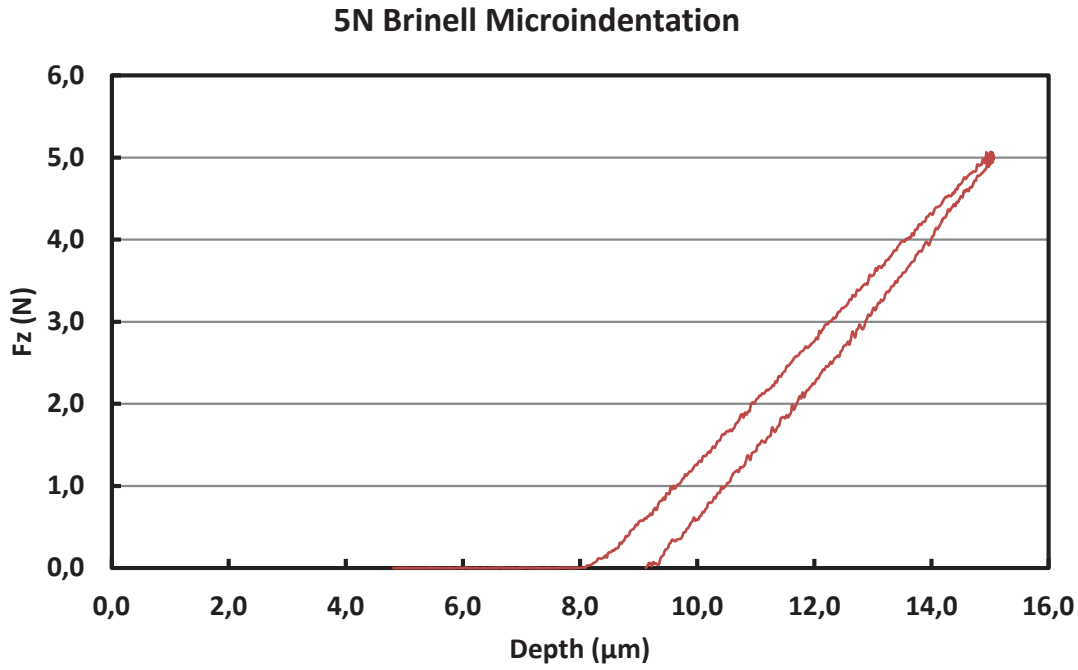

Fig.6.2. 5N Brinell Microindentation Force vs. Depth curve (DA SILVA, 2009)

After the microindentation test it is necessary to evaluate the indented surface, and with that purpose the Laser Interferometry was used.

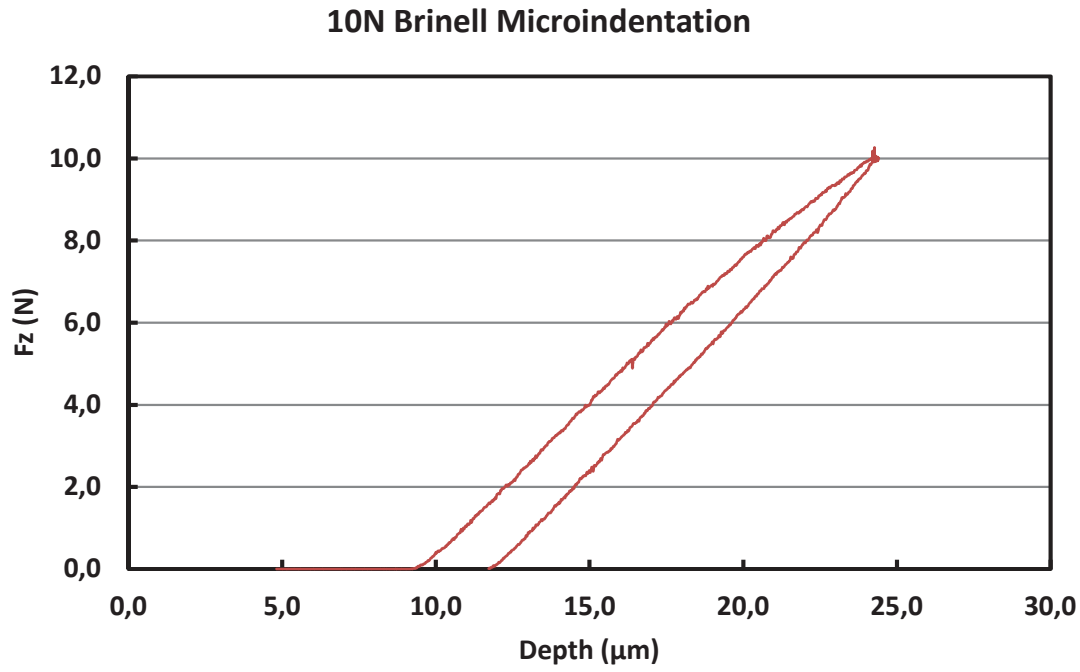

Fig. 6.3. 10N Brinell Microindentation Force vs. Depth curve (DA SILVA, 2009)

6.2. Pile up and Sink in

The microindentation test performs a deformation in the specimen under the tool and that causes deformation in the mark´ surroundings. If the material experience hardening when it undergoes plastic deformation, the surroundings will go up, forming the pile up. On the other hand, if the specimen undergoes annealing during the plastic deformation, the surroundings go down, performing a sink in phenomena. Both the pile up and the sink in are represented by the Figure 6.4. (TALJAT & PHARR, 2004, LEE *at al.,* 2008, TALJAT *at al.,*2011)

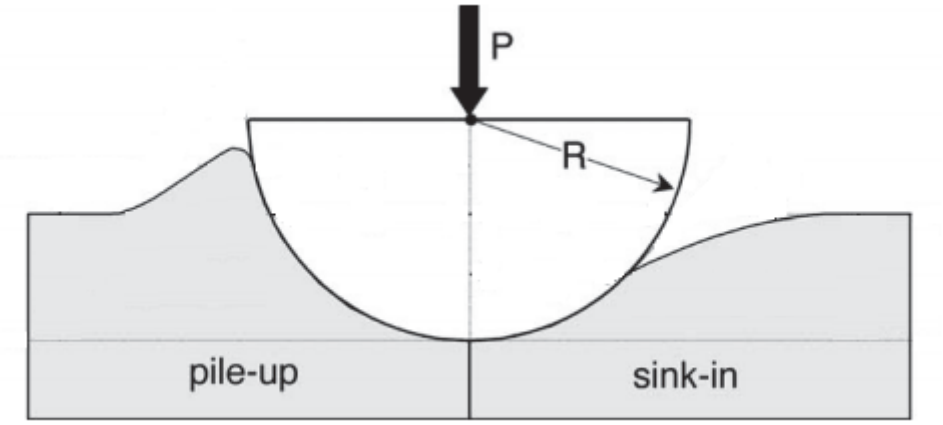

Fig. 6.4. Pile up and sink in phenomena. (Adapted from TALJAT & PHARR, 2004)

6.3. Laser Interferometry

The laser interferometry is a measurement method which uses wave interference to measure distances. A laser beam is divided in two and each beam goes through a different path. The first beam goes to a reference mirror and the second to the specimen surface and then both lasers are reflected together to a detector. The difference in the wave pattern is calibrated to indicate distances and, therefore, the specimen surface roughness. (BUSHAN, 2001)

Figure 6.5 shows the simplified schematic design of the Laser interferometry operation mechanism.

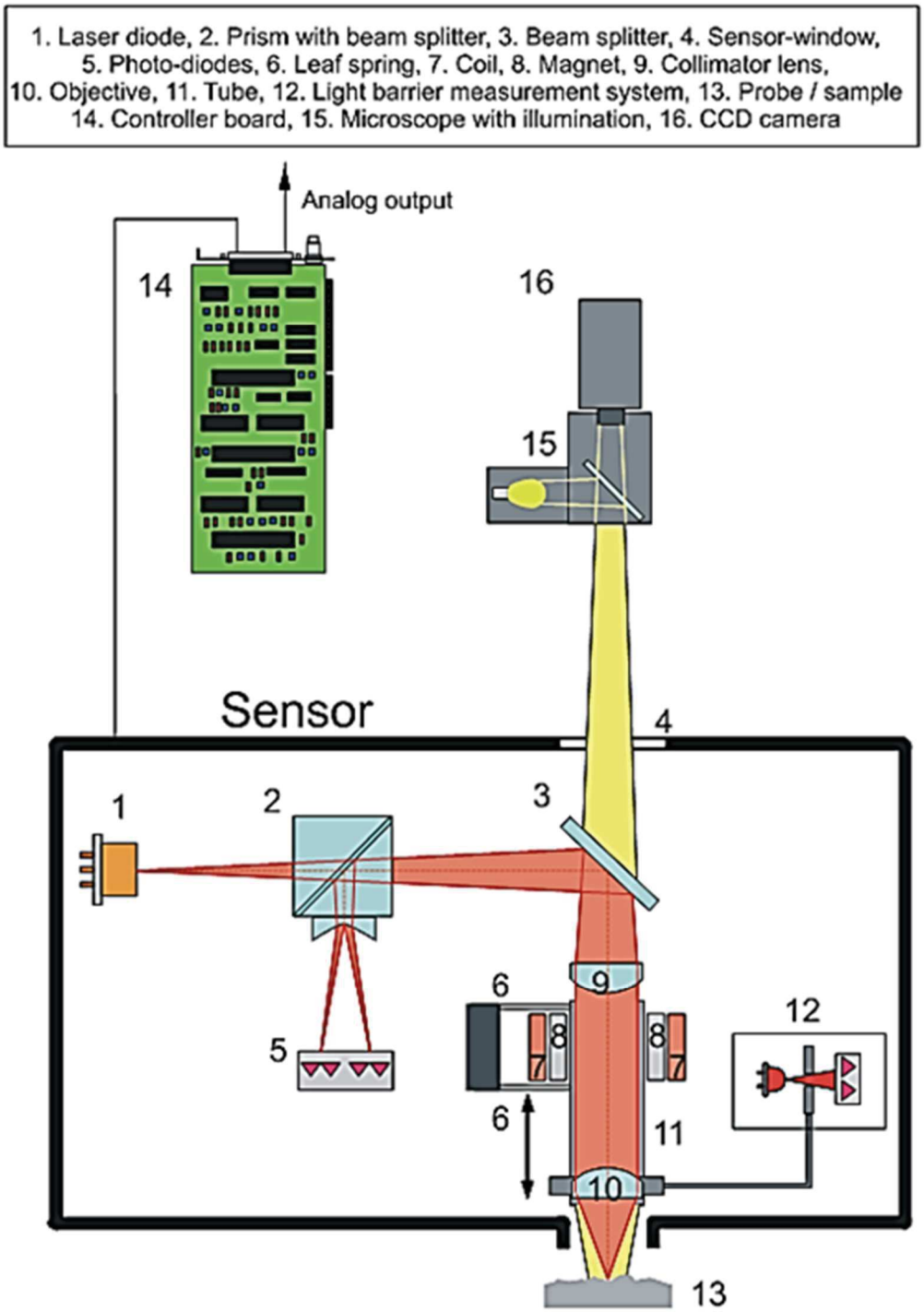

Fig. 6.5. Schematic Design of the Laser Interferometry operation mechanism (UBM, 1999)

The experimental microindented specimens were scanned with a Laser Interferometry and the results for 5N load and 2.5 mm diameter indenter radius (Brinell indenter) are on Figs. 6.6 and 6.7 (DA SILVA, 2008).

There were also scanned with Laser Interferometry a Copper Specimen with 10N load and the same 2.5 mm indenter diameter. Figures 6.8 and 6.9 show the Copper specimen topography and roughness profile for this experiment. (DA SILVA, 2008)

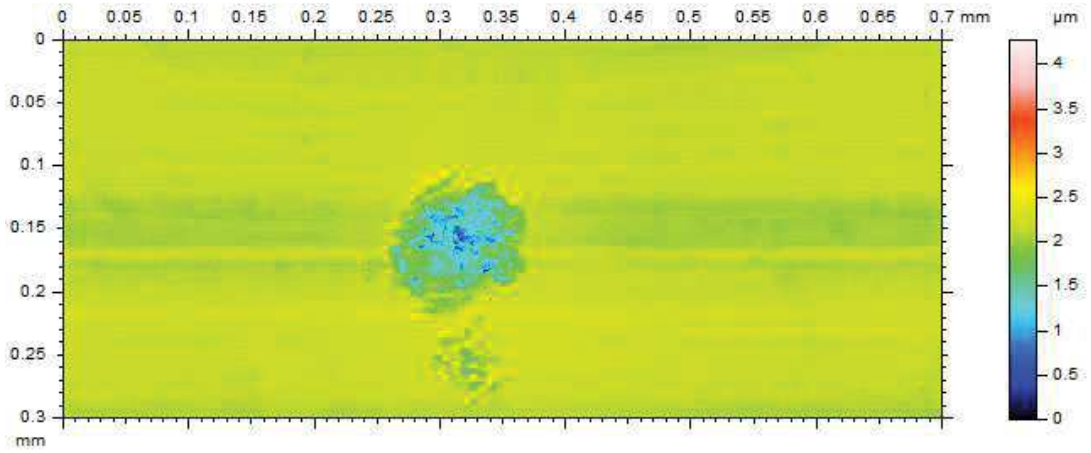

Fig. 6.6. Laser Interferometry of the 5N Brinell microindentation (DA SILVA, 2009)

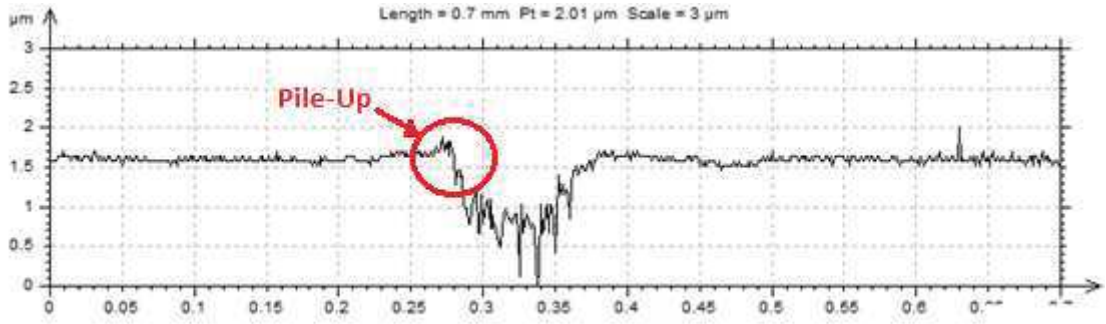

Fig. 6.7. 5N Brinell microindentation roughness profile. (DA SILVA, 2009)

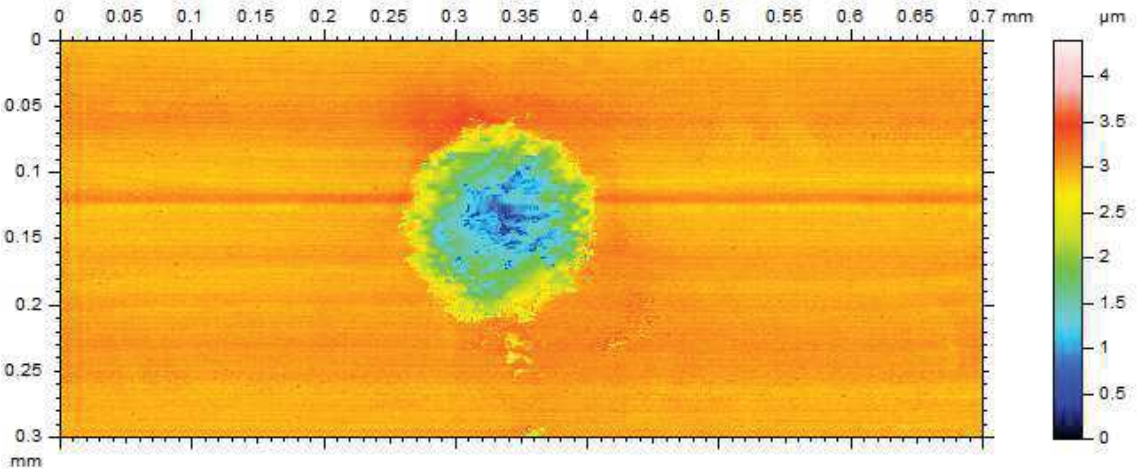

Fig. 6.8. Laser Interferometry of the 10N Brinell microindentation (DA SILVA, 2009)

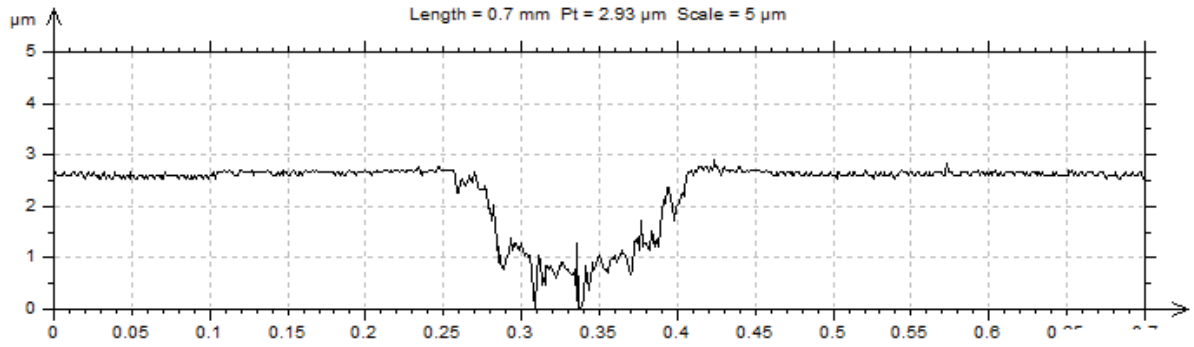

Fig. 6.9. 10N Brinell microindentation roughness profile. (DA SILVA, 2009)

CHAPTER VII

METHODOLOGY

In the previous chapters were discussed the contact problem, theoretically and numerically. After that, were discussed material plastic properties and a formulation (material and contact) to simulate severe contact conditions, such as the microindentation test, reviewed in Chapter 6. This Chapter aims to stablish a methodology to create a contact domain approach in Explicit FEM, inside an existing program, create a Small Elastic and Large Plastic Deformations formulation, validate the method using experimental tensile strength test and simulate a microindentation test.

7.1. Implementing the Constitutive Model in COMFORM

The COMFORM is a Finite Element Method calculation software, developed in the Polytechnic University of Catalonia (UPC) in partnership with other Institutes. This software is FORTRAN90 programmed and has a modular

constitution, making possible to introduce new modules that works with the already existent programming.

The COMFOM software, before this work, was capable of simulating axisymmetric, 2D and 3D problems, with triangular or quadrilateral mesh, all with implicit time integration. The code can be used to simulate general mechanical process, such as stamping, bending, contact and also sintering. To do so, the software uses elastic, plastic, granular and powder material formulations.

Considering the microindentation problem, where the deformation is really punctual (micrometres), the elastic part of the total deformation is small enough to be neglected, and then all the deformation is considered to be plastic. Thus, a Small Elastic Large Plastic (SELP) constitutive law was implemented in the COMFORM software. This material behaviour works now in all implemented modulus.

The second stage was to implement the explicit time integration inside COMFORM, using the methodology from Chapter III. The Explicit Method were also implemented to work with all modulus of COMFORM (2D/3D, material formulations, mesh criteria).

Then, convergence tests were made, just to be sure that the entire system works. After the convergence tests, a validation test were made for a tensile strength experiment.

7.2. Validation of the Implemented Model

To validate the implemented method, is necessary a proper result comparison, which can use benchmark or experimental results. For this work was used a tensile strength experimental test, in a copper specimen. The experiment was carried using the ABNT NBR 6892-1 (2015)

The software COMFORM is a calculus module only, i.e., it doesn't have an interface to create geometry, mesh, boundary conditions and read the post-process data. For that, were used the GiD platform, which provides several tools to build the pre-process and post-process data, including a problem type feature, that enables the user to create a standard data export, making easy to create COMFORM structure data file.

Using the GiD software, were designed two models, with square shaped cross-section area and same length as the experimental test ($100\ mm^2$ and $50\ mm$ respectively). The square shaped cross-section area is different from the experimental specimen cross-section, which is circular, but if the cross-section area is the same, the Stress vs. Strain and Force vs. Displacement curves won't differ. The difference between the models is the element mesh, the first model used tetrahedral and the second hexahedral elements, as shown in Fig. 7.1

Both meshes were created with 5 divisions in the X and Y axis and with 10 divisions in the Z axis, totalyzing 15000 elements and 1102 nodes for the tetrahedrical mesh and 625 elements and 936 nodes for the hexahedrical mesh. For boundary conditions it was imposed that the bottom nodes are fixed (X, Y and Z displacements equals to zero during the whole simulation) and in the top nodes were imposed a curve Force vs. Time, which copies the Force vs. Time curve aspect from the tensile strength experiment. In order to correctly impose the force in the top surface, the total force were divided by the number of the elements in the surface, considering how many elements each element share connections with, as shown in Fig. 7.2.

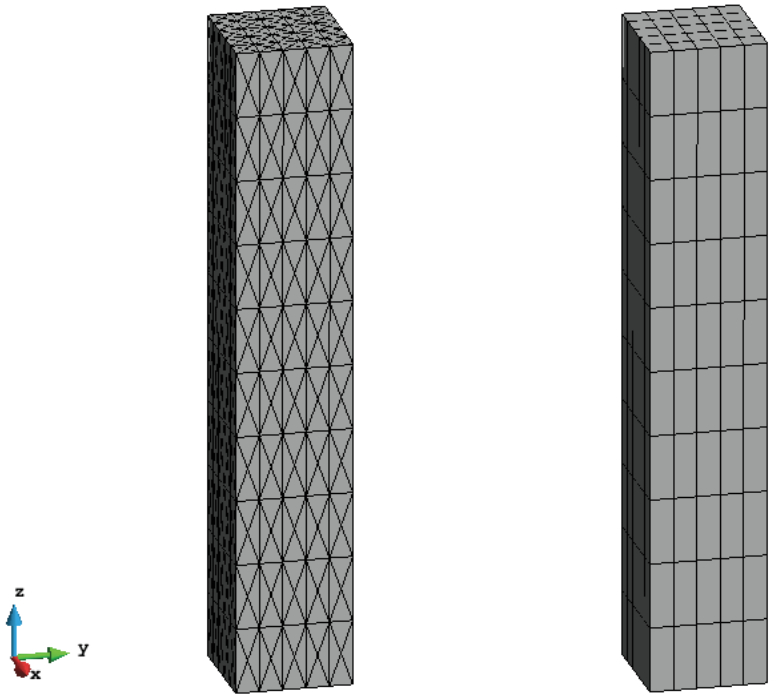

Fig. 7.1 Tensile Strength FEM models with Tetrahedral and Hexahedral Elements.

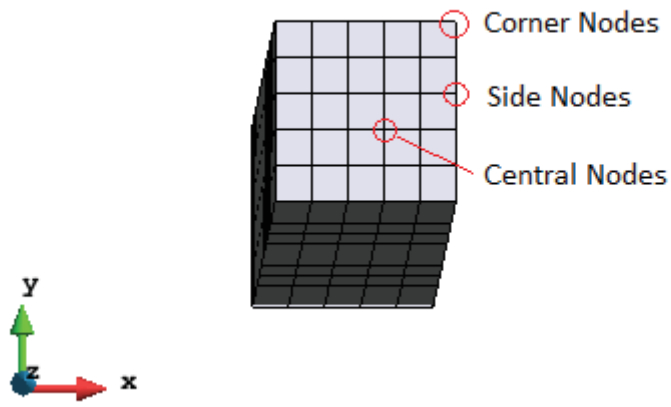

Fig. 7.2. Distribution of nodes in the top surface of the tensile strength experiment test model.

There are 16 central nodes, each of them is connected to 4 elements, 16 side nodes, connected to 2 elements, and 4 corner elements, connected to only one element. Considering that the total force applied to the specimen in the

experimental tensile strength test was 7000 [N], the Equation 7.1 shows the distribution of the force through the elements on the surface.

$$16.(1.'Force') + 16.(0{,}5.'Force') + 4.(0{,}25.'Force') = 7000\ [N] \quad (7.1)$$

So, the curve that represents the Force (F = 280 N) vs. Time that were imposed in the surface elements is shown by Fig.7.3.

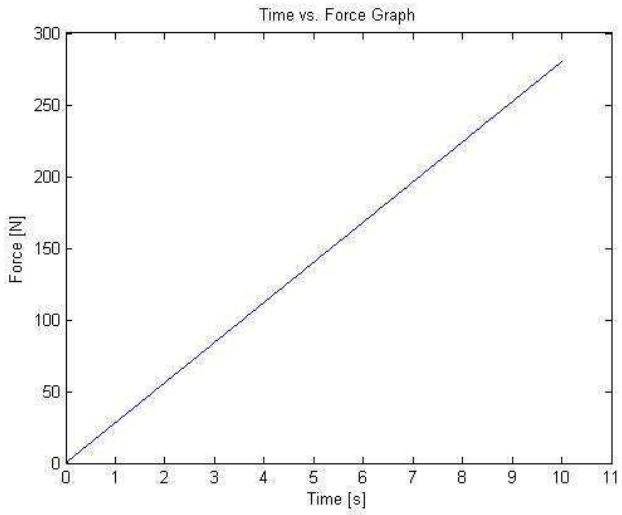

Fig. 7.3. Time vs. Force curve applied to the tensile strength test top nodes.

For the Tetrahedral mesh model, were used a similar approach to distribute the Load trough the top surface elements, considering that the tetrahedral mesh has more elements even with the same number of division in each axis. That can be seen on Fig. 7.1.

To simulate the experiment correctly, all properties data must be the same in the FEM simulation as in the real experiment specimen. In order to get these properties, an error minimization approach was used, as described in the next section.

7.3. Material properties from tensile strength test curve

The tensile strength test provides some material properties directly from the experiment and other properties are given by the bulk material manufacturer, those properties are listed in Table 7.1.

Table 7.1 Copper specimen properties.

Property	Value	Unity
Young Modulus (E)	117	GPa
Yielding Stress (σ_y)	110.83	MPa
Poisson's ratio (ν)	0.3	-
Density (ρ)	8960.0	Kg/m³

Those properties doesn't concern to the plastic deformation hardening and for this phenomenon must be used a hardening model. For this work were used a Ludwik-Nadai model, an exponential hardening law, which performs a good hardening representation of several materials, including Copper. The Ludwik-Nadai hardening law is presented by the equation (5.11).

The plastic part of the deformation can be calculated for the tensile strength test using the initial specimen length(l_0) and the displacement trough the experiment. In this case, the Plastic part of the deformation starts in zero and increases during the experiment, in the form of the equation (7.3). The differential plastic part of the deformation is in the form of the equation (7.4).

$$(\varepsilon_p)_{t+1} = (\varepsilon_p)_t + (\Delta\varepsilon_p)_{t+1} \tag{7.3}$$

$$\left(\Delta\varepsilon_p\right)_{t+1} = (1.5.((\varepsilon_{11})_{t+1} - (\varepsilon_{11})_t)^2 + 2.((\varepsilon_{22})_{t+1} - (\varepsilon_{22})_t)^2)^{\frac{1}{2}} \tag{7.4}$$

Where

$$\varepsilon_{11} = 0.5.\left(1 - \left(\frac{l_0}{l_f}\right)^2\right) \quad (7.5)$$

$$\varepsilon_{22} = 0.5.\left(1 - \left(\frac{l_0}{l_f}\right)\right) \quad (7.6)$$

And l_f is the final length of the specimen.

Using those equations and the experimental curve Force vs. Displacement, it is possible to create a MatLab® minimization function, in which a seed of *k* (hardening modulus) and *n* (hardening exponent) is chosen by the user and the function minimize the error (difference between the calculated and experimental stress) in order to approximate the two curves. It considers a number of evaluations and an error tolerance. The initial seed were chosen considering a common Copper material found in the literature and the evaluations started in 100 (default) until the response value of *k* and *n* does not change anymore (400 evaluations). The algorithm returns the values of *k* and *n* for the minimum calculated error and the complete implemented MatLab® algorithm is presented in the APPENDIX A.

7.4. Simulation of a Micro-indentation test

After the material properties calibration and validation of the explicit time integration for Hexahedral and Tetrahedral elements, the next step is to create a model to simulate a microindentation test.

To decrease the simulation time, the microindentation model created is a quarter of the whole model, i.e., symmetry in the XZ and YZ plans. The indenter is sphere shaped with 2.5 [mm] diameter and has only the tip of the indenter designed, considering that the indenter won't undergo plastic or large elastic deformations because it is constituted by a hard material (tool steel), when compared to the copper specimen (designed with $0.7\ x\ 0.7\ x\ 1.4\ mm$). Figure 7.4 shows the simulation model created for the microindentation test and Tab. 7.2 shows the indenter elastic properties.

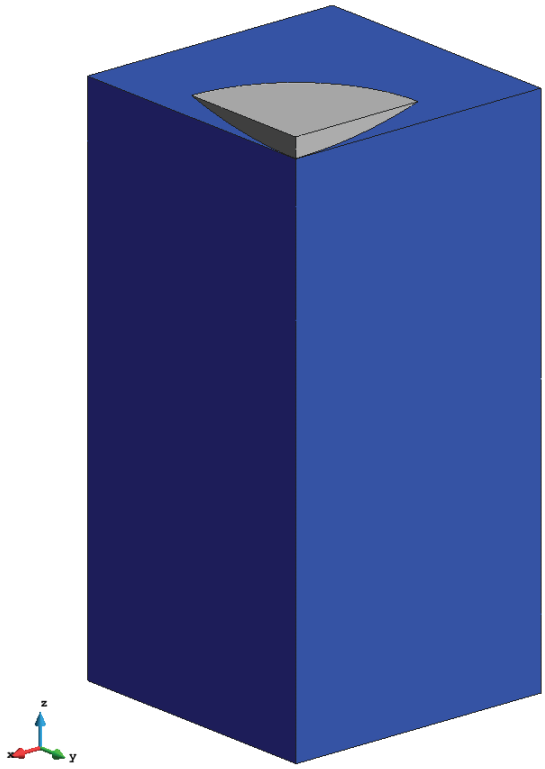

Fig. 7.4. Representation of the microindentation test.

Table 7.2. Microindentation Simulation Indenter properties.

Property	Value	Unity
Young Modulus (E)	210	GPa
Poisson's ratio (ν)	0.3	-
Density (ρ)	7850.0	Kg/m³

Considering that the model was designed considering each model distance as one millimetre, all properties must be re-evaluated to guarantee the unities coherence. Equations (7.7) to (7.9) show the unities transformations made.

$$E = GPa = 10^9 Pa = 10^9 \left(\frac{N}{m^2}\right) = 10^9 \left(\frac{N}{(10^3 mm)^2}\right) = 10^3 \left(\frac{N}{mm^2}\right) \tag{7.7}$$

$$\rho = \frac{kg}{m^3} = \frac{kg}{(10^3 mm)^3} = 10^{-9} \left(\frac{kg}{mm^3}\right) \tag{7.8}$$

$$\sigma_y = MPa = 10^6 Pa = 10^6 \left(\frac{N}{m^2}\right) = 10^6 \left(\frac{N}{(10^3 mm)^2}\right) = \frac{N}{mm^2} \tag{7.9}$$

The Poisson's ration is dimensionless so there is no conversion to be made. The hardening exponent *n* is also dimensionless but the hardening modulus must be converted to millimeters as well, Equation (7.10).

$$k = MPa = 10^6 Pa = 10^6 \left(\frac{N}{m^2}\right) = 10^6 \left(\frac{N}{(10^3 mm)^2}\right) = \frac{N}{mm^2} \tag{7.10}$$

The mesh created is constituted by tetrahedral elements in both bodies (indenter and specimen). The global element size for the unstructured mesh is 0.09. This size were chosen considering the minimum deformation expected in the copper specimen, i.e., the mesh must be small enough to perform the shape of the indentation mark left on the copper specimen surface. The indenter has the global element size for the bottom surface and the global size multiplied by a factor of 10, totalizing 1142 nodes and 5750 elements. The indenter mesh is shown by the Fig. 7.5.

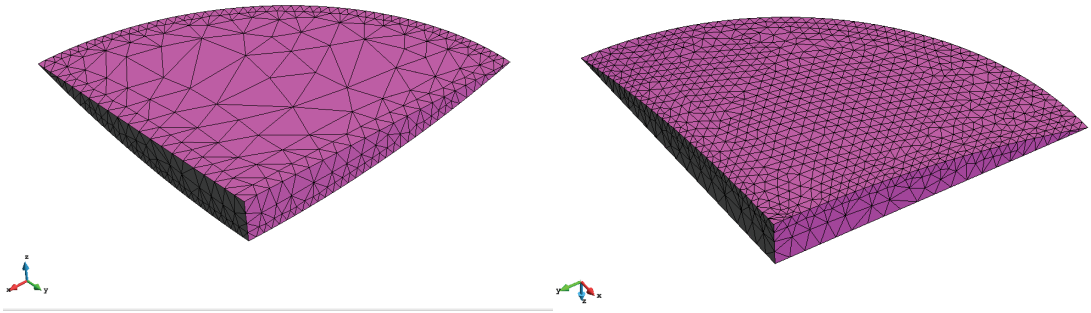

Fig. 7.5. Mesh of the Top and Bottom face of the indenter.

For the specimen, the top surface has the global element size (0.09) and the bottom surface has the global element size multiplied by a factor of 100, totalizing 2636 nodes and 22847 elements. Figure 7.6 represents the mesh created for the specimen in the microindentation test simulation.

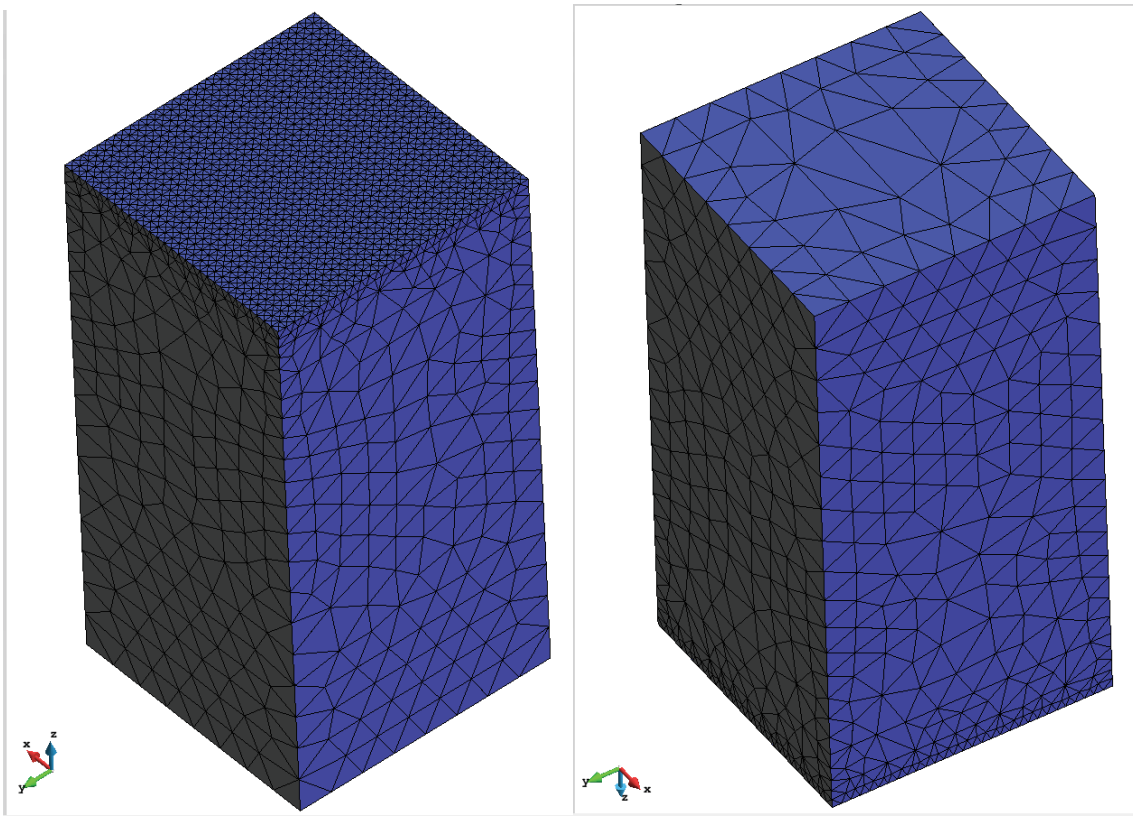

Fig.7.6. Mesh of the Top and Bottom face of the specimen.

The complete mesh model is represented by Fig.7.7.

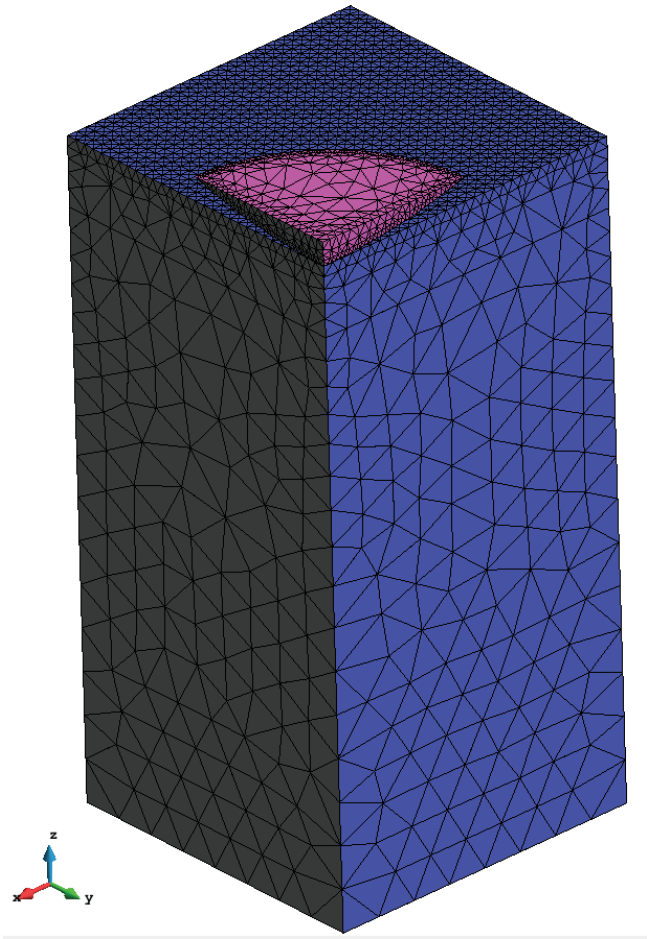

Fig. 7.7. Mesh of the FEM Microindentation model.

The boundary conditions created for this model consists in the restriction of displacement of the bottom surface specimen nodes, in the axis X, Y and Z. The symmetry surfaces, XZ and YZ, had the Y displacement and X displacement equals to zero respectively, to guarantee the model symmetry. The Fig. 7.8 shows the restricted points in the model symmetry surfaces with and without the global mesh.

The indenter moves according to a Time vs. Displacement curve (Fig 7.9), based on the experimental data of the microindentation experimental test, carried by Da Silva (2008).

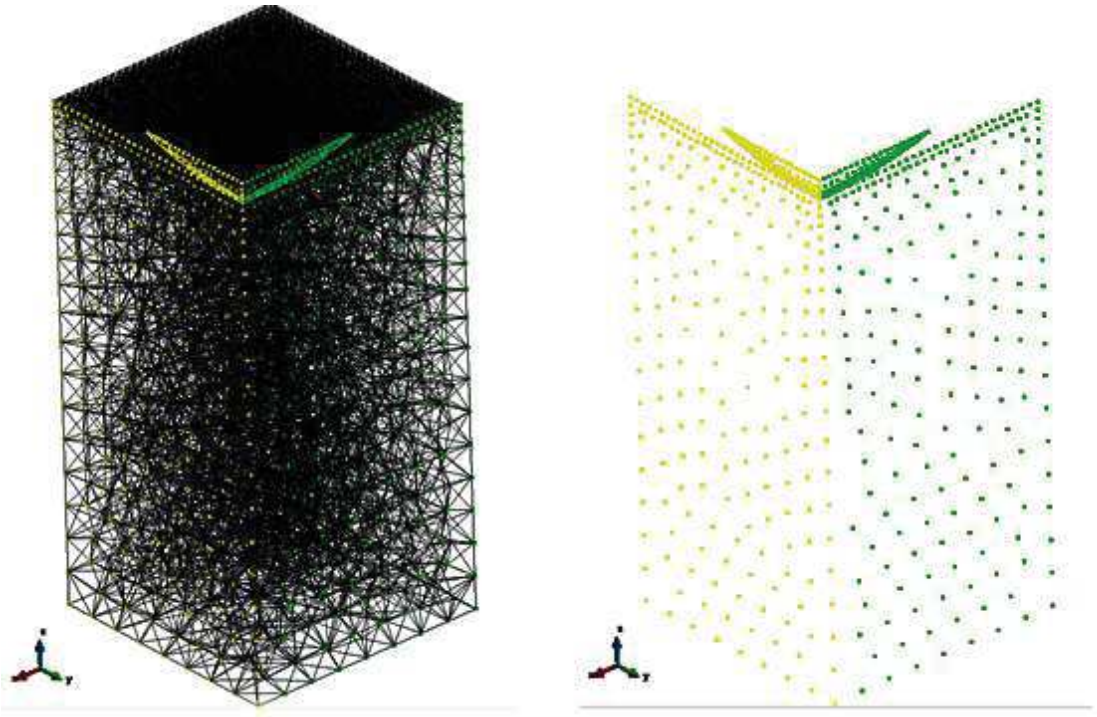

Fig 7.8. Restricted points in the model symmetry surfaces with and without the global mesh.

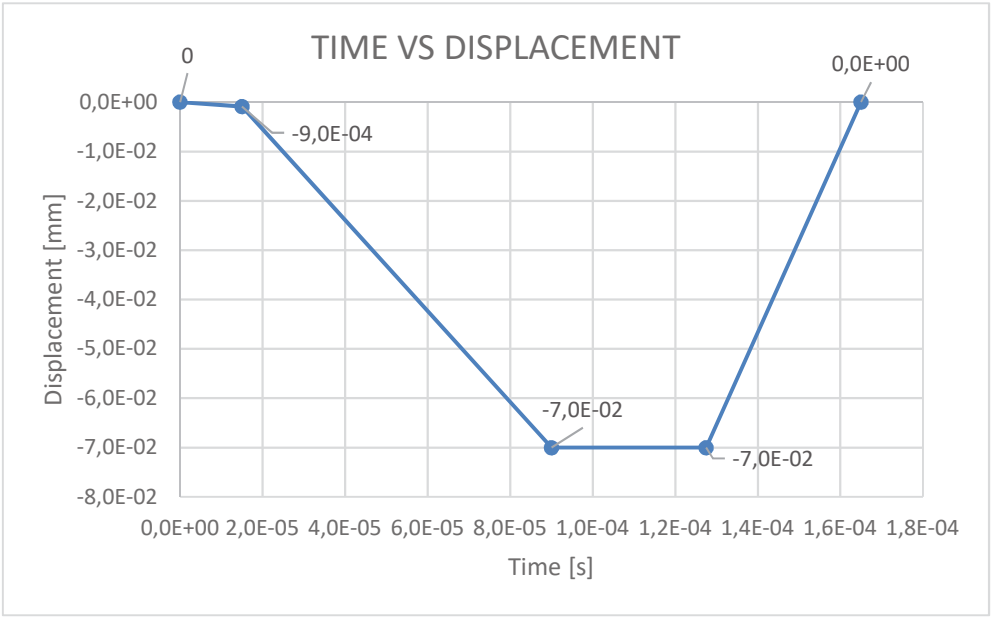

Fig.7.9. Time vs Displacement curve imposed on the top surface indenter nodes

The Time vs. Displacement curve shows 4 stages: i. In the first stage the displacement is in a short range, just to approximate the indenter to the copper specimen. The simulation did not start with the bodies in touch, because of several convergence problems found; ii. In the second stage the Displacement is

increased slowly to guarantee the algorithm convergence, until it comes to the maximum Z axis Displacement; iii. In the third stage the displacement is constant, to be sure that there are no dynamic effect or numerical disturbance, which would make the specimen surface point to move even with the indenter stopped; iv. The fourth stage is the unloading, which can be fast and is really important because the specimen material will undergo a spring-back (elastic deformation recuperation) that will enable the comparison between the final stage of the simulation with experimental specimen surface topography, measured with a Laser Interferometry.

Some other simulation properties were set:

- **Number of post-process:** This variable sets the number of post-process files that are saved in the Hard disk. It is important to choose a number big enough to allow the right visualization of the deformation development. If this parameter became too big, the Hard disk space consumption and the time necessary to read and write files increases. The value used for these simulations was 200 post-process files.
- **Write message step frequency:** This parameter establishes the frequency that simulation information is written on the screen. It is important to keep up with the simulation development, analysing parameters such as the error and the critical time step. On the other hand, a high frequency makes the simulations lasts longer because of the writing process.
- **CPU:** This parameter represents the number of CPU cores that will be dedicated to the simulation. Theoretically, greater the number of CPUs dedicated to the simulation, faster it goes, but non cluster computers are not designed to work with a huge amount of writing and reading at the same time as the simulation needs. This happens because PCs uses the low memory bus, i.e., the calculations are divided between the CPUs but the writing and reading became the process bottleneck. To choose this parameter, a tensile strength test were made, changing just the number of

CPUs used, starting with 1 until 8, which is the total number of CPUs in the simulation computer used.

Based on the FEM model created, both Explicit and Implicit time integration simulationswere performed.

7.4.1. Explicit FEM

The Explicit time integration was carried using the model from the previous section. In addition to the activation of the explicit time integration calculus module, there must be set a critical time step factor, an explicit exclusive property. This factor is multiplied to the critical time step in order to guarantee the simulation stability. The factor value must be greater than zero and with maximum value equals one. By default, the value of this variable is 0.8 and this is necessary because the explicit stability condition depends on the critical time step and working on the stability edge can lead to the divergence of the algorithm.

Considering that the explicit time integration calculates a critical time step that will be the time increment of the simulation, it is interesting to decrease the end time simulation, in order to simulate faster without compromising the accuracy of the results. The counter part of the end time decrease is the fact that a very fast simulation can lead to a dynamic effect, different from the microindentation experiment made, which constitutes a quasistatic process, where dynamic forces can be neglected and there is no need to establish a dumping factor.

Aiming to decrease the end time of the explicit FEM model, three models were created, decreasing the simulation end time 10x for each simulation. For simulations with lower end time, the FEM model diverges.

7.4.2. Scale Problem

Even with XZ and YZ planes symmetry and a gradual mesh to make possible to simulate with lower total time and the whole model being designed with millimetres as the length base unity (which makes the element size needed to represent the phenomenon bigger), the simulation process took an enormous amount of time to finish, making the idea of several simulations unbearable.

In order to reduce the simulation total execution time, properties scale were applied, more specifically a mass scale, which increases the material density aiming to increase the critical time step that leads the whole model simulation.The density were multiplied by 10^3 and became $\rho = 8.96.10^{-3}$.

Another scale made was in the time vs. displacement curve applied as boundary condition to the indenter. The curve shape remained the same but the time axis were all multiplied by 10^{-3}, 10^{-4} and 10^{-5} to check how far the curve time could be reduced , without entering a dynamic problem, which would change the assumptions made.

7.4.3. Implicit FEM

The total execution time problem persists even considering that the explicit time integration converges, the total simulation time is too big to make several simulations in order to study the microindentation test related phenomena. To decrease the total simulation time, was created an implicit time integration model, using the FEM model parameters from section 7.4.

In the implicit time integration, there are also some exclusive properties that must be set to make the FEM model to converge. The adaptive critical time step parameter were activated to allow the time increment to be fragmented (by half) when iteration doesn’t achieve convergence. The Line search parameterwas enabled and it finds the magnitude of the minimum error direction solution vector.

7.4.4. SecondT x D (Time vs. Displacement) Simulation

After simulating the microindentation test, with explicit and implicit time integration and obtaining similar results, these were compared with the experimental data, which had a different outcome.

Considering the possibility that the machine undergoes elastic deformation (machine stiffness), or even had some sort of gap in its assembly that could absorb the tip of the indenter displacement, resulting in milder indentation. To make sure that this was happening, a second simulation were made, with maximum displacement of the microindentation test centre point (measured in the Laser Interferometry), chosen as the maximum displacement of the indenter tip, as shown in the Fig. 7.10, considering the amount of elastic recuperation.

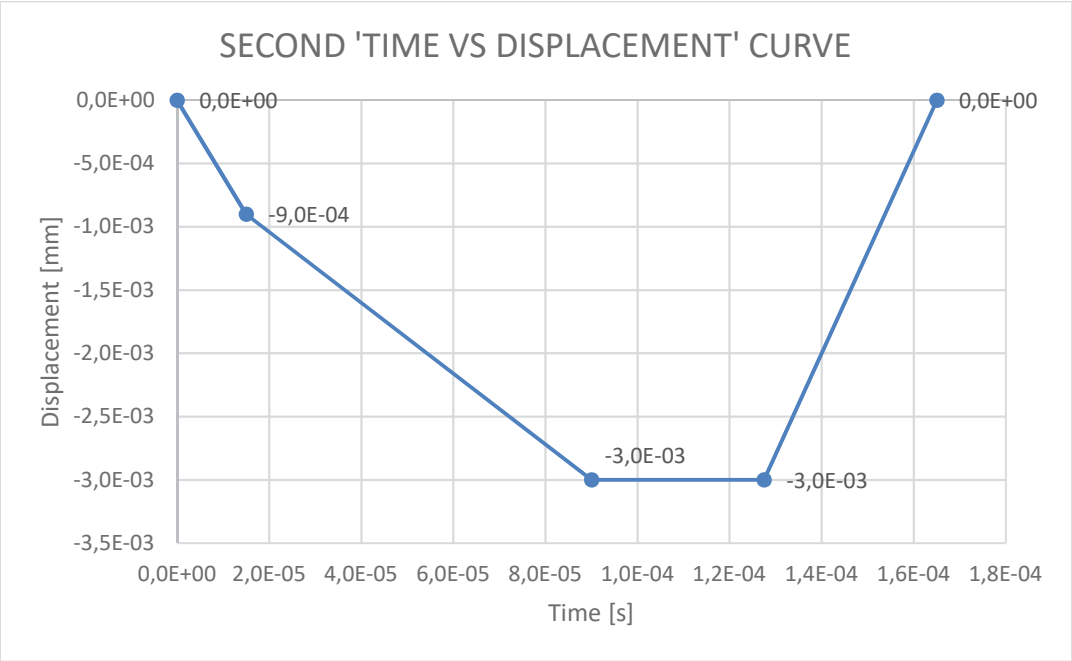

Fig. 7.10. Second ‘Time vs Displacement’ curve imposed on the top surface indenter nodes

For all simulations were used the same hardware, constituted by an 8 Core, 4. GHz and 16.0 MB total cache processor, 32Gb DDR 3 RAM memory, 250 Gb SSD and 1Tb HDD for simulations storage.

CHAPTER VIII

RESULTS AND DISCUSSION

The main contribution of this work is the implementation of an explicit finite element method formulation, which uses the contact mesh approach and the small elastic and large plastic deformations material. All these features must work inside the academic FORTRAN90 based software COMFORM and to test the correct operation of the whole system, a severe contact problem, microindentation test, were proposed.

8.1. Number of Cores convergence

As a preliminary result, it must be pointed the number of CPUs used in all simulations. The tests were made with 1 to 8 cores, according to the number of cores of the used PC and the total simulation time for each number of CPUs composes the Table 8.1. The model used for all tests were the tensile strength experiment, with tetrahedral elements.

The number of CPUs chosen for all simulations were 2, considering that it was the fastest simulation and the results were the same as the simulation with only one core. The increasing in simulation time for more cores is explained by the writing and reading queue formed by the huge amount of simultaneous calculations made. Also the simulation results changed progressively, together with the increasing of time, leading on the algorithm divergence for 6 or more CPUs.

Table 8.1. Simulation time for different number of CPUs

Number of CPUs	Total Simulation Time
1	25 minutes and 36 seconds
2	12 minutes and 51 seconds
3	14 minutes and 58 seconds
4	16 minutes and 12 seconds
5	24 minutes and 23 seconds
6	Divergence of the algorithm
7	Divergence of the algorithm
8	Divergence of the algorithm

8.2. Convergence and Interaction of the implemented modulus inside COMFORM

The convergence and interaction of the implemented modulus with all other COMFORM modules is a qualitative test, based on the convergence of the whole algorithm. The fact that the algorithm worked for models with explicit time integration and Small Elastic and Large Plastic Deformations material model is enough to endorse the implementation coherence, before validate the given results.

8.3. Hardening properties for the Copper Specimen

The MatLab® algorithm created to minimize the error between the experimental and theoretically calculated Stress vs. Strain curve converged for the seeds of the hardening exponent *n* of 0.25 and hardening modulus *k*of 400 MPa (which are common values for a Copper Specimen). The number of function evaluations (iterations) ranged from 10 to 300 and the results are shown in the table 8.2.

Table 8.2. Material Properties approximation Algorithm Results

Number of Function Evaluations	Total Execution Time	*k[MPa]*	*n*
10	1.26 seconds	420.0000	0.2500
50	4.50 seconds	446.1829	0.2797
100	8.51 seconds	446.2089	0.2797
200	16.46 seconds	446.2088	0.2797
300	16.87 seconds	446.2088	0.2797

Even considering that the seeds of *n* and *k* are the normal values for those parameters in Copper Specimens, it was necessary to check the influence of the seeds provided and for that 5 tests were made. The results of those tests are in the table 8.3. To guarantee the function evaluations stabilization, all seed tests were made using 300 function evaluations.

Table 8.3. Minimization Algorithm Seeds Test

Seed *n*	Seed *k*[MPa]	*k* [MPa]	*n*
0.1	**100**	446.2088	0.2797
0.25	**400**	446.2088	0.2797
1.0	**1000**	446.2088	0.2797

The Table 8.3 shows that the seed chosen did not affect the algorithm result and also that the number of evaluations was enough to achieve the minimum error given by this method. Therefore, the hardening properties used for all simulations were 446.2088 [MPa] for the hardening modulus and 0.2797 for the hardening exponent.

Figure 8.1 shows the result given by the error minimization algorithm, a Stress vs. Strain curve, where the blue dashed line is the experimental curve and the red continuous line is the calculated curve.

It is important to note that the experimental data were treated to eliminate the final part of the tensile strength experimental test, where the Stress start decreasing despite of the increasing Strain, characterized by the specimen cross section reduction (necking).

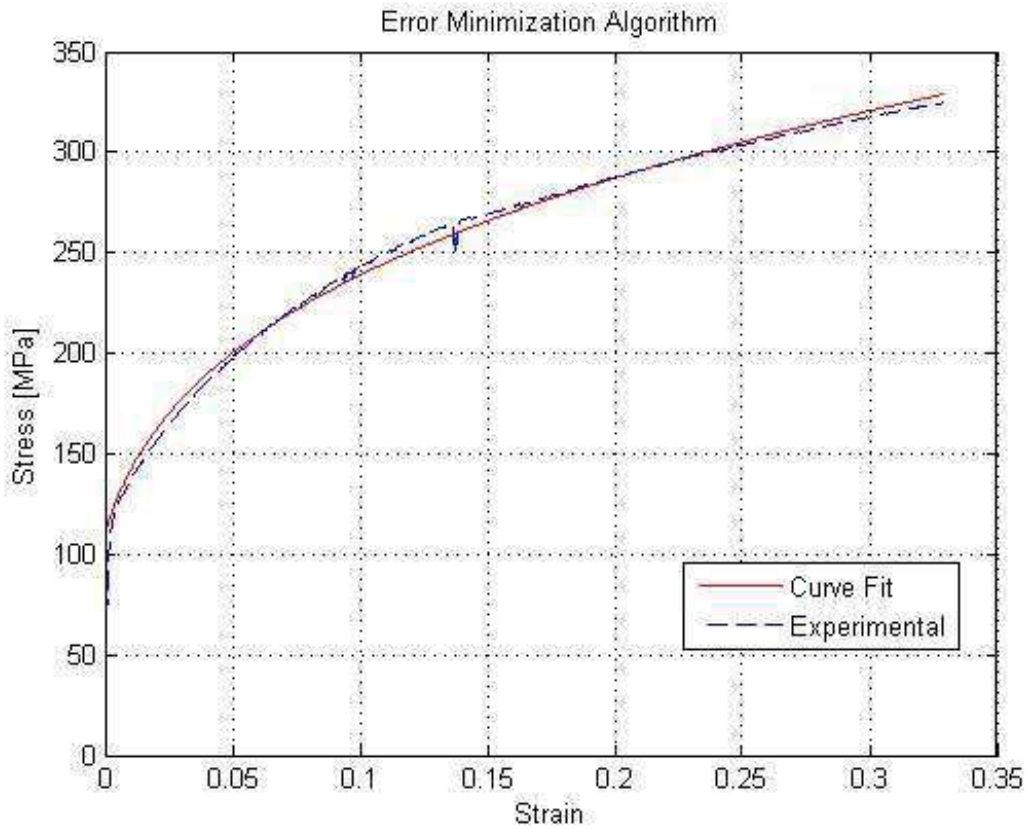

Fig. 8.1. Error minimization algorithm curve

8.4. Validation of the model with tensile strength test

In order to validate the FEM model implemented, two models of tensile strength experimentwere used, one with hexahedral and the other with tetrahedral elements, characterized in section 7.2. Using those models, a Force vs. Displacement set of curves were made and they are in the Fig. 8.2

The red curve is the experimental data from the tensile strength test and it shows a slip region during the plastic deformation zone, probably caused by the extraction process of the extensometer. The calibration curve (blue) is calculated using the constitutive laws for the elastic and plastic zones and uses properties from sections 7.2 and 8.2. The Tetrahedral and Hexahedral COMFORM curves are calculated in a similar way, where all the forces in the top surface nodes are summed and the displacement is taken just for one node (all nodes undergo the same displacement condition, which were imposed as a boundary condition).

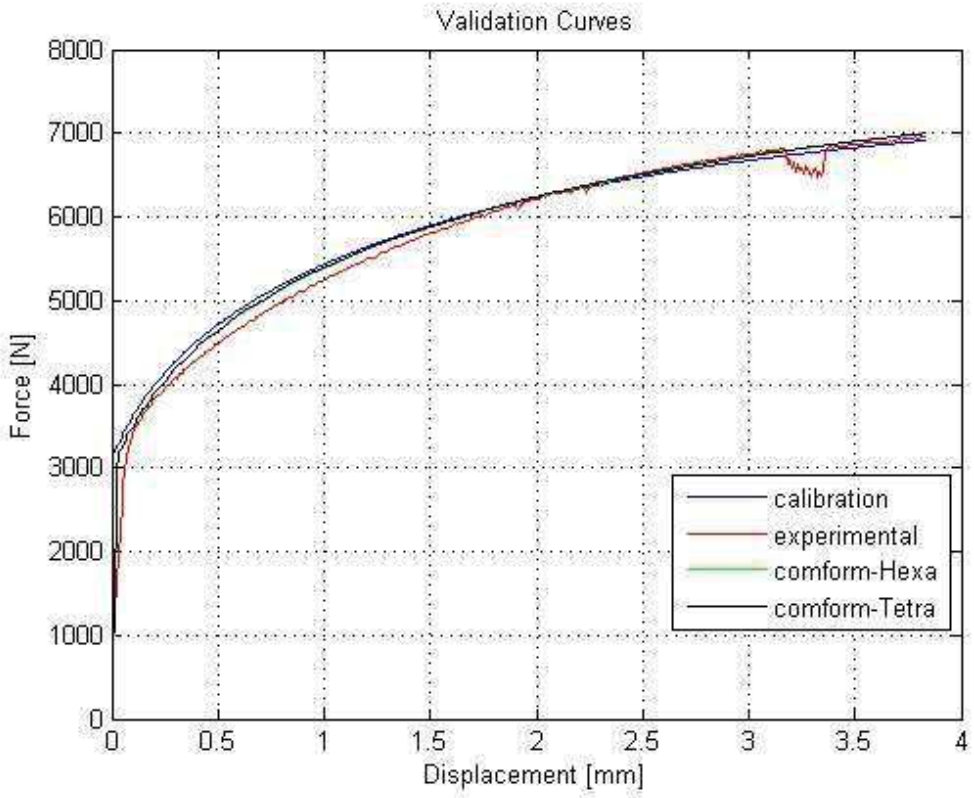

Fig. 8.2. Validation Force vs. Displacement Curves

Figure 8.3 represents the total displacement for tensile strength FEM simulation with Tetrahedral Elements. The model with hexahedral elements is similar, with displacement and force results differing around 1%.

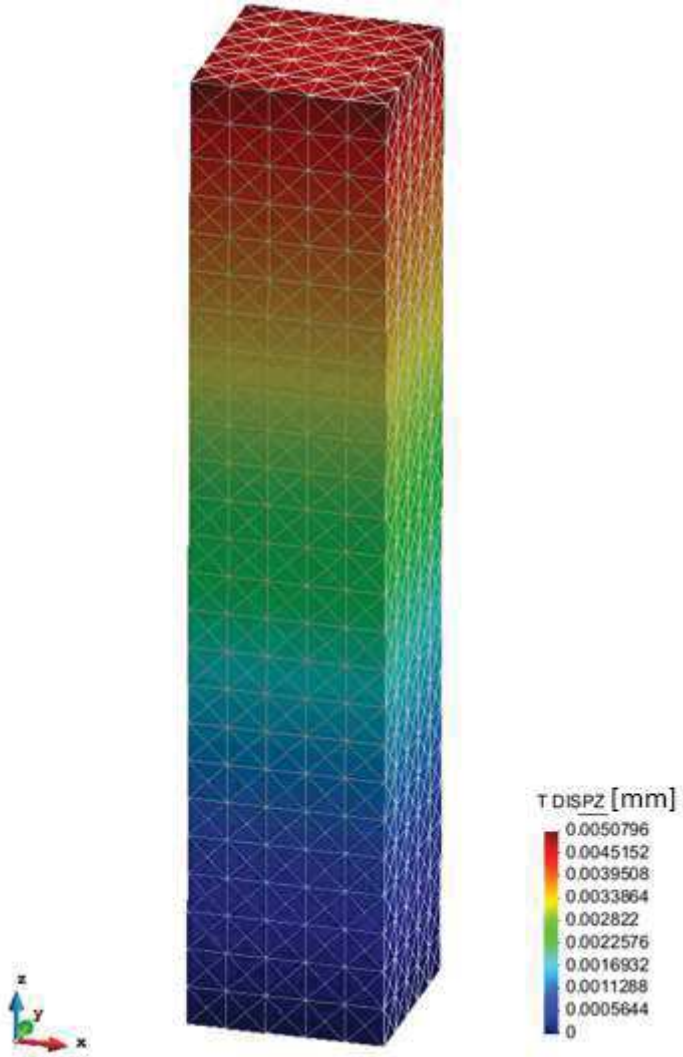

Fig. 8.3. Displacement in the tensile strength FEM simulation

Figure 8.4 shows the equivalent Von Mises stress for the tensile strength test simulation, with tetrahedral elements. It is possible to notice that the corners are stress concentration areas and that the whole specimen undergo similar stress, differing only near the load application areas, according to Saint-Venant principle (NAKAMURA, 1995). The lower part of the specimen show non uniform results because of the X and Y axis restriction.

Validated the FEM model (explicit time integration and Small Elastic and Large Plastic Deformation material model), the next stage were to simulate the microindentation test.

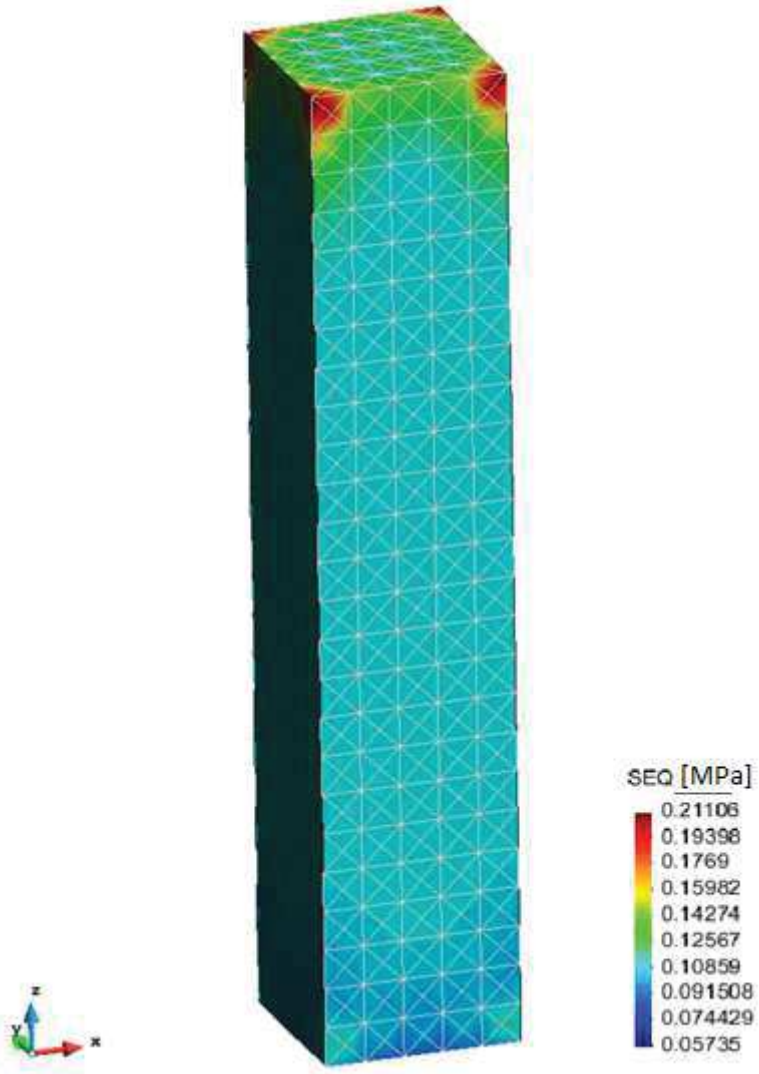

Fig. 8.4. Equivalent Von Mises Stresses for the tensile strength simulation in MPa.

8.5. Microindentation FEM Simulation

The microindentation test simulation started with the explicit time integration resolution, aiming to comprehend the Copper specimen deformation development during the microindentation test and the spring-back phenomenon. Considering that the first simulations predicted a total simulation time of around 300 hours (~ 12 days) and the model already had symmetry and scale, the time axis of the time displacement curve were multiplied by scale factors of 10^{-3}, 10^{-4} and 10^{-5}, virtually increasing the indentation velocity. The increasing of velocities could lead to a dynamic problem, instead of the quasistatic problem proposed. All models converged with total execution time shown in table 8.4.

Table 8.4. Total execution time for different Time vs. Displacement curve scales

Scale	Total Execution Time
10^{-3}	**~70 h**
10^{-4}	**~40 h**
10^{-5}	**~10 h**

The first two scales results in similar results (error around 3%) but the third and bigger scale give different results, probably cause by the non-dumped dynamic phenomenon or even an algorithm divergence. This effect can be seen on Fig. 8.5, which shows the Z axis displacement experienced by the central Copper Specimen node, during the 10^{-5} time scale.

With the scale factor results considered, the Time vs. Displacement curve would be scaled by 10^{-4}, with stage end time of $1.6.10^{-4}$. The Fig. 8.6 shows the Z Displacement of the central specimen node. In this figure, the Time axis was multiplied by 10 for the 10^{-4} factor, to guarantee the correct comparison of results.

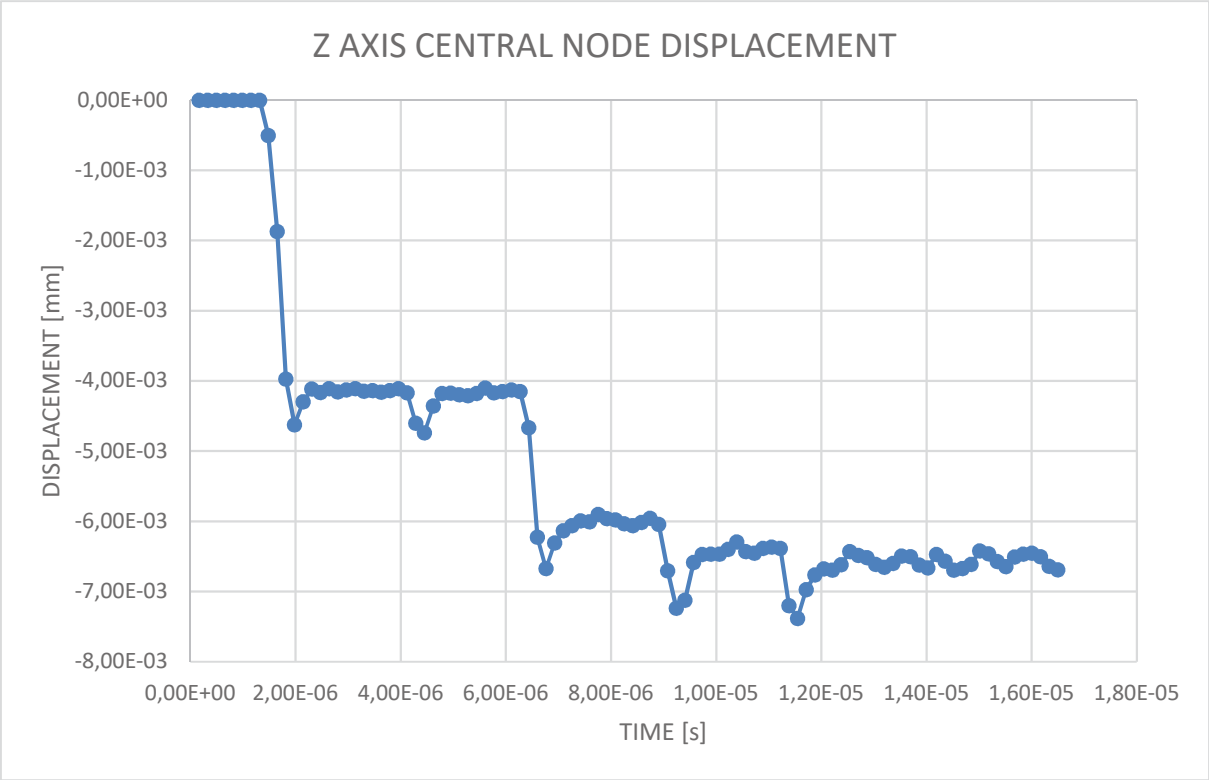

Fig. 8.5. Centre Specimen node Z Displacement for 10^{-5}Scale

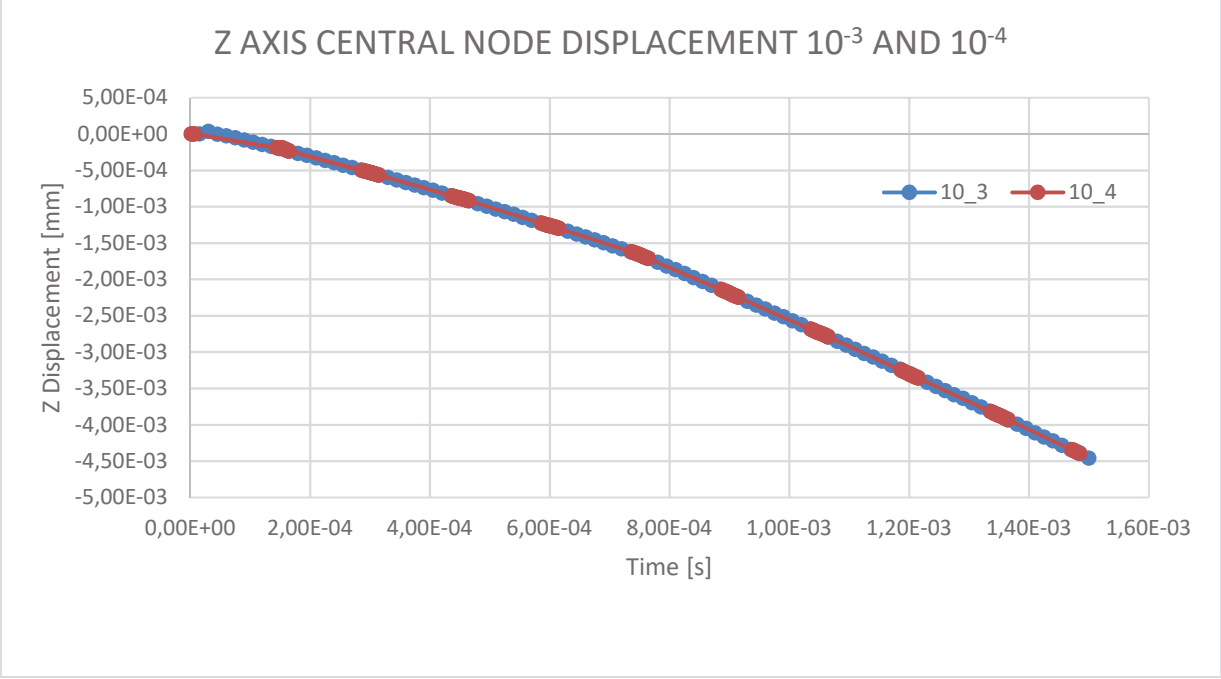

Fig. 8.6. Centre Specimen node Z Displacement for $10^{-3}$and 10^{-4} Scale

In the Fig. 8.6 the different curve aspect between the two scales happens because for the 10^{-4} scale it was not loaded all results. This was made to allow the correct visualization, otherwise only one curve would be seen.

8.5.1. Explicit Time Integration Microindentation FEM Model

Considering the previous results of convergence, properties and scale, the microindentation FEM simulation were made, presenting total displacement in the Z axis in Fig. 8.7.

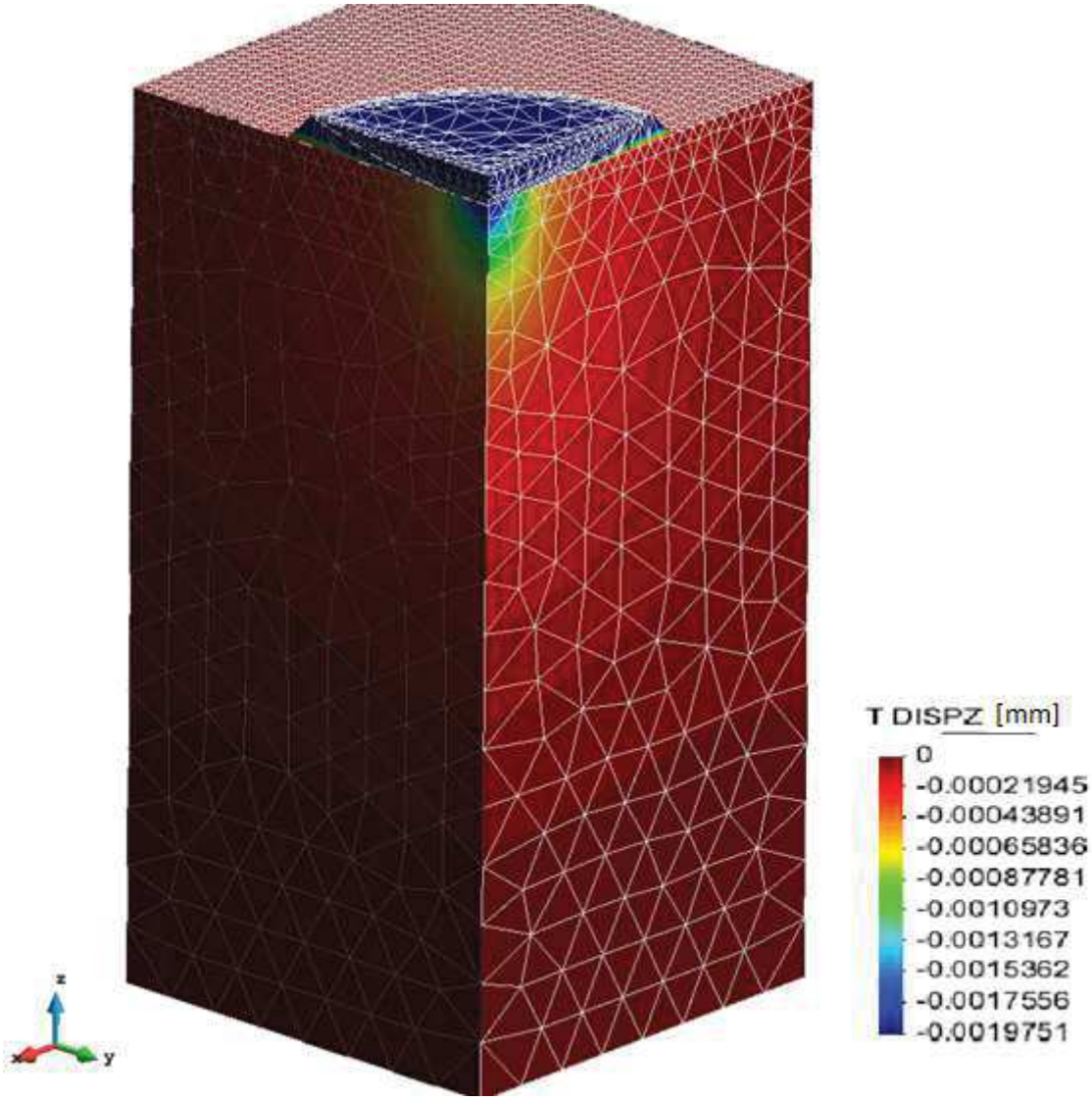

Fig. 8.7. Z Displacement of the Explicit Model.

In order to guarantee better visualization, the model can be subdivided in the Contact Mesh (Fig. 8.8), the Z Displacement for the Copper Specimen (Fig. 8.9) and the Z Displacement for the indenter (Fig. 8.10). It is possible to note in Fig.8.10 that the indenter had gradual distribution of the Z Displacement, suggesting that it undergoes some deformation. The Fig. 8.11 shows that the deformation in the indenter is purely elastic deformation, considering that the Von Mises equivalent stress is lower than the tool steel yield stress.

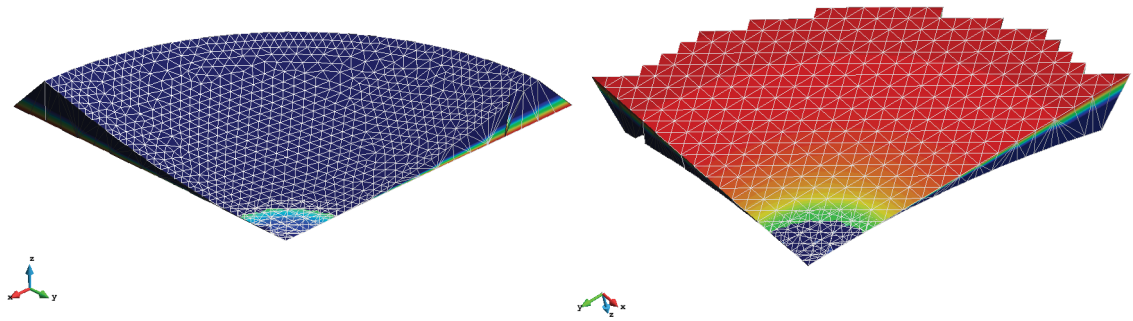

Fig.8.8. Top and Bottom surface of the Explicit Contact Mesh

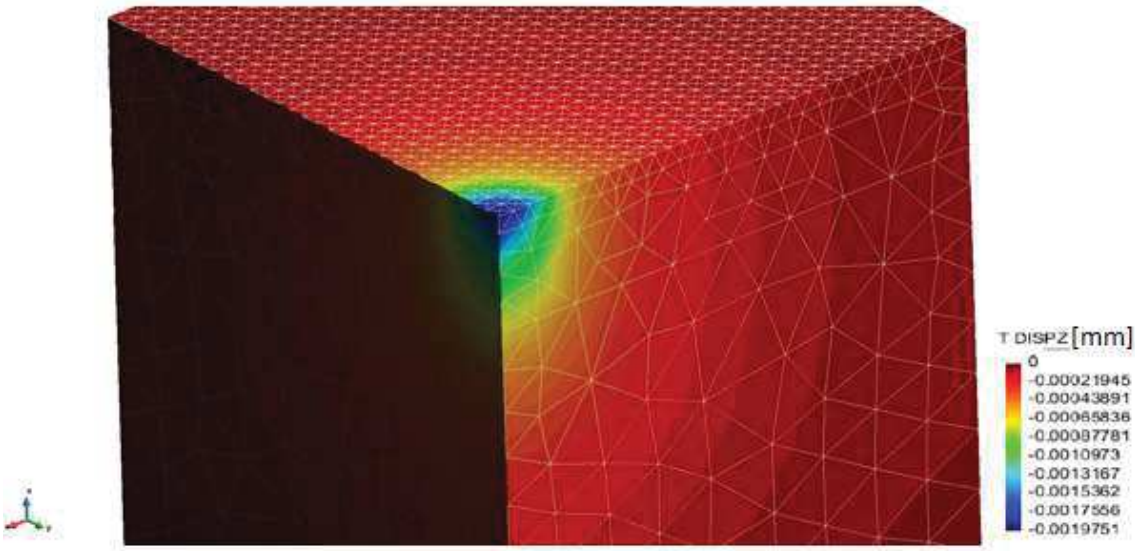

Fig. 8.9. Z Displacement Explicit Results for the Copper Specimen, at the end of the loading.

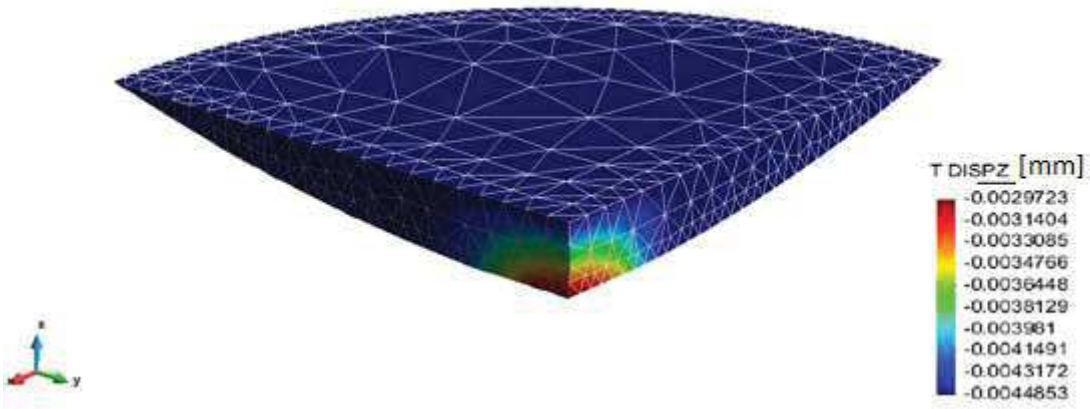

Fig.8.10. Z Displacement Explicit Results for the Indenter.

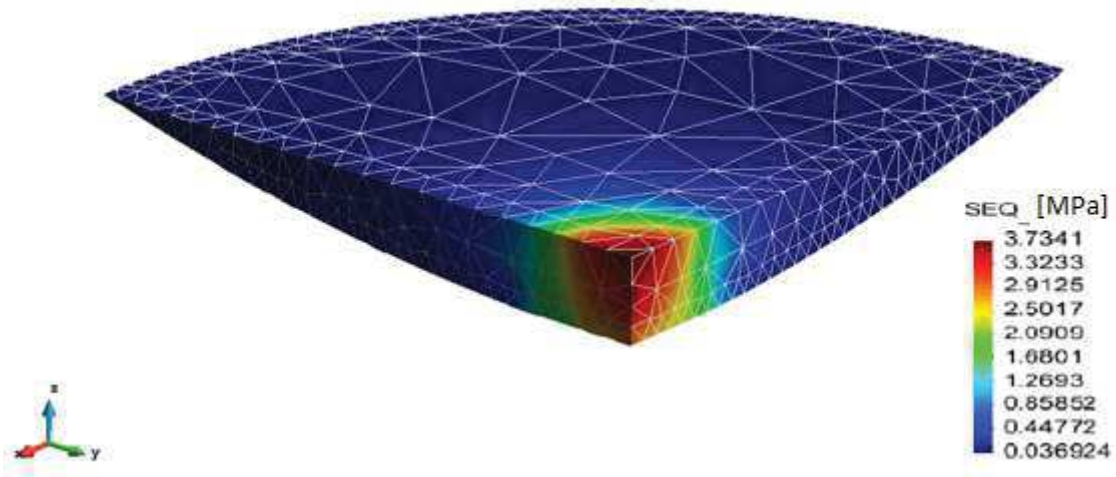

Fig.8.11. Equivalent Von Mises Stress for the Explicit Results for the Indenter.

The explicit simulationsshows smooth transition and algorithm convergence, with FEM internal calculus errors under the tolerance given by the FEM algorithm, which were 10^{-6}. All this suggests a good simulation and results, but the experimental Laser Interferometry results used as parameter to validate shows a total displacement of the centre point of the indentation mark, after the spring-back, ofapproximately 1.5µm, as shown in section 6.2 (Fig. 6.6). The total simulation depth, in the centre node of the copper specimen were 2.64µm.

The difference between the experiment and the FEM simulation could come from different sources.

- **Implementation errors:** The explicit time integration or the Small Elastic and Large Plastic Deformations Material Formulation could be incorrect. This hypothesis is improbable, considering that these implementations were validated with tensile strength experimental data, section 8.3.
- **Contact Problems:** The validation was made in a tensile strength example, which has no contact. This hypothesis is also unlikely to be true, because an incorrect contact approach would be seen in the FEM model as a big penetration of meshes or a rough transition of the simulation results, different from what is shown in the figures above (Figs. 8.7 to 8.11).
- **Experimental error due to the machine stiffness:** This hypothesis suggests that the machine somehow (elastic deformation or construction gap) could mask the deformation actually imposed to the Copper Specimen. To test this hypothesis, it was made a second simulation, with a different Time vs. Displacement curve, section 7.4.4. The results will be shown together in the following sections.

8.5.2. Implicit Time Integration FEM Model

An Implicit approach could solve the total simulation time problem, for future works where several simulations can be made, also could reinforce the machine stiffness problem, considering that the implicit model were simulated first with the second T x D curve from section 7.4.4 and then with the first curve. The total simulation time for the first simulation of the implicit model were 1 hour, 24 minutes and 17 seconds, which constitutes a difference of more than 26 times the value of approximate 40 hours, took by the explicit time integration model.

Similar results for the implicit simulation were obtained, when compared with the explicit one simulated with the second T x D curve, as it can be seen on Figs. 8.12 to 8.15, these results are the Z Displacement of the whole model, top and bottom surface of the contact mesh, Z Displacement for the Copper Specimen, Z Displacement for the indenter and the Von Mises Equivalent Stress for the indenter, respectively.

It is quite notable that the results patterns are almost the same for both models, first and second T x D curves, as expected, considering that the only difference is the depth range.

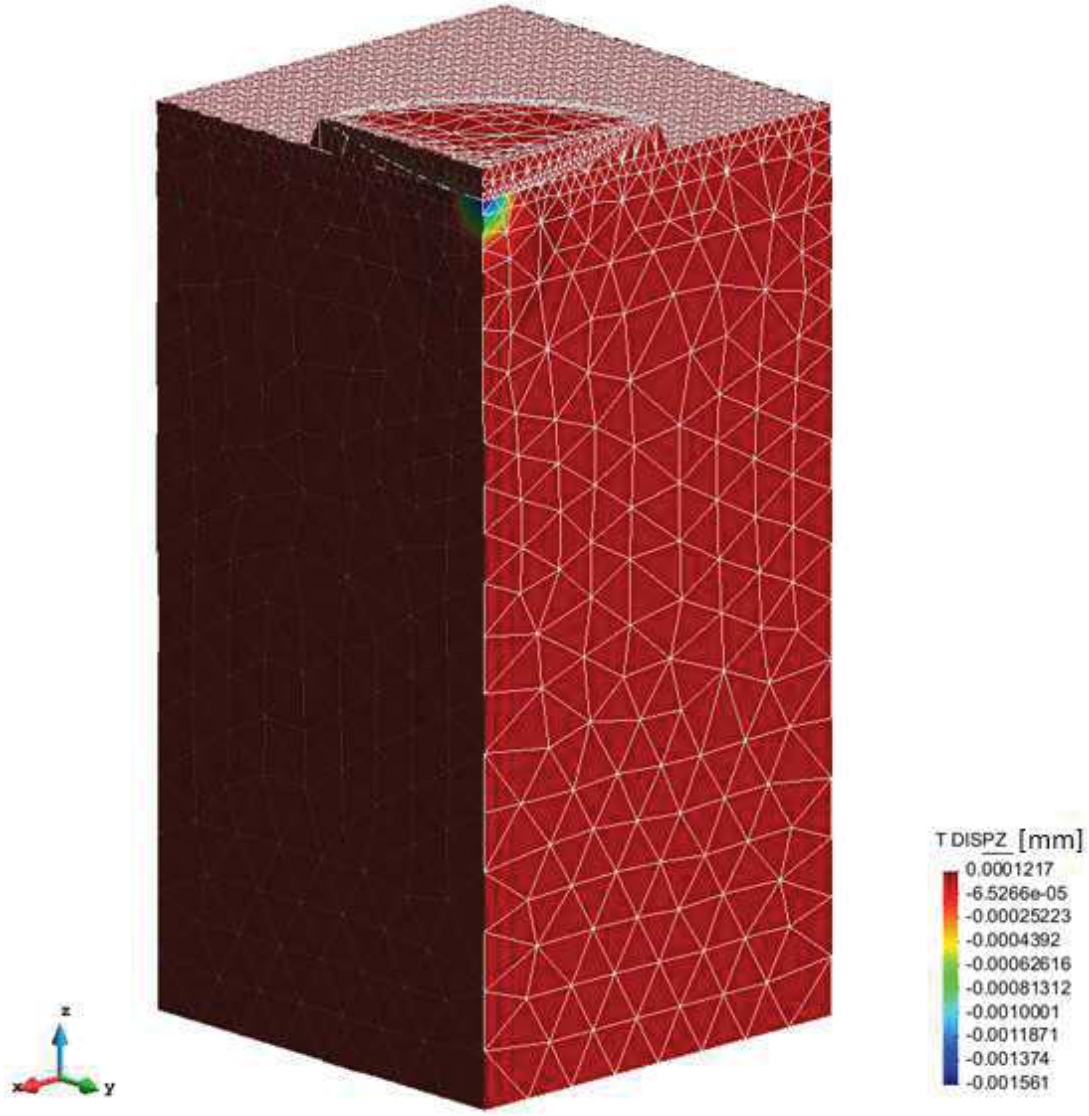

Fig. 8.12. Z Displacement of the Implicit Model.

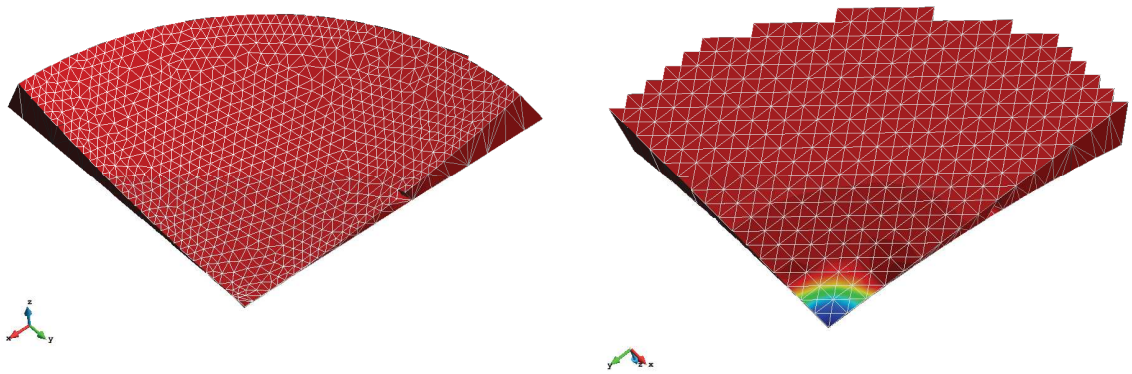

Fig. 8.13.Top and Bottom surface of the Implicit Contact Mesh

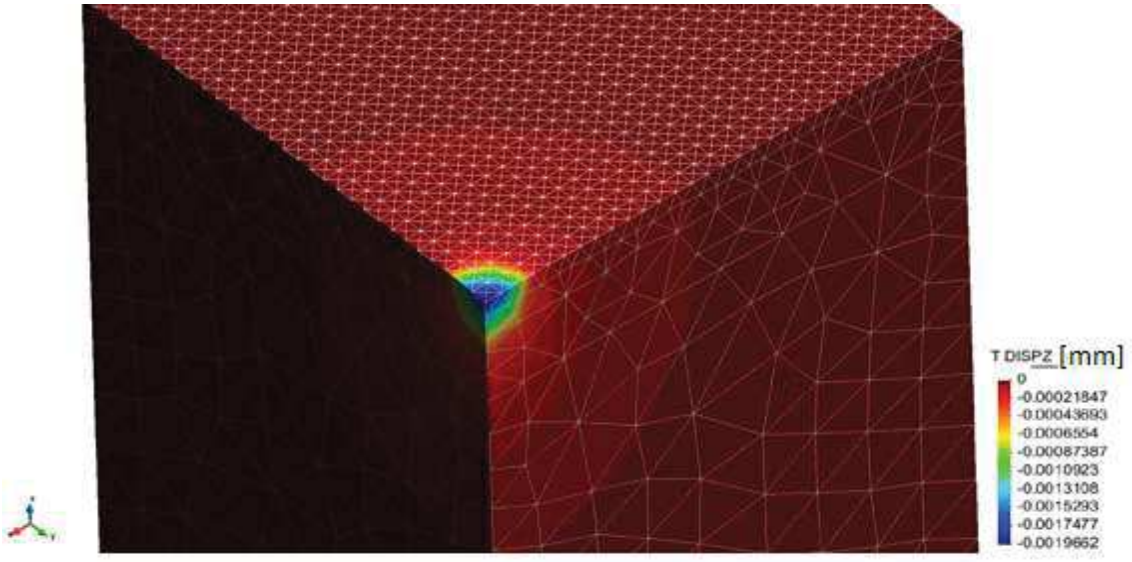

Fig. 8.14. Z Displacement Implicit Results for the Copper Specimen, at the end of the Loading.

For better visualization, the centre and the subsequent nodes in the X axis were taken, as given by Fig. 8.16. The result displayed is the Z Displacement, after the spring-back. And for the Explicit and Implicit time integration, using the second T x D curve, the Z displacement of the selected nodes is in the Fig 8.17.

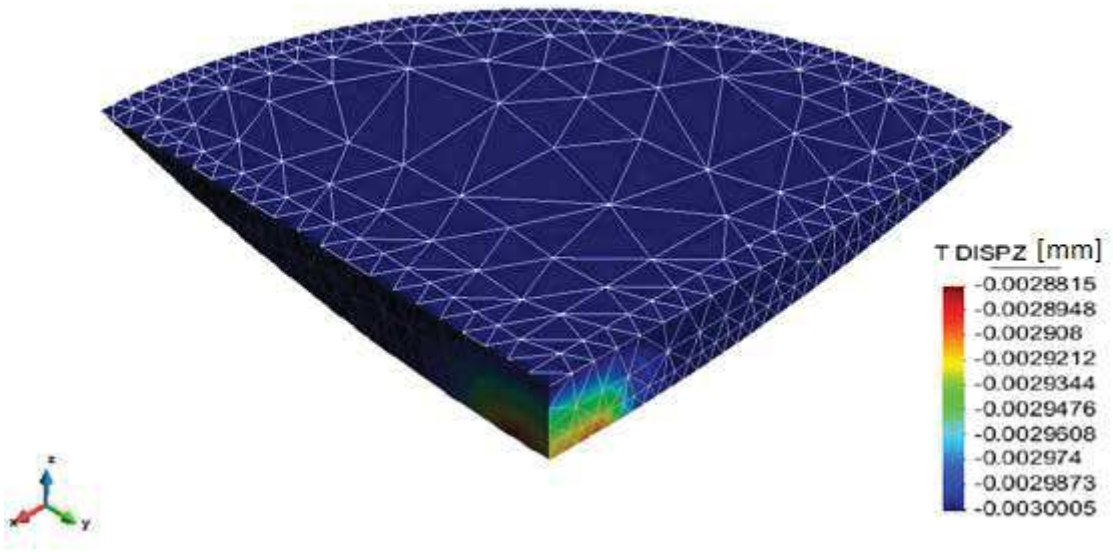

Fig. 8.15.Z Displacement Implicit Results for the Indenter.

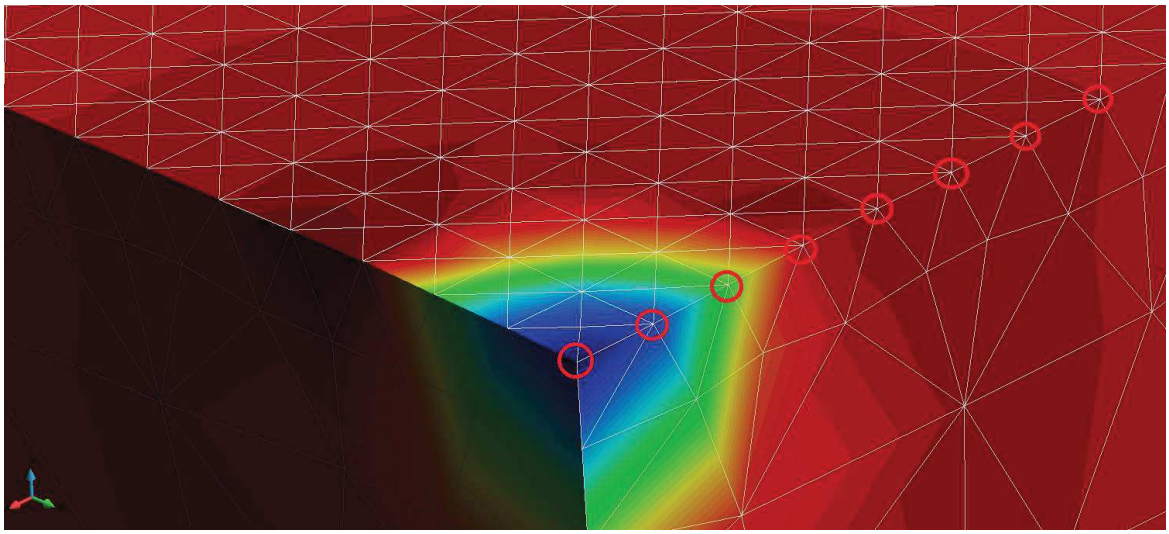

Fig. 8.16. Nodes taken in the surface, X axis, to analysethe microindentation Z displacement profile.

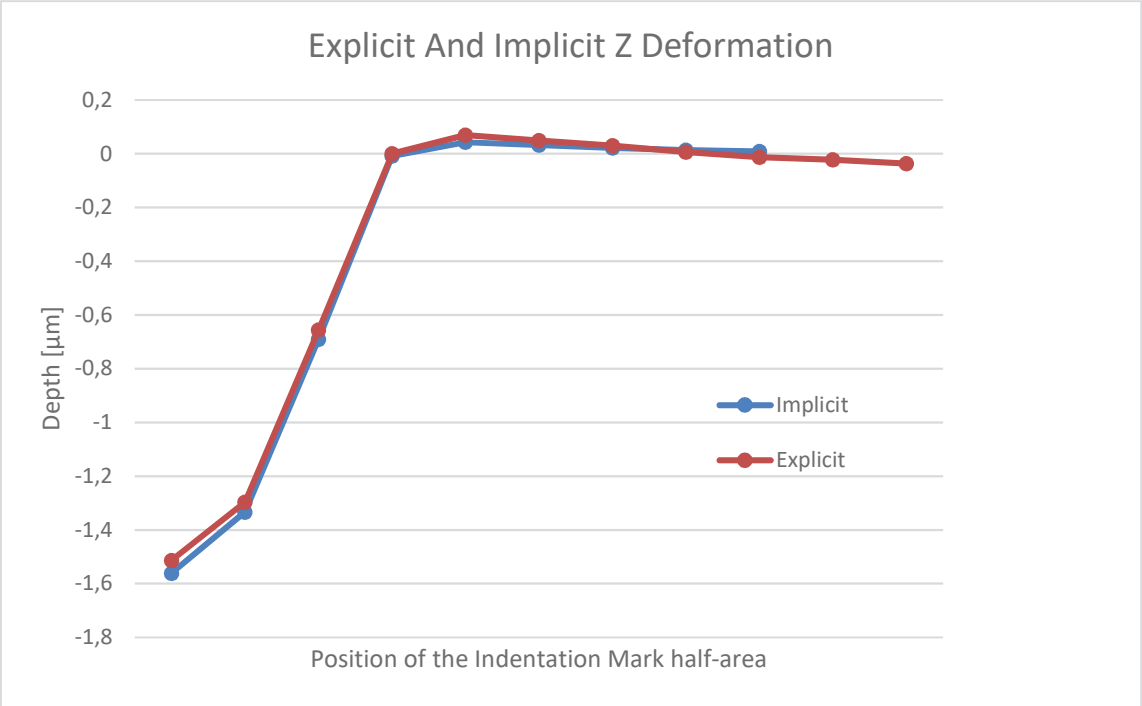

Fig. 8.17. Implicit and Explicit Indentation depth half-area mark

As it can be seen on Fig. 8.17, the implicit and explicit results are close and represent the microindentation test related phenomena, such as the pile up formed just after the indentation mark. Comparing these results with the experimental roughness curve for the 5N Brinell Indentation it is possible to note the results similarity. The centre node maximum depth goes around 1.5µm for the experiment, while the simulation give as results for the explicit and implicit 1.5132 and 1.5610µm respectively.

The Implicit result of the central and X nodes depth using the first Time vs. Displacement is shown in Fig. 8.18. This result of the centre node is 2.6351µm, which is really close from the result obtained for the explicit model, 2.64µm, and also similar to the result obtained by Da Silva (2008) in the experimental microindentation test made with 10N force and 2.5mm Brinell indenter from section 6.2, which were approximately obtained from the roughness profile as 2.6µm.

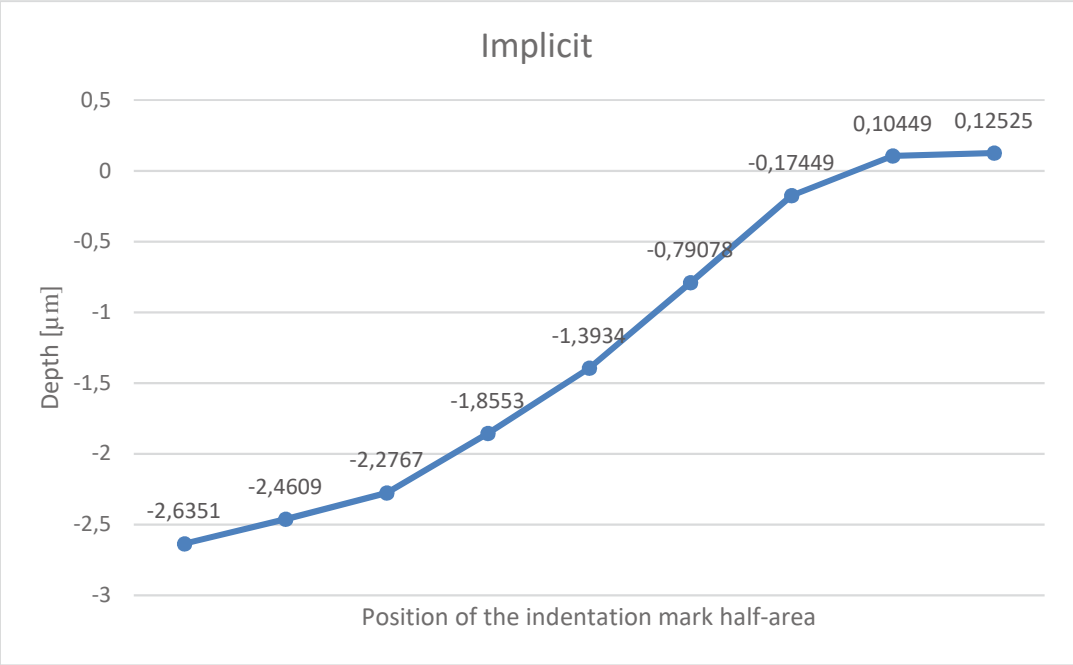

Fig. 8.18.Implicit Indentation depth half-area mark for the first Time vs. Displacement curve

In the Fig. 8.18 is also possible to observe the forming pile up. The Force vs. Displacement curve were also analysed, and for that the force of all nodes from the top surface of the indenter were summed and multiplied by 4 (considering the X and Y axis symmetry), this result is shown in Fig 8.19.

Comparing the Fig. 8.19 with the 5N Brinell Indentation Force vs. Displacement curve (Fig.6.2) it is possible to observe that they start the force application in different points because the indenter distance from the Copper specimen is different. The Load in the simulation is smoother and achieves a greater maximum value. The unloading is fast in both experiment and simulation and the difference from the point where the force leaves and come back to the zero Force (which represents the plastic deformation) is similar, as said above.

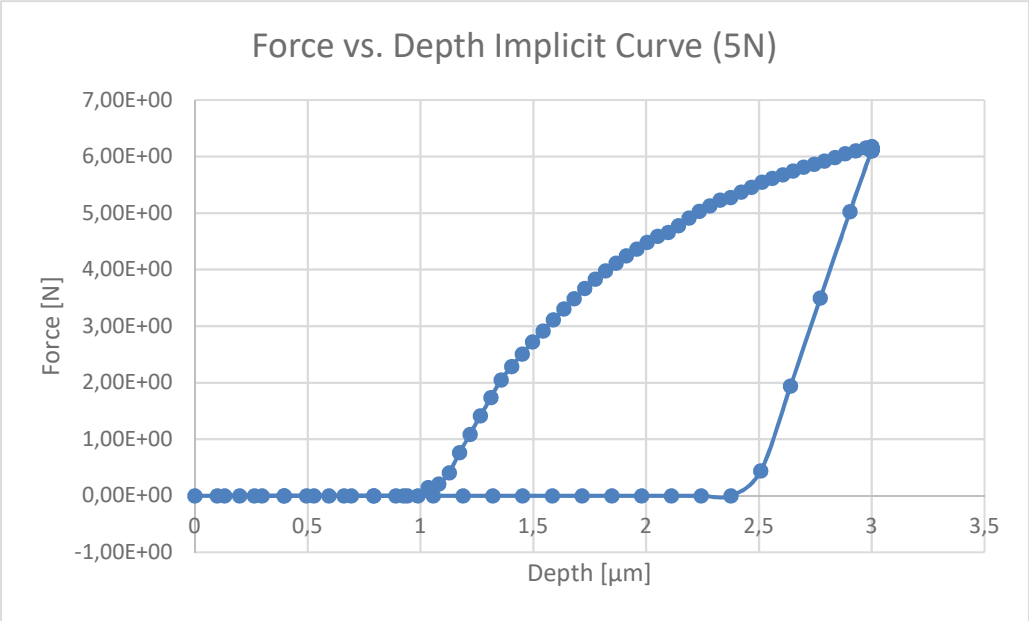

Fig. 8.19. Force vs. Depth Implicit curve for the second T x D curve.

8.5.3. Pile up

The pile up phenomenon is an elevation in the near indentation area, normally seen on indented specimens. Figure 8.20 shows the pile up evolution during the microindentation test for the node with greatest pile up final value, with a Z Displacement vs. Time Curve. The model used in this analysis was the Implicit FEM model with the second T x D curve.

Analysing the Fig. 8.20 in comparison with the Time vs. Displacement curve used as boundary condition for this simulation, the elevation of the node towards the +Z axis, the pile up, is more evident during the unload stage. The unload stage is characterized by the spring-back, which goes against the deformation direction.

Considering that the microindentation test causes a radial mark, the elastic recuperation is radial, from the indentation centre towards to its ends. But when the indentation depth increases, the deformation direction became inclined, making the elastic recuperation to be toward to the surface, causing the pile up.

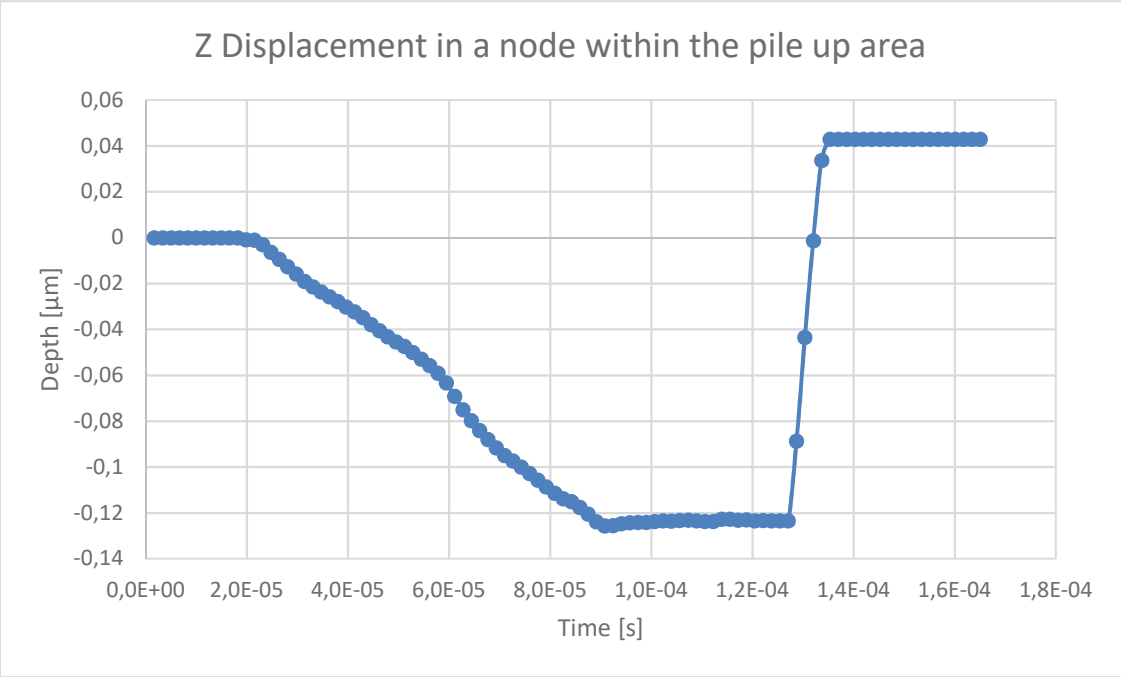

Fig.8.20. Z Displacement in a node within the pile up area

CHAPTER IX

CONCLUSION

This work proposed an implementation of an explicit time integration FEM model that could use an innovative contact approach, the contact domain method or contact mesh. Along with the implementation, the validation and the study of microindentation related phenomena, which are cases where the contact plays an important role in the FEM simulation results. From the results and discussion presented in the previous chapter, it could be concluded that:

1. The COMFORM software is a robust tool to simulate different problems, also to implement new tools for specific cases, because of its language (FORTRAN90) which is consolidated for simulation purposes and for its modular structure, which allows the complete integration of new modules with interaction with all other program modulus.
2. The Explicit time Integration and the Small Elastic and Large Plastic Deformation Material Formulation Modules worked with the other COMFORM modules, stated by the convergence of the whole algorithm.

3. The Methodology of error minimization used to obtain the hardening properties (hardening exponent and hardening modulus) for the Ludwik-Nadai Hardening criteria is valuable.This was affirmed by the direct comparison of the approximated curve with the experimental stress vs. strain curve in the tensile strength test. Other comparison was made between the experimental curve and the FEM simulated tensile strength model curve.
4. In this case, it is possible to use properties scale and remain in a quasistatic problem, decreasing the total simulation time for explicit models, considering that the density and the elastic modulus are used to calculate the critical time step.
5. It is possible to decrease the simulation total time by decreasing the simulation end timeand remain in a quasistatic problem. This configures an increasing of the indentation velocity and for the microindentation model created it was stable and remained quasistatic for a maximum multiplying factor of 10^{-4}.
6. The Explicit and Implicit time integration methods, working with contact mesh, give similar results compared with experimental tests and also with each other.
7. In this case, even with properties and end time scale, the implicit method provides lower total simulation times when compared with the explicit time integration, with similar results.
8. Analysing the Force vs. Displacement curves and the indentation marks, after spring-back, it is possible to infer that the testing machine used to perform the microindentation tests probably has a construction problem which mask the total displacement actually given to the Copper Specimen. This problem probably relies on the machine stiffness, which could undergo elastic deformations during the Force appliance or there could be construction gaps in the machine assembly.
9. The pile up phenomenon is more evident when the specimen is going through the elastic recuperation, the spring-back. This happens because the deformation direction changes from horizontal and

radial(microindentation start) to inclined and towards the Specimen surface, in the positive direction of theZ axis in the FEM model created.

CHAPTER X

FUTURE WORK

Considering that the FEM contact mesh worked for explicit and implicit time integration, with experimental validated results, some problems could be studied in future work, such as:

- Creating a micro scratch simulation model, probably with implicit time integration because of the total simulation time, and performing more than one scratch, changing the distance between the scratches centre mark. The scratches overlap could show interrelated results that would lead to a better abrasion wear comprehension.
- Creating a FEM model of a rolling particle over a specimen surface, also to study the abrasion wear phenomenon.
- Use the methodology to get material hardening properties in other materials and also with other material formulations, in order to validate it for several materials.
- Making other experimental/FEM microindentation tests to comprehend better the pileup phenomena and its influence in the debris generation.

CHAPTER XI

REFERENCES

ADAMS, G.G., NOSONOVSKY, M., **CONTACT MODELING - FORCES**, Tribology International 33, 2000.

ASSOCIAÇÃO BRASILEIRA DE NORMAS TÉCNICAS (ABNT), **NBR ISO 6892-1 2013 VERSÃO CORRIGIDA: 2015,** Materiais Metálicos – Ensaio de Tração Parte 1: Método de ensaio a temperatura ambiente, 2015.

BANDEIRA, A. A.; GUIMARÃES, C. D.; FREITAS, L. A.; SANTOS, L. M., **ALGORITMOS DE OTIMIZAÇÃO APLICADOS À SOLUÇÃO DE SISTEMAS ESTRUTURAIS NÃO-LINEARES COM RESTRIÇÕES: UMA ABORDAGEM UTILIZANDO OS MÉTODOS DA PENALIDADE E DO LAGRANGIANO AUMENTADO**. Revista Exacta, São Paulo, v. 8, n.3, p. 345-361, 2010

BARKANOV, E., **INTRODUCTION TO THE FINITE ELEMENT METHOD**, Institute of Materials and Structures , Faculty of Civil Engineering, Riga Technical University, 2001.

BELYTSCHKO, T., LIU, W. K., MORAN, B., **NONLINEAR FINITE ELEMENTS FOR CONTINUA AND STRUCTURE**, John Wiley & Sons LTD., 2001.

BERTSEKAS, D.P., **NONLINEAR PROGRAMMING**, Massachusetts Institute of Technology, second edition, Athena Scientific, Belmont, Massachusetts, 1995.

BRAGA, F.V.G., **ANÁLISE DE UM MODELO ELASTOPLÁSTICO PARA CONTATO**, Master Thesis, Programas de pós-graduação de engenharia da Universidade Federal do Rio de Janeiro, Rio de Janeiro, 2008.

BUSHAN, B., **SURFACE ROUGHNESS ANALYSIS AND MEASUREMENT TECHNIQUES,** The Ohio State University, CRC Press LCC, 2001.

CHEN, R., YANG, F., LIAW, P.K., FAN, G., CHOO, H., **MICROINDENTATION OF A $Zr_{57}Ti_5Cu_{20}Ni_8Al_{10}$ BULK METALLIC GLASS**, Special Issue on Bulk Metallic Glasses – Selected Papers from the Fifth International Conference on Bulk Metallic Glasses (BMGV), Materials Transactions, vol. 48, No. 7, pp. 1743 to 1747, The Japan Institute of Metals, 2007.

COSTA, H.L., KLEIN, A.N., DE MELLO, J.D.B, **AVALIAÇÃO DA RESISTÊNCIA AO DESGASTE ABRASIVO DE AÇOS CARBONO NITRETADOS A PLASMA**, XVI CONGRESSO BRASILEIRO DE ENGENHARIA MECÂNICA (COBEM), 2001.

COURTNEY, THOMAS H., **MECHANICAL BEHAVIOR OF MATERIALS**, McGraw-Hill series in materials science and engineering, 2005.

DA SILVA, W. M., **SIMULAÇÃO DO DESGASTE ABRASIVO VIA ITERAÇÕES MÚLTIPLAS**, Tese de Doutorado, 177f., Programa de Pós Graduação em Engenharia Mecânica, Universidade Federal de Uberlândia, Uberlandia, 2008.

DESAI, C.S., ABEL, J.F., **INTRODUCTION TO THE FINITE ELEMENT METHOD**, Van Nostrand, 1972.

DEVARAJU, A., **A CRITICAL REVIEW ON DIFFERENT TYPES OF WEAR OF MATERIALS**, International Journal of Mechanical Engineering and Technology (IJMET), Vol. 6, Issue 11, pp 77-83, 2015.

DINIS, L.; Cap-4, **O MÉTODO DAS DIFERENÇAS FINITAS NA ANÁLISE DE PLACAS RECTANGULARES FINAS**, Placas e Casca, FEUP, 2003/2004.

EKMARK, B., **ON LARGE STRAIN THEORIES IN SHEET METAL FORMING**, PhD Thesis, Lulea University, Sweden, 1983.

FELICE-NETO, F.R., **SIMULATION OF A MULTILAYERED MATERIAL MICROINDENTATION BY FINITE ELEMENT METHOD**, MSc. Dissertation, Federal University of Uberlandia, Uberlandia, 2012.

FELLIPA, C., **INTRODUCTION TO FINITE ELEMENT METHODS**, Department of Aerospace Engineering Sciences, University of Colorado, Boulder, 2015.

FISH, J., SHEK, K., **FINITE DEFORMATION PLASTICITY BASED ON ADDITIVE SPLIT OF THE RATE OF DEFORMATION AND HYPERELASTICITY**, Computer Methods in Applied Mechanics and Engeneering, vol 190, issues 1-2, p. 75 - 93, 2000.

FRANCO S. D.; ZUMPANO, P.; DE MELLO, J. D. B**. Abordagem Global do Estudo do Processo do Abrasivo. Parte II: Desenvolvimento e Avaliação de Abrasômetro a Dois e Três Corpos,** 1° SEMINÁRIO BRASILEIRO DE MATERIAIS RESISTENTES AO DESGASTE ABRASIVO, São Paulo, anais do 1° Seminário Brasileiro de Materiais Resistentes ao Desgaste Abrasivo, pp 47-62, ABM-EPUSP, 1989.

GONZALES, A., **DRUCKER-PRAGER: UM MODELO CONTITUTIVO PARA SOLOS**, Artigotécnico, Engineering Simulation and Scientific Software, 2009.

GREENWOOD, J.A., WILLIAMSON, J.B.P., **CONTACT OF NOMINALLY FLAT SURFACES**, Burndy Corporation Research Division, Norwalk, Connecticut, USA, 1996.

GU, Y., NAKAMURA, T., PRCHLIK, L., SAMPATH, S., WALLACE, J., **MICRO-INDENTATION AND INVERSE ANALYSIS TO CHARACTERIZE ELASTIC-PLASTIC GRADED MATERIALS**, Materials Science and Engineering, Elsevier, 2003.

HARTMANN, S, OLIVER, J., WEYLER, R., CANTE, J.C., HERNANDEZ, J.A., **A CONTACT DOMAIN METHOD FOR LARGE DEFORMATION FRICTIONLESS PROBLEM. PART 2: NUMERICAL ASPECTS**, Computational Methods Applied to Engineering, 198, pg 2607-2631, Elsevier, 2009.

HARTMANN, S,WEYLER, R.,OLIVER, J.,CANTE, J.C.,HERNANDEZ, J.A., **A 3D FRICTIONLESS CONTACT DOMAIN METHOD FOR LARGE DEFORMATION PROBLEMS**, Computer Modeling in Engineering & Science (CMES), vol. 55, no. 3, pp.211-269, Tech Science Press, 2010.

HILL, R., **THE MATHEMATICAL THEORY OF PLASTICITY**, Oxford University Press, Oxford, UK, 1950.

HOLMBERG, K, MATTHEWS, A, **COATINGSTRIBOLOGY – PROPERTIES, MECHANISMS, TECHNIQUES AND APPLICATIONS IN SURFACE ENGINEERING**, Second Edition, Tribology and Interface Engineering Series, vol. 56, Elsevier, 2009.

JOHNSON, K.L., **CONTACT MECHANICS**, Press Syndicate of the University of Cambridge, Cambridge, UK, 1985.

JOHNSON, K.L., JEFFERIS, J.A.,**PLASTIC FLOW AND RESIDUAL STRESSES IN ROLLING AND SLIDING CONTACT.** Proc. Inst. Mech. Engrs. Sym. Rolling Contact Fatigue, 1963.

JOHNSON, K.L., **MECHANICS OF ADHESION**,TribolInt, 1998.

JOST, H. P. **LUBRICATION (TRIBOLOGY) EDUCATION AND RESEARCH**, ('Jost Report') UK Department of Education and Science, HMSO (Her Magesty's Stationery Office), 79 p, 1966.

KACHANOV, L. M., **FUNDAMENTALS OF THE THEORY OF PLASTICITY**, MIR Publishers, Moscow, 1974.

LEE, Y.H., HAHN, J.H., NAHM, S.H., JANG, J.I., KWON, D., **INVESTIGATIONS ON INDENTATION SIZE EFFECTS USING A PILE-UP CORRECTED HARDNESS,** Journal of Physics D: Applied Physics, volume 41, number 7, 2008.

MELCONIAN, M.V., "FUNDAMENTAÇÃO TEÓRICA", p. 25-64 In: **MELCONIAN, Marcos Vinícius. Modelagem Numérica e Computacional com Similitude e Elementos Finitos**. São Paulo: Blucher, 2014.

NAKAMURA, S., LAKES, R.S., **FINITE ELEMENT ANALYSIS OF SAINT-VENANT AND EFFECTS IN MICROPOLAR ELASTIC SOLIDS,** Engineering Computations, 12, 571-587, 1995.

NATAL JORGE, R. M., DINIS, L. M. J. S., **TEORIA DA PLASTICIDADE**, Departamento de Engenharia Mecanica e Gestão Industrial, Faculdade de Engenharia, Universidade do Porto, 2004.

NOGUEIRA, R. E. F. Q.; DE MELLO, J. D. B. **ESCLEROMETRIA APLICADA AO ESTUDO DO DESGASTE ABRASIVO: POTENCIALIDADES DA TÉCNICA, CONSTRUÇÃO E AVALIAÇÃO DE ESCLERÔMETRO RETILÍNEO**, 43° CONGRESSO ANUAL DA ABM – ASSOCIAÇÃO BRASILEIRA DE METALURGIA, volume 1, 1988b, Belo Horizonte, MG, Anais do 43° Congresso Anual da ABM, pp 281 – 300.

NOH, G., BATHE, K.J., **AN EXPLICIT TIME INTEGRATION SCHEME FOR THE ANALYSIS OF WAVE PROPAGATIONS**, Computer and Structures 129, 2013.

OLIVER, J., HARTMANN, S., CANTE, J.C., WEYLER, R., HERNANDEZ, J.A., **A CONTACT DOMAIN METHOD FOR LARGE DEFORMATION FRICTIONAL CONTACT PROBLEMS. PART I: THEORETICAL BASIS**, Computational Methods Applied to Engineering, 198, pg 2591-2606, Elsevier, 2009.

OWEN, D. R. J., HINTON, E., **FINITE ELEMENTS IN PLASTICITY: THEORY AND PRATICE**, Pineridge Press, Swansea, UK, 1980.

PENNEC, F., ACHKAR, H., PEYROU, D., PLANA, R., PONS, P., COURTADE, F., **VERIFICATION OF CONTACT MODELING WITH COMSOL MULTIPHYSICS SOFTWARE**, EUROSIM, Toulouse University, 2007.

WEYLER, R., **SIMULACIÓN NUMÉRICA DE PROCESOS DE COMPACTACIÓN Y EXTRUSIÓN DE MATERIALES PULVERULENTOS - APLICACIÓN A LA PULVIMETALURGIA INDUSTRIAL**, Tesis doctoral, Universitat Politécnica de Catalunya, Barcelona, 2000.

RUTHERFORD, K. L.; HUTCHINGS, I. M. **A MICRO-ABRASIVE WEAR TEST, WITH PARTICULAR APPLICATION TO COATED SYSTEMS, SURFACE AND COATINGS TECHNOLOGY**, volume 79, pp 231-239, 1996.

SILVA, P.S. da., **ANÁLISE DO USO DE ESCALAS NAS SIMULAÇÕES DE PROCESSOS DE ESTAMPAGEM.** 100f. Dissertação de Mestrado, Faculdade de EngenhariaMecânica, Universidade Federal de Uberlândia, Uberlândia, 2016.

SVENSSON, D., WALANDER, T., **EVALUATION OF A COHESIVE INTERPHASE ELEMENT USING EXPLICIT FINITE ELEMENT ANALYSIS**, Bachelor degree Project in Mechanical Engeneering, University of Skovde, 2008.

TALJAT, B., PHARR, G. M., **DEVELOPMENT OF PILE-UP DURING SPHERICAL INDENTATION OF ELASTIC-PLASTIC SOLIDS,** International Journal of Solids and Structures, Elsevier, 2004.

TALJAT, B., ZACHARIA, T., PHARR, G. M., **PILE-UP BEHAVIOUR OF SPHERICAL INDENTATIONS IN ENGINEERING MATERIALS,** MRS Procedings, Volume 522, 2011.

UBM MESSTECHNIK GmbH, **OPERATOR MANUAL – UBSOFT VERSION 1.9**, Germany, 1999.

VON MISES, R., **MECHANICS OF SOLID BODIES IN THE PLASTICALLY-DEFORMABLE STATE**, Submitted by C. Runge at the session, translated by D. H. Delphenic, 1913.

WESTERGAARD, H. M., **BEARING PRESSURE AND CRACKS**, Journal of Applied Mechanics, vol.6, 1939.

WEYLER, R., OLIVER, J., SAIN, T., CANTE, J.C., **ON THE CONTACT DOMAIN METHOD: A COMPARISON OF THE PENALTY AND LAGRANGE MULTIPLIER IMPLEMENTATIONS**, Computational Methods Applied to Mechanical Engineering, vol. 205-208, pg 68-82, Elsevier, 2012.

ZIENKIEWICZ, O.C., **THE FINITE ELEMENT METHOD**, 3rd edition, McGraw-Hill BookCo.,1991.

APPENDIX A

1) Algorithm to insert the initial data (seed and parameters) and call the minimization function:

```
clearall

closeall

clc



 K = 400; %Seed for k

n = .25; %Seed for n

 vpo = [K n];

options = optimset('Tolx',1e-15,'Tolfun',1e-
13,'MaxFunEvals',100,'MaxIter', 3000);

figure;

vpans=fminsearch('nova1',vpo,options);
```

2) Function that calculates the Ludwik-Nadai curves and compare with the experimental one.

```
function err = nova(vp)

loadcp01.txt%Load experimental data

disp=(cp01(:,2));

fuerza=(cp01(:,4))*1000;



l0=30;  %comprimento do corpo de prova

y=250;   % Limite de escoamento

d0=4.92;  %diametro do corpo de prova



lf=l0+disp;

df=d0.*(l0./lf).^(1/2);



areaf=df.^2;

sigma_=(fuerza./areaf)';



e11=.5.*(1-(l0./lf).^2);

e22=.5.*(1-(lf./l0));



dp(1)=0;

p(1)=0;

ndf=length(disp(:,1));



fori=2:ndf

dp(i)=(1.5*((e11(i)-e11(i-1))^2+2*(e22(i)-e22(i-1))^2))^(.5);
```

```
    p(i)=p(i-1)+dp(i);

    sigma(i)=vp(1)*((((y/vp(1))^(1/vp(2)) + p(i))^vp(2)));

end

%Determinaçao do erro

err=norm(sigma-sigma_);

figure(29);

plot(p,sigma,'r',p,sigma_,'b--');

xlabel('P');

ylabel('Tensao (MPa)');

title('LEI DE CONVERGÊNCIA');

legend('Ajuste','Experimental');

grid on;

drawnow;
```

ANNEX A

Creación de las "Condiciones de los pares de contacto"

BEGIN_CONTACTS y **END_CONTACTS** son las palabras clave que identifican el comienzo y el final respectivamente del conjunto de datos asociados a los pares de contacto.

BEGIN_CONTACTS

DELETE : CURVE = <*Etiqueta_de_la_curva_a_eliminar*>

NEW_CURVE

<*Cuerpo que define la curva*>

END_NEW_CURVE

DELETE : [MASTER=<*etiqueta*>] [SLAVE=<etiqueta>] [ALL_MASTER]

[ALL_SLAVE] [ALL_PAIRS]

NEW_PAIR

MASTER = <etiqueta>

ALL_SLAVE

SLAVE = <etiqueta>

ALL_MASTER

TYPE = <tipo_contacto>

BEGIN_PARAMETERS

< Lista de parámetros >

END_PARAMETERS

END_NEW_PAIR

END_CONTACTS

COMANDOS

- **BEGIN_CONTACTS** : es la palabra clave que indica el inicio de los datos correspondiente a la definición de los pares de contacto.
- **END_CONTACTS** : es la palabra clave que indica el final de los datos correspondiente a la definición de los pares de contacto.
- **END_CONTACTS** : es la palabra clave que indica el final de los datos
- **NEW_CURVE** : Palabra clave que abre el campo para interpretar una curva (ver campo *Definición de curvas*).
- **END_NEW_CURVE** : Palabra clave que cierra el campo de curvas que especifican las condiciones de contorno sobre los grados de libertad.

● **DELETE**[1]: es la palabra clave para especificar que se va a eliminar una curva o un par de contacto de la base de datos. Esta opción debe ir obligatoriamente acompañada de una de las siguientes palabras clave:

- **CURVE** : Palabra clave para especificar la eliminación de una curva. Esta palabra debe ir seguida de la etiqueta de la curva que se desea borrar.
- **ALL_PAIRS** : Palabra clave para especificar la eliminación de todos los pares de contactos definidos en etapas (*stages*) anteriores así como las curvas que tienen asociadas.
- **MASTER** : Palabra clave para especifica parcialmente (identificando el *master*) el par de contacto a eliminar. Esta palabra clave le precede la etiquita correspondiente al cuerpo que actúa como *master* en el par de contacto. Para completar la especificación del par de contacto a esta palabra clave le debe acompañar un comando que especifique el *slave*. En este sentido, dependiendo del comando empleado, existe la posibilidad de identificar a uno o a todos los pares de contacto asociados a este *master*.
- **SLAVE** : Palabra clave para especifica parcialmente (identificando el *slave*) el par de contacto a eliminar. Esta palabra clave le precede la etiquita correspondiente al cuerpo que actúa como *slave* en el par de contacto. Para completar la especificación del par de contacto a esta palabra clave le debe acompañar un comando que especifique el *master*. En este sentido, dependiendo del comando empleado, existe la posibilidad de identificar a uno o a todos los pares de contacto asociados a este *slave*.
- **ALL_MASTER** : Palabra clave que acompaña al comando SLAVE o ALL_SLAVE y que se emplea para especificar múltiples pares de contacto. Esta combinación de comandos eliminan todos los pares de contactos en los que el cuerpo identificado con el comando SLAVE actúa como *slave* (a excepción del caso de auto-contacto) o elimina todos los pares del contacto si se emplea el comando ALL_SLAVE (a excepción del caso de auto-contacto).

---

[1]NOTA: los dos puntos que siguen a la palabra **DELETE** son opcionales y se emplea por motivos de claridad para indicar que se trata de un comando asociado a otros comandos.

- **ALL_SLAVE** : Palabra clave que acompaña al comando MASTER o ALL_MASTER y que se emplea para especificar múltiples pares de contacto. Esta combinación de comandos eliminan todos los pares de contactos en los que el cuerpo identificado con el comando MASTER actúa como *master* (a excepción del caso de auto-contacto) o elimina todos los pares del contacto (a excepción del caso de auto-contacto).

● **NEW_PAIR** : es la palabra clave que abre el campo con los datos que definen el par de contacto. Este campo contiene los siguientes comandos:

- **MASTER** : Palabra clave que identifica el cuerpo que actúa como *master*.
- **SLAVE** : Palabra clave que identifica el cuerpo que actúa como *slave*.
- **ALL_MASTER** : Palabra clave que acompaña al comando SLAVE o ALL_SLAVE y que se emplea para especificar múltiples pares de contacto. Para el *slave* especificado con el comando SLAVE se crea un par de contacto con cada uno de los cuerpos del problema que harán de *master*, a excepción del caso de auto-contacto. Si se emplea el comando ALL_SLAVE se crea un par de contacto entre todos los cuerpos existentes a excepción de los casos de auto-contacto aunque sin controlar que cuerpo es el *master* y cual es el *slave*.
- **ALL_SLAVE** : Palabra clave que acompaña al comando MASTER o ALL_MASTER y que se emplea para especificar múltiples pares de contacto. Para el *master* especificado con el comando MASTER se crea un par de contacto con cada uno de los cuerpos del problema que harán de *slave*, a excepción del caso de auto-contacto. Si se emplea el comando ALL_MASTER se crea un par de contacto entre todos los cuerpos existentes a excepción de los casos de auto-contacto aunque sin controlar que cuerpo es el *master* y cual es el *slave*.
- **TYPE** : Especifica el tipo o modelo de contacto a definir.
- **BEGIN_PARAMETERS** y **END_PARAMETERS** : Define el principio y el final del campo que contiene todos los datos necesarios para definir el par de contacto.

● **END_PAIR** : es la palabra clave que cierrra el campo con los datos que definen el par de contacto.

REGLAS

Este campo permite la comunicación con la base de datos que definen los pares de contacto, permitiendo crear, modificar o borrar estos pares en cada etapa (*stage*).

Como norma general, se tendrá en cuenta que los pares de contacto definidos en una etapa se mantendrán en las subsiguientes etapas a no ser que estos sean expresamente eliminados o modificados.

Para crear o eliminar un par de auto-contacto, hay que definirlo o eliminarlo específicamente poniendo la etiqueta del cuerpo en el comando MASTER y en el comando SLAVE simultáneamente. Los comandos ALL_MASTER y ALL_SLAVE no incluyen el auto-contacto, por lo que los pares de auto-contacto deben definirse de forma específica.

Si se emplean simultáneamente los comandos ALL_MASTER y ALL_SLAVE se crean todos los pares de contacto entre cuerpos existentes en el *stage* (a excepción de los pares de auto-contacto). No obstante, con esta metodología no se puede controlar el cuerpo que actúa de *master* y el que actúa de *slave* por lo que no debe usarse con métodos de contacto donde sea relevante distinguir entre que cuerpo es el *master* y cual es el *slave*.

EJEMPLO

```
BEGIN_CONTACTS
   DELETE ALL_PAIRS
   NEW_PAIR
```

TYPE = CONTACT_DOMAIN

MASTER = Probeta_Autocontacto

SLAVE = Probeta_Autocontacto

BEGIN_PARAMETERS

END_PARAMETERS

END_NEW_PAIR

END_CONTACTS

“Contact Domain”

BEGIN_PARAMETERS y **END_PARAMETERS** son las palabras clave que identifican el comienzo y el final respectivamente del conjunto de datos asociados al modelo de contacto *Contact Domain*.

BEGIN_ PARAMETERS

CONTACT_STRATEGY = <*Etiqueta_método_contacto*>

MESH_STRATEGY = < *Etiqueta_método_generación_mallas*>

MESH_GENERATOR = <*Etiqueta_mallador*>

SHRINKAGE_STRATEGY = <*Etiqueta_método_contracción_contorno*>

SHRINKAGE_FACTOR = <*Número:factor_contracción_contorno*>

SHRINKAGE_LEVEL = <*Número_entero:número_de_capas_elementos*>

REMESH_START = <*Tipo_de_criterio_para_iniciar_el_remallado*>

BEGIN_START_PARAMETERS

<*Cuerpo de los parámetros sobre la realización del remallado*>

END_START_PARAMETERS

PENALTY_VALUE = <*Número:penalty*>

PENALTY_VALUE_N = <*Número:penalty_normal*>

PENALTY_VALUE_T = <*Número:penalty_friccion*>

PENALTY_CURVE = <*Etiqueta:curva_de_penalty*>

PENALTY_CURVE_N = <*Etiqueta:curva_de_penalty_normal*>

PENALTY_CURVE_T = <*Etiqueta:curva_de_penalty_friccion*>

PENALTY_ARGUMENT = <*Numero_entero*>

FRICTION_VALUE = <*Número:penalty*>

FRICTION_CURVE = <*Etiqueta:curva_de_penalty*>

FRICTION_ARGUMENT = <*Numero_entero*>

STAB_FACTOR = <Parámetro_de_regularización>

STAB_FACTOR_N = <Parámetro_de_regularización_comp_normal>

STAB_FACTOR_T = <Parámetro_de_regularización_comp_tangencial>

YOUNG_MIN = <Modulo_para_calculo_parámetro_de_regularización>

YOUNG_MIN_LIM = <Límite_minimo_para_el_E_equivalente>

TAU_FACTOR = <Parámetro_penalty_multiplier>

TAU_FACTOR_N = <Parámetro_penalty_multiplier_comp_normal>

TAU_FACTOR_T = <Parámetro_penalty_multiplier_comp_tangencial>

PRED_FACTOR = <Factor_relajación_predicción_active_set>

WEIGACTSET_FACTOR = <Peso_predicción_active_set_SLM>

ALPHASHAPE_FACTOR = <*Número_factor_AlphaShape*>

ALPHASHAPE_METHOD = <*Etiqueta_método_AlphaShape*>

MESH_SIZE_METHOD = <*Etiqueta_método_evaluación_tamaño*>

SELFCONTACT_LIMIT_ANGLE = <*Ángulo_límite_de_autocontacto*>

ITER_CT_MAX = <*Número_límite_de_oscilaciones_ActiveSet*>

TOL_ANGLE_B = <*Ángulo_de_toler._para_la_normal_elemento_B_(3D)*>

END_ PARAMETERS

COMANDOS

● **BEGIN_PARAMETERS** : es la palabra clave que indica el inicio de los datos correspondiente a la definición del tipo de contacto.

● **END_POINT_LOADS** : es la palabra clave que indica el final de los datos correspondiente a la definición del tipo de contacto.

● **CONTACT_STRATEGY** : es la palabra clave para especificar el método de contacto que se va a emplear. Esta opción debe ir obligatoriamente acompañada de una palabra clave que especifique el método de contacto. Actualmenteestánimplementadoslossiguientesmétodos de contacto:

- **PENALTY**: Palabra clave para especificar el método de penalty.
- **LAGRANGE_MULTIPLIER** : Palabra clave para especificar el método de Multiplicadores de Lagrange.

● **MESH_STRATEGY** : es la palabra clave para especificar la estrategia de generación de mallas. Esta opción debe ir obligatoriamente acompañada de una

palabra clave que especifique la estrategia de generación de mallas. Actualmenteestánimplementadas las siguientesmetodologías:

- **ALPHASHAPE** : Palabra clave para definir las mallas de contacto por el método de Alpha-Shape.
- **MAXIMUM_EDGE**: Palabra clave para definir las mallas de contacto eliminando los elementos con una arista mayor que un valor límite (similar al *ALPHASHAPE* pero utilizando las longitudes de las aristas en lugar del radio).

● **MESH_GENERATOR** : es la palabra clave para especificar el mallador. Esta opción debe ir obligatoriamente acompañada de una palabra clave que especifique el generador de mallas. Actualmenteestánimplementadoslossiguientesmalladores:

- **TRIANGLE**: Ejecuta el mallador "Triangle". (Opción por defecto para problemas 2D). Mallador de dominios 2D con triangulos.
- **TETGEN**: Ejecuta el mallador "Tetgen". (Opción por defecto para problemas 3D). Mallador de dominios 3D con tetraedros.

● **SHRINKAGE_STRATEGY** : es la palabra clave para especificar el método de contracción del contorno. Esta opción debe ir obligatoriamente acompañada de una palabra clave que especifique el método. Actualmenteestánimplementadas las siguientesmetodologías:

- **GEOVARDISP** : palabra clave para especificar un desplazamiento normal al contorno y variable en función del tamaño de los elementos que en el programa se denomina "Desplazamiento geométrico variable".

● **SHRINKAGE_FACTOR** : Valor numérico que especifica la proporción entre el desplazamiento de contracción del contorno y el tamaño del elemento (en tanto por uno) el cual se define a partir de la cara contenida sobre el contorno.

● **SHRINKAGE_LEVEL** : Valor numérico entero que especifica el número de capas de elementos en la que se permitirá desplazar la contracción del contorno (Valor por defecto 5).

● **REMESH_START** : es la palabra clave para especificar el criterio sobre cuando debe realizarse el remallado, y en consecuencia que datos se necesitan y como

se deben interpretar. Debe ir precedida de una palabra clave predefinida por el programa según el tipo de criterio empleado. Debe estar declarado antes que el campo **BEGIN_START_PARAMETERS**.

Actualmente están implementados los siguientes criterios:

- **TIME_FREQ** : Ejecución del remallado según una frecuencia de tiempo. Este criterio tiene asociado un parámetro adicional que corresponde a la frecuencia de tiempo.
- **TIME_SET** : Ejecución del remallado en un conjunto de instantes definidos por el usuario. Este criterio tiene asociado tantos parámetros como instantes de tiempo se deseen definir.
- **STEP_FREQ** : Ejecución del remallado según una frecuencia de *steps* (incrementos de tiempo en el cálculo incremental). Este criterio tiene asociado un parámetro adicional que corresponde a la frecuencia de tiempo.
- **STEP_SET** : Ejecución del remallado en un conjunto de *steps* definidos por el usuario. Este criterio tiene asociado tantos parámetros como *steps* se deseen definir.

NOTA: Ver el apartado *Definición del criterio para cuando "remallar" un "Par de Contacto"* para la definición de estos criterios.

● **BEGIN_START_PARAMETERS** : es la palabra clave que indica el inicio de los datos que caracterizan el tipo de remallado especificado con el comando **REMESH_START**.

● **END_START_PARAMETERS** : es la palabra clave que indica el final de los datos que caracterizan el tipo de remallado especificado con el comando **REMESH_START**.

● **PENALTY_VALUE** : Valor numérico que especifica numéricamente el Penalty (se define la componente normal y la fricción simultáneamente con el mismo valor de penalty). Aunque no se generará un error, este valor únicamente se interpreta para el método de Penalty o de Lagrangiano Aumentado (no implementado). Este parámetro es incompatible con los parámetros

PENALTY_VALUE_N , *PENALTY_VALUE_T* , *PENALTY_CURVE* , *PENALTY_CURVE_N* o *PENALTY_CURVE_T*.

● **PENALTY_VALUE_N** : Valor numérico que especifica el valor de penalty sólo para la componente normal. Aunque no se generará un error, este valor únicamente se interpreta para el método de Penalty. Este parámetro es incompatible el parámetro *PENALTY_VALUE* o *PENALTY_CURVE*.

● **PENALTY_VALUE_T** : Valor numérico que especifica el valor de penalty sólo para la fricción. Aunque no se generará un error, este valor únicamente se interpreta para el método de Penalty. Este parámetro es incompatible el parámetro *PENALTY_VALUE* o *PENALTY_CURVE*.

● **PENALTY_CURVE** : Etiqueta que especifica un penalty variable según una curva (se define la componente normal y la fricción simultáneamente con el mismo valor de penalty). Aunque no se generará un error, esta etiqueta únicamente se interpreta para el método de Penalty o de Lagrangiano Aumentado (no implementado). Este parámetro es incompatible con los parámetros *PENALTY_VALUE ,PENALTY_VALUE_N* , *PENALTY_VALUE_T*, *PENALTY_CURVE_N* o *PENALTY_CURVE_T*.

● **PENALTY_CURVE_N** : Etiqueta que especifica un penalty variable según una curva sólo para la componente normal. Aunque no se generará un error, este valor únicamente se interpreta para el método de Penalty. Este parámetro es incompatible el parámetro *PENALTY_VALUE* o *PENALTY_CURVE*.

● **PENALTY_CURVE_T** : Etiqueta que especifica un penalty variable según una curva sólo para la fricción. Aunque no se generará un error, este valor únicamente se interpreta para el método de Penalty. Este parámetro es incompatible el parámetro *PENALTY_VALUE* o *PENALTY_CURVE*.

● **PENALTY_ARGUMENT** : Valor entero correspondiente a la etiqueta interna que especifica la variable empleada como argumento en la curva de penalty (por defecto se emplea el tiempo). Aunque no se generará un error, esta etiqueta únicamente se interpreta para el método de Penalty o de Lagrangiano Aumentado (no implementado).

● **FRICTION_VALUE** : Valor numérico que especifica numéricamente el coeficiente de fricción. Actualmente, este parámetro está implementado para el método de Multiplicadores de Lagrange (con el método de Penalty todavía no implementado).

● **FRICTION_CURVE** : Etiqueta que especifica un coeficiente de fricción variable según una curva. Actualmente, este parámetro está implementado para el método de Multiplicadores de Lagrange (con el método de Penalty todavía no implementado).

● **FRICTION_ARGUMENT** : Valor entero correspondiente a la etiqueta interna que especifica la variable empleada como argumento en la curva que define el coeficiente de fricción (por defecto se emplea el tiempo). Actualmente, este parámetro está implementado para el método de Multiplicadores de Lagrange (con el método de Penalty todavía no implementado).

● **STAB_FACTOR** : Valor numérico que especifica el parámetro alpha de estabilización (se define la componente normal y la fricción simultáneamente con el mismo parámetro). Aunque no se generará un error, este valor únicamente se interpreta para el método de Multiplicadores de Lagrange. Este parámetro es incompatible con los parámetros *STAB_FACTOR_N*, *STAB_FACTOR_T*, *TAU_FACTOR*, *TAU_FACTOR_N* o *TAU_FACTOR_T*.

● **STAB_FACTOR_N** : Valor numérico que especifica el parámetro alpha de estabilización sólo para la componente normal. Aunque no se generará un error, este valor únicamente se interpreta para el método de Multiplicadores de Lagrange. Este parámetro es incompatible el parámetro *STAB_FACTOR*, *TAU_FACTOR*, *TAU_FACTOR_N* o *TAU_FACTOR_T*.

● **STAB_FACTOR_T** : Valor numérico que especifica el parámetro alpha de estabilización sólo para la fricción. Aunque no se generará un error, este valor únicamente se interpreta para el método de Multiplicadores de Lagrange. Este parámetro es incompatible el parámetro *STAB_FACTOR*, *TAU_FACTOR*, *TAU_FACTOR_N* o *TAU_FACTOR_T*.

● **YOUNG_MIN** : Comando empleado cuando no se desea que el programa estima un modulo elástico equivalente para el calculo del parámetro de estabilización. Si YOUNG_MIN está presente, en lugar de la estimación del módulo elástico se emplea el valor fijo definido por este comando.

● **YOUNG_MIN_LIM** : Comando empleado para definir un valor mínimo del módulo elástico equivalente empleado en la adimensionalización del parámetro de estabilización (*penalty multiplier* τ). NOTA: Este valor únicamente tiene sentido cuando se estima el módulo elástico, quedando inutilizado cuando se emplea YOUNG_MIN.

● **TAU_FACTOR** : Valor numérico que especifica el parámetro *penalty multiplier* (se define la componente normal y la fricción simultáneamente con el mismo parámetro). Aunque no se generará un error, este valor únicamente se interpreta para el método de Multiplicadores de Lagrange. Este parámetro es incompatible con los parámetros *STAB_FACTOR*, *STAB_FACTOR_N*, *STAB_FACTOR_T*, *TAU_FACTOR_N* o *TAU_FACTOR_T*.

● **TAU_FACTOR_N** : Valor numérico que especifica el parámetro *penalty multiplier* sólo para la componente normal. Aunque no se generará un error, este valor únicamente se interpreta para el método de Multiplicadores de Lagrange. Este parámetro es incompatible el parámetro *STAB_FACTOR*, *STAB_FACTOR_N*, *STAB_FACTOR_T*, *TAU_FACTOR* o *TAU_FACTOR_T*.

● **TAU_FACTOR_T** : Valor numérico que especifica el parámetro *penalty multiplier* sólo para la fricción. Aunque no se generará un error, este valor únicamente se interpreta para el método de Multiplicadores de Lagrange. Este parámetro es incompatible el parámetro *STAB_FACTOR*, *STAB_FACTOR_N*, *STAB_FACTOR_T*, *TAU_FACTOR* o *TAU_FACTOR_N*.

● **PRED_FACTOR** : Valor numérico que especifica el factor de relajación en la predicción inicial del *Active Set*. Un valor 0 indica el mismo Active Set que el instante *n*, un valor 1 predice el mismo incremento que el del paso anterior. (Valor por defecto 1.0). Aunque no se generará un error, este valor se interpreta únicamente para el método de Multiplicadores de Lagrange.

● **WEIGACTSET_FACTOR** : Valor numérico que especifica el peso de la tensión en la predicción del active set. Un valor 0 degenera en un criterio geométrico basado únicamente en el gap, un valor 1 es para el método de Multiplicadores de Lagrange teórico (Valor por defecto 1.0). Aunque no se generará un error, este valor se interpreta únicamente para el método de Multiplicadores de Lagrange. NOTA: La fricción se relaja pero sin degenerar en el caso de Penalty Regularizado.

● **ALPHASHAPE_FACTOR** : Valor numérico que especifica el factor Alpha-Shape para la exclusión de elementos por tamaño. Aunque no se generará un error, este valor se interpreta únicamente para el método Alpha-Shape.

● **ALPHASHAPE_METHOD** : es la palabra clave para especificar el criterio para definir el tamaño del elemento a partir del valor definido en los nodos del elemento. Esta opción debe ir obligatoriamente acompañada de una palabra clave que especifique el criterio a emplear. Aunque no se generará un error, este valor se interpreta únicamente para el método Alpha-Shape.

Actualmente están implementados los siguientes criterios:

- **MAXSIZE** : Palabra clave para especificar tamaño límite del elemento como el máximo de los valores nodales del elemento.
- **MINSIZE** : Palabra clave para especificar tamaño límite del elemento como el mínimo de los valores nodales del elemento.

● **MESH_SIZE_METHOD** : es la palabra clave para especificar el criterio para definir el tamaño del elemento evaluados en los nodos a partir del tamaño de los elementos del contorno *master/slave*. Esta opción debe ir obligatoriamente acompañada de una palabra clave que especifique el criterio a emplear. Aunque no se generará un error, este valor se interpreta únicamente para el método Alpha-Shape.

Actualmente están implementados los siguientes criterios:

- **MAXSIZE** : Palabra clave para especificar tamaño del elemento de contorno como el valor del elemento mayor que contiene al nodo de contorno.

- **MINSIZE** : Palabra clave para especificar tamaño del elemento de contorno como el valor del elemento menor que contiene al nodo de contorno.

● **SELFCONTACT_LIMIT_ANGLE** : Valor numérico que especifica el ángulo límite a partir del cual el elemento de auto-contacto que contenga una arista de la superficie de auto-contacto no será creado (por defecto se consideran 90°). Las unidades del ángulo se definen en grados.

● **ITER_CT_MAX** : Número máximo de iteraciones a partir del cual las oscilaciones sobre el Active Set comienzan a impedirse de manera externa al algoritmo. NOTA: Este comando sólo tiene sentido para la estrategia de contacto "LAGRANGE_MULTIPLIER". El valor asignado por defecto es 5.

● **TOL_ANGLE_B** : Tolerancia de ángulo para considerar al elemento de contacto tipo *B* como correcto (únicamente se tiene en cuenta en el caso 3D). El valor corresponde al ángulo límite que la normal del elemento de contacto tipo *B* (caso 3D sólo) puede estar fuera del rango definido por las normales a los dos elementos vecinos del contorno. NOTA: Este valor debe estar suministrado en grados (valor por defecto 0.0 grados).

REGLAS

Este campo permite la comunicación con los pares de contacto de la base de datos que emplean el modelo de contacto "Contact Domain". Estos parámetros son independientes para cada par de contacto (aunque se hayan creado simultáneamente múltiples pares de contacto) y su eliminación o modificación se debe realizar eliminando el par de contacto al que están asociados.

NOTA: El parámetro "SELFCONTACT_LIMIT_ANGLE" únicamente tiene sentido para el caso de autocontacto.

El parámetro "SELFCONTACT_LIMIT_ANGLE" se emplea (principalmente en el caso 3D) para evitar que las superficies de autocontacto discretizadas y que

queden ligeramente cóncavas por el *shrinkage* generen falsos elementos de autocontacto que pueden activarse indebidamente.

El parámetro STAB_FACTOR es incompatible con los parámetros STAB_FACTOR_N y STAB_FACTOR_T. Si se emplea el parámetro STAB_FACTOR entonces se asigna internamente este valor a los parámetros STAB_FACTOR_N y STAB_FACTOR_T. Si no se emplea STAB_FACTOR (caso en el que se deseen valores distintos para la componente normal y la fricción), entonces se debe utilizar específicamente los parámetros STAB_FACTOR_N para la componente normal del parámetro alpha de estabilización y STAB_FACTOR_T para el parámetro alpha de estabilización de la fricción, ya que de no estar presentes alguno o ambos se asignará la unidad como por defecto. Cualquiera de los parámetros STAB_FACTOR es incompatible con los parámetros TAU_FACTOR.

El parámetro TAU_FACTOR es incompatible con los parámetros TAU_FACTOR_N y TAU_FACTOR_T. Si se emplea el parámetro TAU_FACTOR entonces se asigna internamente este valor a los parámetros TAU_FACTOR_N y TAU_FACTOR_T. Si no se emplea TAU_FACTOR (caso en el que se deseen valores distintos para la componente normal y la fricción), entonces se debe utilizar específicamente los parámetros TAU_FACTOR_N para la componente normal del parámetro *penalty multiplier* y TAU_FACTOR_T para el parámetro *penalty multiplier* de la fricción, ya que de no estar presentes alguno o ambos se asignará la unidad con valor negativo por defecto para inactivar internamente dicho parámetro. Cualquiera de los parámetros TAU_FACTOR es incompatible con los parámetros STAB_FACTOR.

El parámetro PENALTY es incompatible con los parámetros PENALTY_N y PENALTY_T. Si se emplea el parámetro PENALTY entonces se asigna internamente este valor a los parámetros PENALTY_N y PENALTY_T. Si no se emplea PENALTY (caso en el que se deseen valores distintos para la componente normal y la fricción), entonces se debe utilizar específicamente los parámetros PENALTY_N para el penalty de la componente normal y PENALTY_T para el penalty de la fricción, ya que de no estar presentes alguno

o ambos se asignará la unidad como por defecto. Estos parámetros definen un valor constante para el penalty.

De manera similar, se sigue los mismos criterios con los parámetros PENALTY_CURVE para la definición del penalty mediante una curva.

EJEMPLO

```
NEW_PAIR
    TYPE = CONTACT_DOMAIN
    MASTER = Viga
    SLAVE = Esfera
    BEGIN_PARAMETERS
       CONTACT_STRATEGY = PENALTY
PENALTY_VALUE = 1.0e+6
MESH_STRATEGY = ALPHA_SHAPE
       MESH_GENERATOR = TRIANGLE
       ALPHASHAPE_FACTOR = 2.5e+0
       ALPHASHAPE_METHOD = MAX_SIZE
       SELFCONTACT_LIMIT_ANGLE = 60
       MESH_SIZE_METHOD = MIN_SIZE
       SHRINKAGE_STRATEGY = GEO_VAR_DISP
       SHRINKAGE_FACTOR = 0.25e+0
```

```
    REMESH_START = STEP_FREQ
    BEGIN_START_PARAMETERS
        FREQUENCY = 2
    END_START_PARAMETERS
END_PARAMETERS
END_NEW_PAIR
```

Definición del criterio para cuando "*remallar*" un "*Par de Contacto*"

TIPO DE CRITERIO

El criterio para definir cuando un *Par de Contacto* debe remallarse se define a través del comando **REMESH_START** descrito en el apartado "*Asignación de parámetros para el modelo de contacto*".

Los parámetros correspondientes al criterio de remallado se definen en el campo **BEGIN_START_PARAMETERS** - **END_START_PARAMETERS**.

Los criterios actualmente disponibles son:

- **TIME_FREQ**: Ejecución del remallado según una frecuencia de tiempo.
- **TIME_SET**: Ejecución del remallado en un conjunto de instantes definidos por el usuario.
- **STEP_FREQ**: Ejecución del remallado según una frecuencia de steps (incrementos de tiempo en el cálculo incremental).
- **STEP_SET**: Ejecución del remallado en un conjunto de steps definidos por el usuario (incrementos de tiempo en el cálculo incremental).

Criterio: TIME_FREQ

Se trata de realizar un remallado sobre el Par de Contacto con una frecuencia de tiempo (tiempo el cual es objeto la simulación) definida por el usuario. Eneste campo se debeespecificar el parámetro:

- **FREQUENCY**: Palabra clave que especifica el periodo de tiempo sobre el cual efectuar un remallado. Debe ir precedida de un valor real positivo correspondiente a dicho parámetro.

Criterio: TIME_SET

Se trata de realizar un remallado sobre el Par de Contacto en una serie de instantes (referidos al tiempo el cual es objeto la simulación) definidos por el usuario. En este campo se deben especificar tantas veces como sea necesario el parámetro:

- **TIME**: Palabra clave que especifica el instante de tiempo sobre el cual efectuar un remallado. Debe ir precedida de un valor real correspondiente a dicho instante. Este parámetro se repite tantas veces como instantes de tiempo se deseen especificar.

Criterio: STEP_FREQ

Se trata de realizar un remallado sobre el Par de Contacto con una frecuencia de pasos de cálculo (incrementos de tiempo) definida por el usuario. Eneste campo se debeespecificar el parámetro:

- **FREQUENCY**: Palabra clave que especifica el periodo de paso sobre el cual efectuar un remallado. Debe ir precedida de un entero positivo correspondiente a dicho parámetro.

  NOTA: En el caso de especificar un valor real se escogerá el entero más próximo.

Criterio: STEP_SET

Se trata de realizar un remallado sobre el Par de Contacto en una serie de pasos de cálculo (incrementos de tiempo) definidos por el usuario. En este campo se deben especificar tantas veces como sea necesario el parámetro:

- **STEP**: Palabra clave que especifica el paso de tiempo sobre el cual efectuar un remallado. Debe ir precedida de un valor entero correspondiente a dicho instante. Este parámetro se repite tantas veces como pasos de tiempo se deseen especificar.

  NOTA: En el caso de especificar un valor real se escogerá el entero más próximo.